



DISSERTATION

Titel der Dissertation

Structural and functional studies on yeast mitochondrial magnesium transporter Mrs2

Verfasser

Muhammad Bashir Khan MSc

angestrebter akademischer Grad

Doktor der Naturwissenschaften (Dr.rer.nat.)

Wien, 2011

Studienkennzahl lt. Studienblatt: A 091490
Dissertationsgebiet lt. Studienblatt: Molekulare Biologie
Betreuerin: Prof. Dr. Kristina Djinovic-Carugo

**To my beloved.....Only and only to my parents especially to my
mother, sisters and elder brother Akhto Jan Bhattani**

Though you look at others with contempt,
It's you whose body will be reduced to dust.

Rehman BaBa

TABLE OF CONTENTS

ABSTRACT.....	1
ZUSAMMENFASSUNG.....	4
1. INTRODUCTION.....	7
1.1 Magnesium Transport.....	7
1.2 Chemical and Biological Properties of Magnesium.....	8
1.3 Classes of magnesium transporters in prokaryotes.....	10
1.3.1 The CorA transporter class.....	10
1.3.1.1. Three-dimensional structure of Tm-CorA.....	13
1.3.1.2. Mechanism of magnesium transport in CorA.....	15
1.3.2 The MgtE transporter class.....	16
1.3.2.1. Three-dimensional structure of MgtE.....	17
1.3.2 The MgtA/MgtB transporter class.....	18
1.4 Eukaryotic magnesium transport systems.....	21
1.4.1 Yeast transport systems.....	21
1.4.2 Mammal transport systems.....	24
1.4.3 Plant transport systems.....	26
2. AIM OF THE THESIS.....	28
3. MATERIALS AND METHODS.....	30
3.1 Constructs and nomenclature.....	30
3.2 DNA manipulation.....	32
3.2.1 DNA amplification PCR and colony PCR.....	32
3.2.1.1 Soluble domain constructs: Mrs2 ₃₃₋₂₇₀ Mrs2 ₃₃₋₃₀₈ Mrs2 ₄₈₋₃₀₈ , Mrs2 ₄₈₋₃₁₀ , Mrs2 ₄₈₋₃₁₂ , Mrs2 ₄₈₋₃₁₄ , Mrs2 ₄₈₋₃₁₆ , Mrs2 ₄₈₋₃₁₈ , Mrs2 ₄₈₋₃₂₀	34
3.2.1.2 Full-length Mrs2.....	34
3.2.2 DNA agarose gel electrophoresis.....	35
3.2.3 Restriction endonuclease reactions.....	35
3.2.4 DNA purification.....	35
3.2.5 Transformation.....	36
3.2.6 Selection of positive clones using antibiotics.....	36
3.2.7 Plasmid extraction in mini scale (miniprep).....	36
3.2.8 DNA sequencing.....	36
3.2.9 Cloning in <i>Pichia pastoris</i>	38

3.3 Protein expression.....	39
3.3.1 Over-expression of recombinant proteins.....	39
3.3.2 Purification of recombinant N-terminal soluble constructs	
Mrs2 ₃₃₋₂₇₀ , Mrs2 ₃₃₋₃₀₈ Mrs2 ₄₈₋₃₀₈ , Mrs2 ₄₈₋₃₁₀ , Mrs2 ₄₈₋₃₁₂ ,	
Mrs2 ₄₈₋₃₁₄ , Mrs2 ₄₈₋₃₁₆ , Mrs2 ₄₈₋₃₁₈ , Mrs2 ₄₈₋₃₂₀ of Mrs2.....	40
3.3.2.1 Purification of constructs containing trans-membrane helices	
Mrs2 ₃₃₋₃₃₇ , Mrs2 ₄₈₋₃₃₇ , Mrs2 ₃₃₋₃₆₉ , Mrs2 ₄₈₋₄₇₀ , and full-length	
Mrs2 ₃₃₋₄₇₀ of Mrs2.....	41
3.3.3 Cleavage of His ₆ -tag by <i>Tobacco etch virus</i> (TEV) protease.....	42
3.3.4 Protein dialysis.....	42
3.3.5 Protein concentration.....	43
3.3.6 Sodium dodecyl sulfate polyacrylamide gel electrophoresis	
(SDS-PAGE).....	43
3.3.7 Protein concentration determination.....	43
3.3.8 Protein storage.....	43
3.3.9 Differential scanning fluorimetry (DSF) or Thermo Fluor.....	44
3.3.10 Dynamic light scattering (DLS).....	48
3.3.11 Protein reductive methylation.....	48
3.3.12 Limited proteolysis	49
3.3.14 Circular dichroism (CD).....	50
3.3.15 Mrs2 ₄₈₋₃₀₈ soaking and co-crystallization.....	50
MANUSCRIPT 1.....	51
MANUSCRIPT 2.....	57
MANUSCRIPT3.....	108
DISCUSSION.....	130
REFERENCES.....	145
ACKNOWLEDGEMENTS.....	156
CURRICULUM VITAE.....	158

ABSTRACT

Mg^{2+} is one of the most abundant divalent cations in cells and organelles. Magnesium is unique in its chemical properties compared to the other cations. It plays an important role in stabilizing macromolecules and in binding to nucleotides. Furthermore, it acts as a cofactor of a number of different enzymes. Mg^{2+} also influences cell volume and signalling processes by modulating the activities of ion channels and transporters. The magnesium transporters discovered to date have unique characteristics, which correlate with the typical physicochemical properties of Mg^{2+} cations. The CorA/Mrs2 family of Mg^{2+} transporters belongs to a class of transporters known as 2-TM-GxN with no homology to other ion transporters. This class of ion transporters is wide spread in all domains of life and belongs to the metal ion transporter superfamily. The best studied members of this family are the CorA protein of prokaryotes, and the eukaryotic Alr1/2 and Mrs2/Lpe10 proteins.

Mrs2 transporters form the major mitochondrial Mg^{2+} uptake system in yeast, plants and mammals and are essential for mitochondrial Mg^{2+} homeostasis. Human Mrs2 is involved in promoting multidrug resistance in gastric cancer cells by regulating p27, expression of cyclin D1 and release of cytochrome C.

Common features of all of these proteins are the presence of two adjacent transmembrane helices (TM1, TM2) near their C-terminus and the highly conserved GMN sequence motif at the very end of TM1. The N-terminus is characterized by a large soluble domain which forms a funnel like structure and is shown to constitute an allosteric regulatory module that can be designed to promote an open or closed state.

In the absence of sufficient intracellular Mg^{2+} levels, Mg^{2+} ions bound between monomers are released, the N-terminal domains move as a rigid body, whereas the willow helices undergo a rearrangement with respect to one another and relative to the stalk helices (pore forming helices). This causes a torque along the stalk helix. The torque propagates onto the intracellular hydrophobic gates and possibly activates the periplasmic gate by interaction of the cytoplasmic, acidic residues and

the C-terminal, basic residues. This causes an infringe on periplasmic gating residues through movement of TM2 and the MPEL motif loop and thus allow Mg²⁺ ions to flow through.

Mrs2 from *Saccharomyces cerevisiae* is being extensively studied biophysically and biochemically by our collaborative group of Prof Rudolf J. Schweyen (late) who discovered the *MRS2* gene in the late eighties.

In this work, a number of efforts based on biophysical methods and structural studies have been carried out in order to elucidate the mechanism of magnesium transport at the molecular level across the membrane and to enhance insights into the regulation of the transport.

In this thesis, several constructs of Mrs2 were prepared, focusing on the soluble N-terminal inner mitochondrial domain of Mrs2. They were designed based on bioinformatics, limited proteolysis in order to determine the construct which behaves as a functional protein and at the same time being suitable for structural studies. The inner mitochondrial domain of Mrs2 from *Saccharomyces cerevisiae* was crystallized in four different conditions in the monomeric form and its crystal structure solved by a single-wavelength anomalous dispersion exploiting sulphur anomalous signal at 1.83 Å. This structure was then further refined against the high resolution data set at 1.28 Å, collected at European Synchrotron Radiation Facility (ESRF).

The N-terminal domain of Mrs2 is a six-stranded anti-parallel β-sheet sandwiched between two sets of α-helices and adopts the expected, a prokaryotic CorA N-terminal like fold. Analytical gel filtration and dynamic light scattering showed that the N-terminal domain of Mrs2 forms pentamers at low salt concentration. Extension of the C-terminus shows that a portion of the trans-membrane helix is necessary for the oligomerisation of the soluble domain, this is also supported by our analysis of the inter-domain interface of the Mrs2 model generated on the CorA pentameric crystal structure.

Based on the structural comparison with known functional homologues (CorA, the bacterial magnesium transporter, ZntB, the bacterial zinc transporter) of Mrs2, we have identified the presumed active site which is formed by an Asp 97 of $\alpha 3$, located in close proximity to the neighbouring monomer in a functional reconstructed pentameric form. A sequence alignment of eukaryotic magnesium transporters reveals that the carboxylate residues of Glu 270 possibly coordinate the metal ion together with Asp97 of the adjacent protomer in the functional pentamer, and that both residues are highly conserved in the whole family of eukaryotic Mrs2 proteins. In the crystal structure of the monomeric N-terminal domain no bound metal was found at the putative metal binding site. The analysis of the pentameric Mrs2 model constructed on the known structure of CorA together with structure based amino acid sequence alignment, allowed us to identify the putative gate forming residues forming the narrowest constriction along the pore.

ZUSAMMENFASSUNG

Mg^{2+} ist eines der am häufigsten vorkommenden zweiwertigen Kationen in Zellen und Organellen. In seinen chemischen Eigenschaften ist es im Vergleich mit anderen zweiwertigen Kationen einzigartig. Es spielt eine wichtige Rolle bei der Stabilisierung von Makromolekülen, in der Bindung an Nukleotide und als Kofaktor für zahlreiche Enzyme. Weiters beeinflusst Mg^{2+} das Volumen der Zelle und Signalprozesse, indem es die Aktivität von Ionenkanälen und Transportern reguliert. Die bisher charakterisierten Magnesiumtransporter sind an die einzigartigen physiochemischen Eigenschaften dieses Ions angepasst. Die Mg^{2+} -Transporter der CorA/Mrs2 Familie gehören zur Klasse der 2-TM-GxN Proteine und zeigen keine Homologie mit anderen Ionentransportern. Sie sind in allen Domänen des Lebens vertreten und gehören zur Superfamilie der Metallionentransporter. Die am besten charakterisierten Vertreter dieser Klasse sind das Protein CorA der Prokaryoten, sowie die eukaryotischen Proteine Alr1/2 und Mrs2/Lpe10.

Mrs2 bildet das Haupttransportsystem für Mg^{2+} in Mitochondrien bei Hefe, Pflanzen und Säugetieren und ist außerdem für die mitochondriale Mg^{2+} Homöostase essentiell. Das menschliche Mrs2 Protein vermittelt multiple Wirkstoffresistenz bei Magenkarzinomzellen indem es die Expression von p27 und Cyclin D1 sowie die Cytochrom C-Freisetzung reguliert.

Gemeinsamkeiten dieser Proteine sind zwei nahe aneinander liegende Transmembran-Helices (TM1, TM2) im C-terminalen Bereich des Proteins und das hochkonservierte F/Y-G-M-N Motiv am C-terminalen Ende von TM1. Der N-terminale Teil des Proteins besteht aus einer großen, löslichen Domäne, die eine trichterförmige Struktur besitzt. Es wurde bereits experimentell gezeigt, dass dieser Bereich ein allosterisches Regulationsmodul bildet, das so verändert werden kann, dass ein offener oder geschlossener Zustand des Kanals erreicht wird. Ist die intrazelluläre Mg^{2+} -Konzentration niedrig, werden Mg^{2+} -Ionen, die zwischen zwei benachbarten Monomeren gebunden sind, freigesetzt und die N-terminale Domäne des Proteins führt als insgesamt starrer Körper eine Bewegung aus. Im Gegensatz dazu kommt es bei den „willow“ Helices, zu einer Umlagerung zueinander und in

Bezug auf die langen Helices, die den Trichter bilden. Diese führt schlussendlich zu einer Drehung der Helices die den Trichter bilden. Diese Drehung setzt sich bis zu den intrazellulären hydrophoben Schleusenstellen fort und aktiviert möglicherweise auch die periplasmatische Schleuse durch eine Interaktion der cytoplasmatischen, sauren Aminosäurenreste mit den C-terminalen, basischen Aminosäurenreste. Die Bewegung von TM2 und der MPEL Schleife führt dann zur Öffnung der periplasmatischen Schleuse und erlaubt schlussendlich den Einstrom von Mg^{2+} -Ionen.

Mrs2 der Hefe *Saccharomyces cerevisiae* wurde in der Gruppe unseres Kollaborationspartners Prof. Schweyen zum ersten Mal als Magnesiumkanal charakterisiert und wird mit biophysikalischen und biochemischen Methoden intensiv studiert.

In dieser Arbeit wurden verschiedene biophysikalischen und strukturbasierte Methoden angewendet, um den Mechanismus des Ionentransports durch diesen Kanal und seine Regulation auf molekularer Ebene zu klären

Eine Reihe von MRS2-Konstrukten, mit Fokus auf den N-terminalen, löslichen Teil des Proteins wurden hergestellt. Das Design der Konstrukte basierte auf Bioinformatik und Ergebnissen eines begrenzten proteolytischen Abbaus des Proteins mit dem Ziel, ein funktionelles Protein zu erhalten, das aber gleichzeitig auch für die Strukturanalyse geeignet ist.

Die inner-mitochondriale Domäne von Mrs2 von *Saccharomyces cerevisiae* wurde, in monomerischer Form, unter vier verschiedenen Bedingungen kristallisiert. Die Kristallstruktur wurde durch Einzelwellenlänge anomale Dispersion unter Ausnützung der anomale Signale des Schwefels mit einer Auflösung von 1,83 Å bestimmt. Mit den am European Synchrotron Radiation Facility (ESRF) akquirierten hoch-auflösenden Daten wurde die Struktur weiter bis zu einer Auflösung von 1,28 Å verfeinert.

Die N-terminale Domäne von Mrs2 besteht aus einem sechs-strängigen β -Faltblatt, dass zwischen zwei Sets von α -Helices liegt. Die Faltung war, wie erwartet,

vergleichbar mit der N-terminalen Faltung des prokaryotischen CorA Proteins. Analytische Gelfiltration und dynamische Lichtstreuungs-Analyse haben gezeigt, dass die N-terminale Domäne von Mrs2 unter niedriger Ionenstärke Pentamere bildet. Versuche mit einer Verlängerung des C-Terminus des Proteins haben aber gezeigt, dass ein Teil der Transmembran-Helix für die Oligomerisierung der löslichen Domäne notwendig ist. Diese Beobachtung wird auch durch die von uns, auf Basis der pentamerischen CorA Kristallstruktur durchgeführte Analyse des Inter-Domänen Interface des generierten Mrs2 Modells unterstützt.

Basierend auf Strukturvergleichen von Mrs2 mit seinen bekannten, funktionellen Homologen (dem bakterielle Magnesiumtransporter CorA und dem Zinktransporter ZntB) haben wir mit Asp 97 von Helix $\alpha 3$ das vermutliche aktive Zentrum des Proteins identifiziert. Diese Aminosäure befindet sich in großer räumlicher Nähe zum benachbarten Monomer in der funktionellen, rekonstruierten, pentamerischen Form. Ein Sequenzabgleich mit anderen eukaryotischen Magnesiumtransportern zeigt, dass im funktionellen Pentamer, die Carboxylgruppen der Aminosäuren Glu 70, vermutlich zusammen mit Asp 97 im angrenzenden Protomer das Metallion koordinieren. Beide Aminosäuren sind in der gesamten eukaryotischen Transporterfamilie hochkonserviert. In der Kristallstruktur der monomeren N-terminalen Domäne konnte kein gebundenes Metallion gefunden werden. Dennoch hat die Analyse des, auf der Basis der bereits bekannten Struktur von CorA, erzeugten pentameren Mrs2 Modells, in Kombination mit strukturbasiertem Sequenzabgleich, es uns erlaubt, die Aminosäurenreste, zu identifizieren die vermutlich die stärksten Verengungen der Pore und damit die Schleusen des Kanals bilden.

1. INTRODUCTION

1.1 Magnesium Transport

Proteins involved in the transport of ions (cations and anions) across the membrane can be divided into channels and carriers. Carriers in general, can be divided into three distinct subgroups: symport, antiport and uniport. When carriers transport a molecule against its concentration gradient, two primary sources are used to provide the desired energy (Wipf et al, 2002) (1) from ATP hydrolysis and (2) energy acquired when one species is coupled to other gradient (e.g. Na^+ , K^+ -ATPase). (3) The third sub-group are the uniporters, alleviating diffusion down a concentration gradient (facilitating diffusion) (Lalonde et al, 2004). The main difference between the channels and carriers is towards their substrate selectivity, as channels in general are non-saturable and exhibit less stereo specificity towards their substrates compared to carriers (Bruce Alberts, 2002; Yan, 2003)(Fig.1.1).

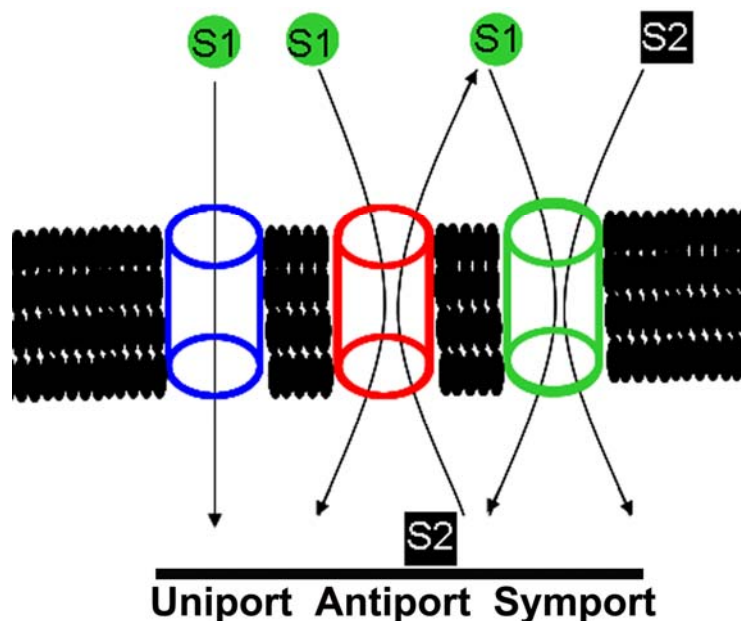


Fig. 1.1: Examples for the three different types of transport.

The differences between the three types of transporters are the direction of transport and the number of substrate transported. This type of classification does not consider whether the process is energy dependent (active transport) or independent (passive transport) (Saier, 2000).

1.2 Chemical and Biological Properties of Magnesium

Mg^{2+} is one of the most abundant divalent cation present in living cells, at a total concentration of about 15-25 mM both in prokaryotic and eukaryotic organisms (Maguire and Cowan, 2002; Romani and Scarpa, 1992; Scarpa and Brinley, 1981). Insufficient Mg^{2+} leads to dissociation of ribosomes into their subunits, serves as an essential structural element both for ribosomes and membranes and acts as a cofactor for ATP in the active sites of a number of enzymes. In prokaryotes, Mg^{2+} also regulates cell volume and signalling processes, which are essential for virulence. (Garcia Vescovi et al, 1996; Ikari et al, 2008; Mobasheri et al, 1998; Soncini et al, 1996; Stephenson & Hoch, 2002).

The chemical properties of divalent magnesium are unusual among all the biologically important cations (Maguire & Cowan, 2002). The hydrated radius of Mg^{2+} is approximately 400 times bigger than the dehydrated radius. This difference is much larger as compared to Na^+ and Ca^{2+} (approximately 25-fold) or K^+ (4-fold). Of all the biological cations, Mg^{2+} is the most charge dense, holding the water molecules within its hydration shell stronger by a factor of about 104 compared to Ca^{2+} , K^+ , Na^+ and is a hard Lewis acid (Fig.1.2) (Maguire & Cowan, 2002). In addition, Mg^{2+} cations are more rigid than other cations in terms of the coordination sphere. It is always hexacoordinated, and prefers to coordinate with oxygen molecules. Moreover, compare to other divalent metal ions, exchange rate of solvent, i.e., waters around is very slow (about three to four times of magnitude than Na^+ and Ca^{2+}), probably due to its strong bond with oxygen of water molecule (Diebler & Winkler., 1969). Proteins that transport Mg^{2+} must be able to recognize the very large hydrated cation, remove the strongly bound hydration shell from the cation, and only then transport the fully or partially dehydrated form of magnesium. Thus, the chemical properties of Mg^{2+} predict that the proteins which recognize and transport Mg^{2+} into cells or organelles, will possess unusual features in nature (Grubbs & Maguire, 1987; Maguire, 2006).

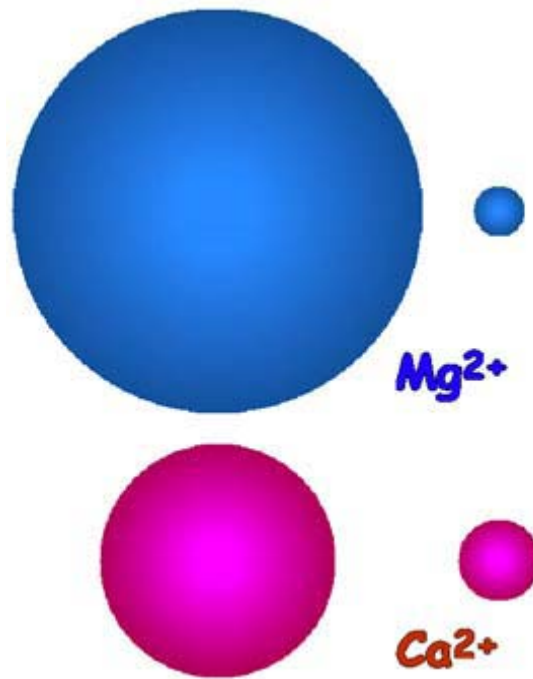


Fig.1.2: Schematic comparison of atomic and hydrated radii of magnesium and calcium

The hydrated (**left**) and dehydrated/atomic (**right**) sizes of Mg^{2+} and Ca^{2+} is illustrated to its size (Maguire & Cowan, 2002). Figure adapted from (Maguire, 2006).

Regarding, concentration of the magnesium in the body, it is the fourth most common and after potassium the second most abundant intracellular cation (Altura, 1994; Iseri & French, 1984; Rude, 1998). In serum and red blood cells very less amount of magnesium is present (less than 1 %) of the total human body. Magnesium exists in three different forms ionized, bound (mainly to albumin) and in the complex form with other anions such as phosphate and citrate. It exists primarily between bone, intracellular compartment of muscle and soft tissues with a ratio of 53 %, 27 %, and 19 %, respectively. In organelles it is mostly concentrated in mitochondria, the endoplasmic reticulum and the nucleus, involved there in different biochemical reaction (Romani & Scarpa, 1992). About ninety percent of intracellular magnesium is restricted to organic matrices (Elin, 1987; Elin, 1994). This frequent occurrence of magnesium in the body indicates its involvement in different biochemical reactions (i.e., more than 300 biochemical reactions). Magnesium

deficiency in humans resulting from insufficient Mg^{2+} intake in the food is a worldwide clinical problem.

1.3 Classes of Magnesium Transporters in Prokaryotes

As described briefly above, the unique chemical characteristics of the magnesium ion, it has been hypothesized that the proteins participating in the transport of this particular divalent cation would have a different structure as compare to other transporters and will represent novel types of transporters or channels. Indeed, this is quite true for the so far described Mg^{2+} transporters characteristics and its structures (Lunin et al, 2006; Moomaw & Maguire, 2008).

In the late 1960's, Webb (1966) observed the importance of magnesium for microbial growth. Since then investigation on magnesium metabolism and its transport in prokaryotes started. In the 1960's and 1970's genetic studies were carried out on *Escherichia coli* in the laboratories of Silver and Kennedy. Both groups discovered the first Mg^{2+} transport system of prokaryotes by transport kinetics experiments using the radio label isotope $^{28}Mg^{2+}$ (Lusk & Kennedy, 1969; Silver, 1969; Silver & Clark, 1971; Snavely et al, 1989). They discovered mutants of *E.coli* which exhibit an unusual behavior towards Co^{2+} ions (Nelson & Kennedy, 1971). In short, until now three distinct magnesium transport systems CorA, MgtE and MgtA/MgtB are discovered. All of them transport magnesium in prokaryotes across the bacterial cell membrane but are expected to have different mechanism of transport and its regulation (Romani, 2007; Smith & Maguire, 1995; Smith & Maguire, 1998). They are described briefly in the following paragraphs.

1.3.1 The CorA transporter class

CorA transporter is the first magnesium transport system identified in *E. coli*, constitute the primary Mg^{2+} uptake system of bacteria and archaea and is the most studied magnesium transporter among all the magnesium transporters (Hmiel et al, 1986; Kehres et al, 1998; Park et al, 1976). The name CorA was derived from the mutant phenotype of increased resistance against the ordinarily toxic levels of Co^{2+} (Cor = Co^{2+} resistance, (Park et al, 1976)). CorA mainly transport divalent cations,

especially magnesium in prokaryotes and is widely distributed throughout gram negative bacteria (Niegowski & Eshaghi, 2007; Smith & Maguire, 1995).

CorA was successfully cloned for the first time in 1986 in *S. enterica* (Hmiel et al, 1986). The transport parameters of the CorA system have been studied in the bacteria *S. typhimurium*, *E. coli* and the Archaeon *Methanococcus jannaschii*. CorA does not solely transport Mg^{2+} but also mediates the influx of Ni^{2+} and Co^{2+} (Hmiel et al, 1986; Snavely et al, 1989; Xia et al, 2011). Mn^{2+} is a poor, non-competitive inhibitor of CorA and is not transported by CorA. Other divalent cations, e.g. Ca^{2+} , Sr^{2+} , Ba^{2+} , Fe^{2+} , Mn^{2+} , and Zn^{2+} do not inhibit CorA significantly. Transport kinetics of CorA demonstrates that Fe^{2+} and Fe^{3+} is neither a substrate of CorA nor its inhibitor (Maguire, 2006; Papp & Maguire, 2004). The CorA affinity for Mg^{2+} is 15 μM . Affinities for Ni^{2+} and Co^{2+} have been quantified in *E. coli* and *S. typhimurium* and are in the range of 200 to 400 and 20 to 40 μM , respectively. As the K_a values of CorA for Co^{2+} and Ni^{2+} are relatively high (explained above), the concentrations required to achieve significant levels of Co^{2+} and Ni^{2+} uptake are toxic for the cell (Maguire, 2006). Therefore, the uptake of Ni^{2+} and Co^{2+} is unlikely to be important due to physiological reasons (Maguire, 2006). As physiological requirement of Ni^{2+} and Co^{2+} is very low compare to other ions, their simple diffusion through CorA may fulfil the cellular requirements under different environmental circumstances (Maguire, 2006). The high K_a value of CorA for Co^{2+} and Ni^{2+} point out the fact, that the transport of Co^{2+} and Ni^{2+} is not the primary function of CorA (Hmiel et al, 1989; Hmiel et al, 1986). It has recently been reported by Xia et al. that CorA from some species transports Co^{2+} more efficiently than Mg^{2+} (Xia et al, 2011). Transport of cations is controlled by the membrane potential like Mrs2 (discuss below) and does not seem to involve ATP hydrolysis for acquiring energy (Smith & Maguire, 1998). As CorA initially interacted with the hexahydrated Mg^{2+} ions which leads to the fact that being of similar size, cobalt hexaammines, can be a potent inhibitor of CorA (Eshaghi et al, 2006; Kucharski et al, 2000; Snavely et al, 1989).

In most bacteria CorA encodes a protein of approximately 310-360 amino acids that has a variable N-terminal hydrophilic domain of about 260 amino acids followed by fairly well conserved two transmembrane helices (TM1 and TM2) of approximately 55 amino acids. On gel electrophoresis like most of the membrane

proteins, CorA runs slightly anomalously at 42 kDa instead of the expected 36-37 kDa. The large majority of CorA proteins has only a short conserved hydrophilic sequence of about six amino acids at the very C-terminus that always contains positively charged residues followed by either one or two aromatic residues resulting in a KKKKWX motif (where as, X is most often aromatic residues) (Maguire, 2006) (Fig.1.3. and 1.4). Some CorA homologues have longer C-terminal tails of about 30 - 35 amino acids, which always retain the positively charged and aromatic residues near both the membrane interface and the conduction pathway (Maguire, 2006).

The structure of the CorA protein is quite unique compared to other cation transporters (Moomaw & Maguire, 2008). It contains a large soluble, N-terminal cytoplasmic domain, constituting about 75 % of the total protein and two transmembrane (TM1, TM2) helices at the C-terminus, each one of about 20 residues (Lunin et al, 2006). Besides the conserved GMN motif at the end of the TM1 helix, the overall general structural features are also conserved over the entire CorA homologues in bacteria and archaea (Eshaghi et al, 2006; Lunin et al, 2006; Payandeh et al, 2008). The CorA transporters represent a major part of the 2-TM-GxN type of proteins in the superfamily of metal ion transporters (MIT) (Knoop et al, 2005; Lunin et al, 2006). To transport metal ions across the plasma membrane CorA must oligomerize to form an ion conducting pathway through the membrane. Previously, it has been reported biochemically that it exists as a homo-tetramer (in *S. enterica*; (Warren et al, 2004) and homopentamer (the yeast homologue Mrs2, (Kolisek et al, 2003)). This oligomerization ambiguity was finally solved by analyzing the crystal structure of the CorA transporter from *Thermotoga maritima* (Tm-CorA), which revealed that it is made of five subunits and is thus function as a homopentamer (Fig.1.3) (Lunin et al, 2006).

The TM1 helices of the five subunits are involved in the formation of the pore in the plasma membrane, while the large N-terminal domains build a funnel like structure in the cytoplasm which monitor the concentration of Mg^{2+} in the cytoplasm (Lunin et al, 2006). The conserved GMN motif is located at the periplasmic surface of the transporter and was implicated in ion selectivity as well as in its dehydration (Payandeh & Pai, 2006). Due to the size of the pore (6-2.5 Å), it is strongly believe that the ion must first be dehydrated completely or partially in order to pass through

the conduction pathway (Eshaghi et al, 2006; Lunin et al, 2006; Payandeh & Pai, 2006).

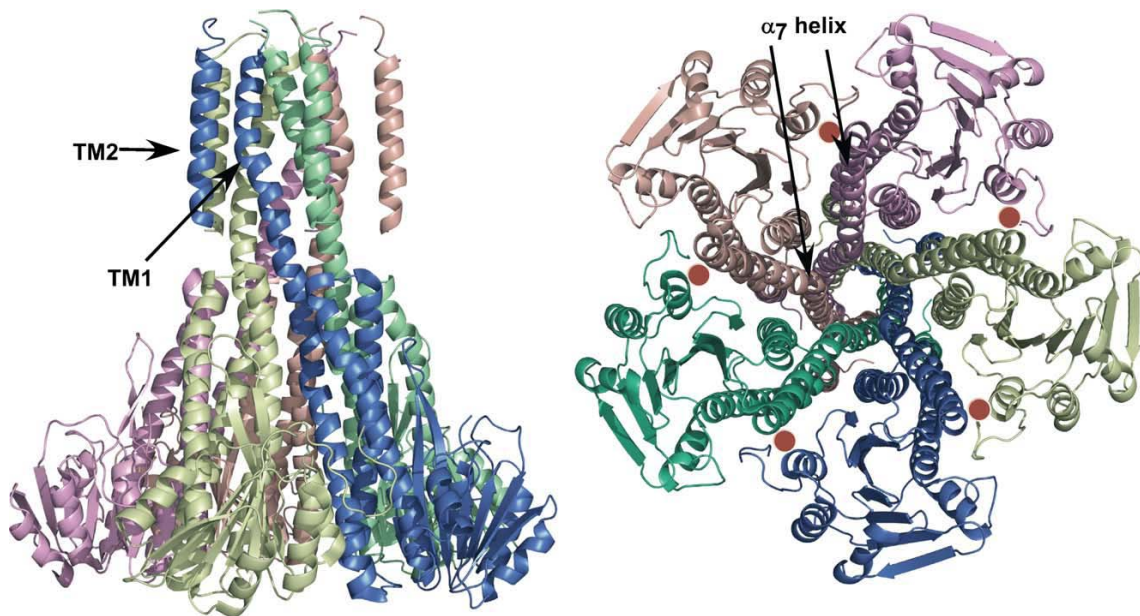


Fig.1.3: Three dimensional crystal structure of the Tm-CorA homopentamer

Figure **(left)** shows the CorA homopentamer side view, with the membrane domain at the top. Each monomer is represented with different colored, and the TM1 and TM2 helices are indicated by an arrow. The loop between the two transmembrane including the conserved GMN motif is not resolved in any of the available crystal structure. Figure **(right)** shows the homopentamer from the cytosol (bottom) facing out through the conduction pathway (pore) in close conformation. The five red dots represent the Mg^{2+} bound between the adjacent monomers. The $\alpha 7$ helices indicated by an arrow Figure adapted from (Papp-Wallace & Maguire, 2007).

1.3.1.1. Three-dimensional structure of Tm-CorA

Lunin et al. (2006) solved the crystal structure of Tm-CorA in the closed conformation (Lunin et al, 2006) at 3.9 Å resolution. The crystal structure of Tm-CorA suggests the importance of the conserved GMN motif and hydrophobic residues in the ion conduction pathway for recognition and transport of Mg^{2+} as previously observed by analysis of *S. enterica* mutants (Eshaghi et al, 2006; Payandeh & Pai, 2006; Smith et al, 1998b; Szegedy & Maguire, 1999). It was proposed previously by biophysical experiments (Smith et al, 1993b), that each monomer possess three TM helices in the *S. enterica* CorA, seems very unusual within the 2-TM-GxN proteins'

family. It is now very well clear that this third proposed TM helix following the two C-terminal helices is the prolonged α -helical portion of the first TM helix making the side wall of the conduction pathway as well as the funnel-shaped cytoplasmic domain, the $\alpha 7$ known as the “stalk helix” (Lunin et al, 2006). The structure of the full-length CorA revealed strong electron density for magnesium at residue Asp 89 of $\alpha 3$ from one protomer and Asp 253 $\alpha 7$ of the adjacent protomer in the cytoplasmic domains, while no electron density were observed at the pore or at the GMN motif (Eshaghi et al, 2006; Lunin et al, 2006; Payandeh & Pai, 2006).

Another research group reported the crystal structure of the Tm-CorA transporter at a higher resolution (2.9 Å versus 3.9 Å), and identified a second Mg^{2+} ion binding site, which can also be occupied by Co^{2+} ions, corroborate that magnesium is not the only substrate of Tm-CorA (Eshaghi et al, 2006; Xia et al, 2011). This site is formed by residues Glu88, Asp175 Asp253 and His257 and coordinates the hydrated Mg^{2+} ion via water. They called them M1 and M2, respectively (Fig.1.4) (Eshaghi et al, 2006).

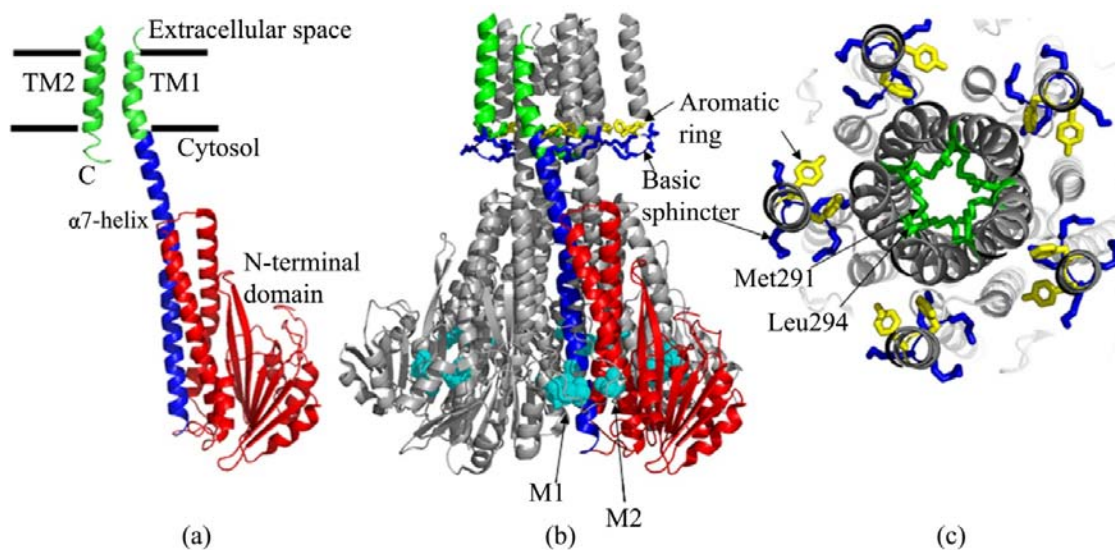


Fig.1.4: Structure of the Tm-CorA Mg^{2+} transporter

(a) Single monomer: green – transmembrane domains TM1 and TM2, blue - $\alpha 7$ helix and red N-terminal domain. **(b)** Side view of the full-length homopentamer: cyan – metal binding sites M1 and M2. **(c)** View from the top of Tm-CorA, representing, blue – the basic sphincter (K4KK), yellow – the aromatic ring and green - the hydrophobic gate forming residues Leu294 and Met291. Figure adapted from (Svidova et al, 2010)

1.3.1.2. Mechanism of magnesium transport in CorA

As the full-length structure of CorA is only available in the close conformation (Lunin et al, 2006), Payandeh et al. (2006) reconstitute the open conformation of the full-length transporter from the crystal structure of the N-terminal soluble domain (Payandeh & Pai, 2006). They then proposed a mechanism for magnesium transportation for the bacterial transporter Tm-CorA (Eshaghi et al, 2006; Lunin et al, 2006; Payandeh et al, 2008; Payandeh & Pai, 2006). In the absence of sufficient intracellular Mg^{2+} levels, Mg^{2+} ions bound between subunits are released, the N-terminal domains of the oligomer moves as a rigid body, whereas the willow helices (two antiparallel helices the $\alpha 5$ and $\alpha 6$ at the N-terminus) undergoes a rearrangement not only with respect to one another, but also to the stalk helices (the pore forming helices) (Payandeh & Pai, 2006). The release of magnesium from the binding site and the rearrangement of the helices cause a torque along the stalk helix. The torque move up into the intracellular hydrophobic gates (Met 291 and Leu 294) and possibly activates the periplasmic gate by interaction of the cytoplasmic N-terminal, acidic residues and the C-terminal, basic residues (Lunin et al, 2006). This causes an impingement on the gating residues through movement of TM2, the MPEL motif (located in the loop connecting TM1 and TM2, following the GMN motif) and thus allowing Mg^{2+} ions to flow through into the cytoplasm (Eshaghi et al, 2006; Lunin et al, 2006; Payandeh et al, 2008) (Fig.1.5). As described above the residues Asp253, Asp89 and Glu88 which are involved in both the magnesium binding sites are from $\alpha 7$ and $\alpha 3$ respectively, indicates the importance of these positions in the transporter regulation. As the conserved GMN motif are located at the entrance of the pore, may provide a polar region for interacting with cations and thus may act as a selectivity filter (Eshaghi et al, 2006; Lunin et al, 2006; Payandeh et al, 2008; Payandeh & Pai, 2006).

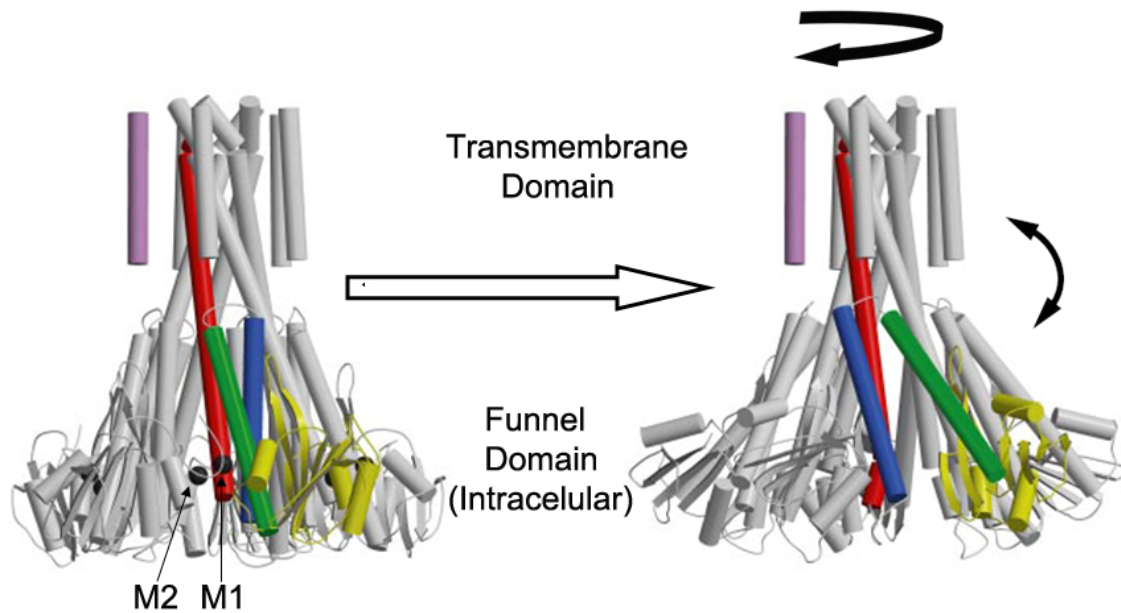


Fig. 1.5: Tm-CorA gating model

A proposed electrostatic interaction between the funnel domain (FD) (acidic residues) and TM2 basic residues (side arrow). The movement of the periplasmic gating residues through a movement of TM2 and the MPEL motif loop (top arrow) upon removal of magnesium from magnesium binding sites M1 and M2. Figure adapted from (Payandeh et al, 2008).

1.3.2 The MgtE transporter class

This type of transporters lacks the GMN motif and does not belong to the 2-TM-GxN family of transporter (Hmiel et al, 1989). It constitutes the second magnesium transport system, which is ubiquitously distributed transporter in all phylogenetic domains (Townsend et al, 1995). Human homologues of MgtE have been functionally characterized and proposed to be involved in magnesium homeostasis, however, compare to CorA transporter they are less widespread (Townsend et al, 1995). Like CorA, MgtE is also unique in nature and shows no homology to other known cation transporters. MgtE initially was cloned both from the Gram-negative and Gram-positive bacterium (*Providencia stuartii* and *Bacillus firmus* OF4) (Smith & Maguire, 1995; Townsend et al, 1995) Evidence exists that, MgtE transport Mg^{2+} and Co^{2+} ; but Ni^{2+} is not transported by this kind of transporter. Expression of MgtE regulated constitutively (Kehres & Maguire, 2002; Maguire, 2006). MgtE has a number of homologues in the eukaryotes (Kehres & Maguire, 2002). It has recently

reported that MgtE are also involved in the regulation of Type III Secretion System of *Pseudomonas aeruginosa* (Anderson et al, 2010).

1.3.2.1. Three-dimensional structure of MgtE

Hattori et al. (2007) determined the full-length crystal structure of MgtE from bacteria *Thermus thermophilus* to a resolution of 3.5 Å (Hattori et al, 2007a; Hattori et al, 2007b) (Fig.1.6). It is a 40 kDa protein, exists as a homodimer with five transmembrane segments per monomer, forming a general architecture similar to some extent to that of Tm-CorA, (i.e., an N-terminal soluble domain and a C-terminal transmembrane domain), but with 10 TM segments in total (Hattori et al, 2007a). The cytosolic domain is composed of two highly acidic sub domains, the helical rich N domain and the cystathionine-β-synthase (CBS) like domain. The CBS and the TM domain are connected by a stretching helix known as “connecting helix,” which is pointed perpendicular to the membrane interface (Hattori et al, 2007a). The first N-terminal domain (the N domain) is located at the N-terminal region of the cytosolic region and is a right-handed super helix with 10 α-helices. The CBS domain, which follows the N domain, is a tandemly repeated, very well-known dimerization domain in various transporters (Ignoul & Eggermont, 2005; Moomaw & Maguire, 2008). Hattori et al. (2007) proposed that the cytosolic domain might function as a Mg²⁺ sensor like that of Tm-CorA which regulates the hydrophobic gating in response to elevated intracellular Mg²⁺ (Hattori et al, 2007a). Recently it has been reported by Hattori et al. (2009) that in presence of high intracellular Mg²⁺ concentration, the close conformation of the transporter stabilized, which is an indication that MgtE might be regulated in the same pattern as the CorA. The exact mechanism of Mg²⁺ transport via MgtE and its regulation is still unknown (Hattori et al, 2009).

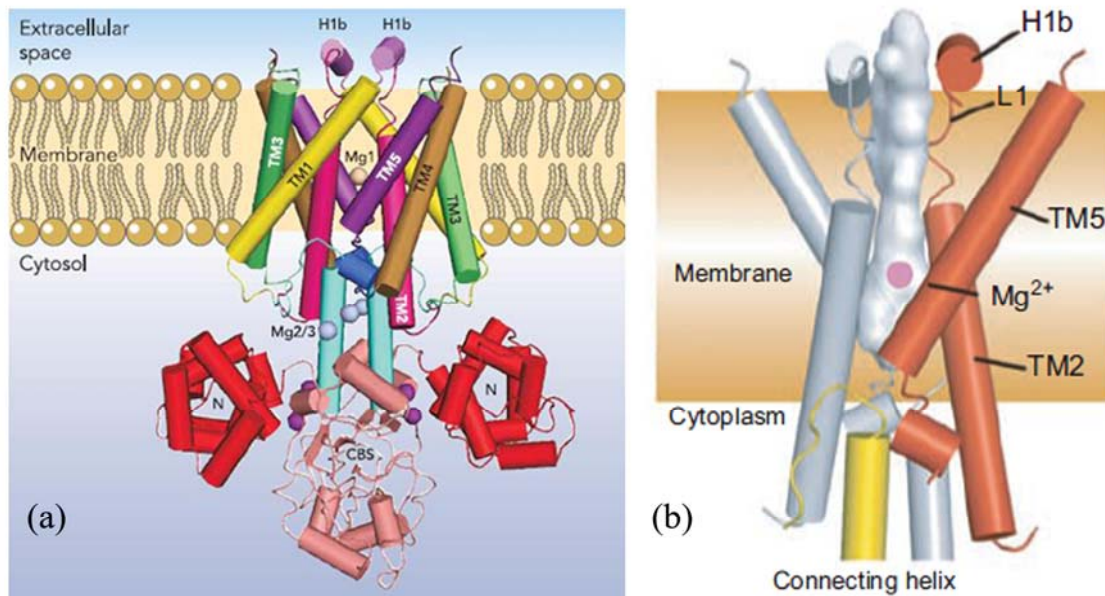


Fig.1.6: Structure of MgtE Mg²⁺ transporter.

(a) The MgtE dimer is viewed in the site of the plane of the membrane, highlighting the N domain (red), CBS domain (beige), connecting helix (blue). The TMs helix of individual monomer are shown in different colors and labeled as TM1 to TM5. The extracellular H1b helices are represented in purple. The five bound magnesiums are labeled according to their position in the protein. **(b)** Solvent-accessible surface of the pore with pore-forming transmembrane helices. The bound Mg²⁺ is shown in purple in the transmembrane region (figure modified from Andrea S. Moomaw et al. (2008) and Motoyuki Hattori et al. (2007)).

1.3.3 The MgtA/MgtB transporter class

Another family of prokaryotic Mg²⁺ transporters that lack the GMN signature motif and thus belong to the non 2-TM-GxN family of transporter (Hmiel et al, 1989). The MgtA and MgtB (Mgt = Magnesium transport) transporters comprise the third magnesium transport system of *Salmonella enterica* that transport Mg²⁺ across the lipid bilayer (Hattori et al, 2009; Quamme, 2010). This class of transporter are quite different from the class of CorA-transporters in many characteristics (Hmiel et al, 1986). MgtA and MgtB have a molecular weight of about 95 kDa and 102 kDa respectively and generally have ten TM helices (like MgtE), with both N-terminal and C-terminal sequences in the cytoplasm (Fig.1.6.) (Hmiel et al, 1989; Tao et al, 1995). The MgtA/MgtB transporters belong to the superfamily of P-type ATPases, which are

cations transport enzymes and has ATP binding domain, acquired energy from the hydrolysis of ATP for the transport process (Smith et al, 1993a). During the process of magnesium transport, phosphorylation of the conserved aspartyl residues takes place by ATP hydrolysis, which causes conformational changes in the protein. (Smith et al, 1993a; Smith & Maguire, 1998). The identity between MgtA/MgtB and mammalian Ca^{2+} -ATPases is 50 % and is 25 % with any other prokaryotic ATPases, respectively (Maguire, 1992), thus MgtA/MgtB is more similar to mammalian Ca^{2+} -ATPases than to any known P-type ATPases (Maguire et al, 1992).

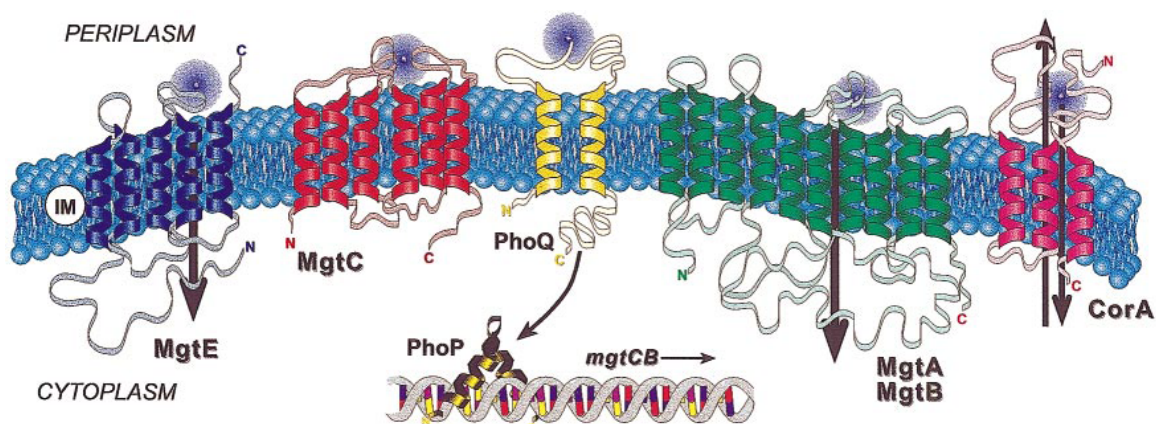


Fig.1.6: Bacterial Mg^{2+} receptors and its transport systems.

The Mg^{2+} transport systems of *Salmonella enterica* are shown with their membrane topologies. The topologies of MgtE, MgtC, PhoQ, MgtA, MgtB and CorA have been shown based on different experimental evidence. The topology for MgtE here is depicted from hydropathy analysis. The crystal structures of CorA and MgtE have resolved their topology ambiguity, which is quite different from their predicted topologies (Hattori et al, 2007a; Kyte & Doolittle, 1982; Lunin et al, 2006). Figure adapted from Moncrief and Maguire (1999).

The PhoPQ (PhoP-PhoQ) is a two component signal transduction system and is responsible for the regulation of MgtA and MgtB in response to the extracellular magnesium level (Kier et al, 1979) (Fig.1.6). The PhoPQ system can be found in different type of bacteria, its regulation was first described in *Salmonella enterica* serovar Typhimurium (Garcia-Calderon et al, 2007; Groisman, 2001; Kato & Groisman, 2008). When Mg^{2+} binds to the membrane-bound PhoQ receptor it

causes inactivation of this protein. If the magnesium concentration decreases, Mg^{2+} and PhoQ dissociation takes place, leading to phosphorylation of the transcription factor PhoP which in turn activates and regulates transcription of a series of genes (about 40), two of which are MgtA and MgtB (Groisman, 1998; Vescovi et al, 1997). MgtA and MgtB maintain a constant intracellular Mg^{2+} concentration (Snaveley et al, 1991). Moreover, Ca^{2+} and manganese can repress the transcription of PhoP-activated genes. The PhoPQ system acts as an essential control element in virulence of *S. enterica* and other bacterial species. (Monsieurs et al, 2005). It is now very well-known, that not only, PhoPQ system is responsible for the regulation of these transporters, but their expression is directly monitored by the intracellular concentration of Mg^{2+} via the gene's 5' UTR (5' untranslatable region) (Cromie et al, 2006; Quamme, 2010).

MgtA is similar to a P-type ATPase of *S. enterica*. The MgtB is encoded by the *mgtCB* operon, which has a size of about 17 k bases. This operon also encodes another hydrophobic protein known as MgtC of an unknown function, which has a molecular weight of about 22.5 kDa (Moncrief & Maguire, 1998). As the *S. enterica* strains knockout for the MgtC gene are avirulents in the mouse. It was hypothesized that MgtC might be necessary for magnesium transport by stabilising magnesium transporting channels/transporters in the membrane and thus required for the virulence in mice (Blanc-Potard & Groisman, 1997; Gunzel et al, 2006; Retamal et al, 2009). Unlike CorA and MgtE, MgtA and MgtB both transport Ni^{2+} besides Mg^{2+} . *E. coli* lacks an MgtCB operon, only the MgtA protein represents the P-type ATPase (Blattner et al, 1997; Park et al, 1976; Smith et al, 1998a). Compared to CorA the Mgt proteins are quite specific in its distribution in different organisms. Most of the sequenced bacterial and archaeal genomes do not possess MgtA or MgtB homologues (Kehres & Maguire, 2002).

1.4 Eukaryotic magnesium transport systems

The three magnesium transport systems (CorA, MgtA/MgtB and MgtE), identified and characterized so far in prokaryotes have, to some extent, homologues in eukaryotes. The CorA homologues exist throughout the genome of the eukarya (Knoop et al, 2005). The MgtE homologues are widely distributed in eukaryotes, including humans, but their homologous proteins are not yet discovered in lower eukaryotes like fungi (Kehres & Maguire, 2002; Maguire, 2006). The prokaryotic MgtA/B transporter has P-type ATPase homologues in eukaryotes, until now no structure and mechanism of transport are described for the eukaryotic magnesium transporters. (Kehres & Maguire, 2002; Maguire, 2006). The inhomogeneous distribution of the prokaryotic types of Mg^{2+} transporters within the eukarya, provide a reason to suggest that, an additional Mg^{2+} transport system may be exist in this domain of life. Below are briefly described the so far characterized transport systems in yeast, mammals and plants.

1.4.1 Yeast transport systems

The eukaryotic homologue of CorA is mostly studied in the fungal model organism *Saccharomyces cerevisiae*, commonly known as “baker’s yeast”. In fungi CorA-like proteins exist for distribution and uptake of magnesium. Alr1 and Alr2 are the homologues proteins of CorA in yeast, located in the plasma membrane (Lee & Gardner, 2006a). These are among the first transporters cloned, which mediate magnesium through the plasma membrane of yeast (Gebert et al, 2009; Graschopf et al, 2001; Lee & Gardner, 2006a; MacDiarmid & Gardner, 1998; Pisat et al, 2009). The names “Alr” were derived, due to their ability to exhibit resistance to the toxic effects of Al^{3+} when over-expressed (Alr = Al^{3+} resistance; (MacDiarmid & Gardner, 1998)). Mrs2 and Lpe10 are also, the homologues of CorA in yeast, located in the inner mitochondrial membrane and mediate the transport of Mg^{2+} into mitochondria (Bui et al, 1999; Gregan et al, 2001a; Moomaw & Maguire, 2008). The sequence identity of Mrs2 with Lpe10 is about 32 % (Sponder et al, 2010).

Mrs2 (Mrs2 = mitochondrial RNA splicing 2) was originally identified in the laboratory of Prof. Schweyen, (Wiesenberger et al, 1992). Later it was confirmed

that the deficiency in splicing with *Mrs2* deletion was due to deficiency of Mg^{2+} for ribozyme structure and function (Gregan et al, 2001b). All homologues of the CorA in yeast exhibit typical structural features of 2-TM-GxN proteins, which is a large cytoplasmic N-terminal domain in case of Alr1 and Alr2 or a mitochondrial matrix domain in case of Mrs2 and Lpe10. The N-terminal soluble domain is followed by the two TM helices with the universally conserved GMN motif at the end of the first transmembrane helix, followed by a flexible loop between the two transmembrane helices (Fig.1.8) (Knoop et al, 2005). The orientation of these transporters in their membranes is such that both the large N-terminus and the shorter C-terminus are oriented towards the mitochondrial matrix in case of Mrs2 and to the cytoplasm in case of Alr1, creating the $N_{in} - C_{in}$ topology (Daley et al, 2005). Despite the low sequence homology, it was suggested that in general Mrs2 and Alr1/2 likely exhibit a similar fold to that of Tm-CorA (Eshaghi et al, 2006; Lunin et al, 2006). Lee et al. (2006) demonstrated by stepwise truncation experiments that 239 amino acids at the N-terminus and 53 amino acids at the C-terminus has no role in the magnesium uptake of the Alr1/2 transporters, but may be required for protein regulation (Lee & Gardner, 2006b). Unlike CorA, yeast Mrs2 transporters has longer C-terminus, with a surplus of positively charged residues and no conserved motif (Weghuber et al, 2006).

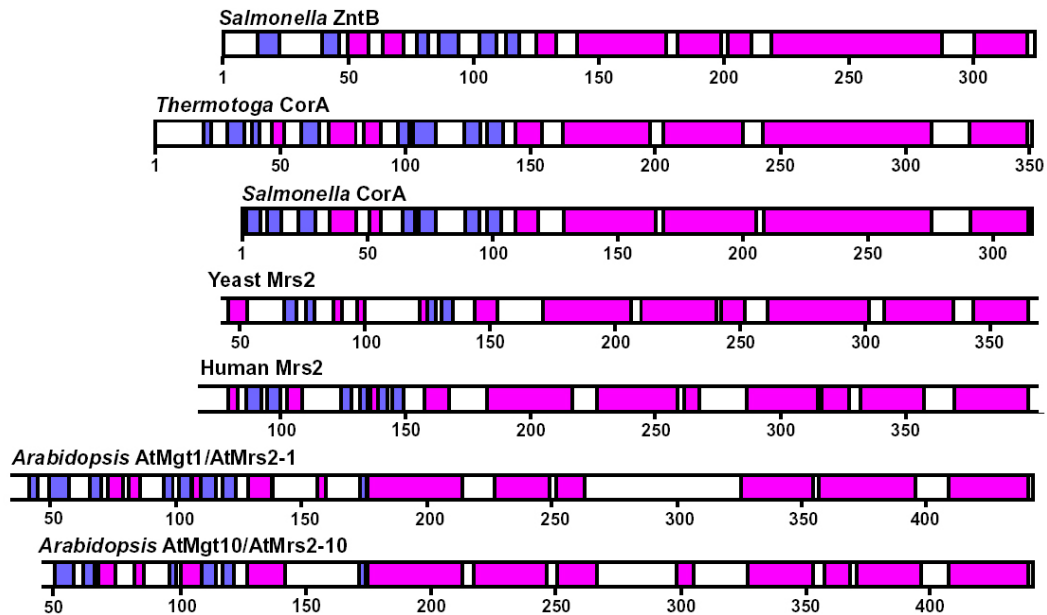


Fig.1.8: Secondary structure comparison of Mrs2 homologues.

The secondary structures features of the indicated sequences were predicted and plotted along the linear sequence with α -helices in magenta and β -sheets in blue. The human, yeast and *Arabidopsis* proteins have an additional N-terminal sequence, and the human and yeast proteins have additional C-terminal sequences not homologous to CorA. These additional sequences did not present here and indicated by the open ends of the bars. The prediction also demonstrates that most of the proteins exhibit a high α -helical content (Figure adapted from Michael E. Maguire 2006).

The *MRS2* knockout strain (*mrs2 Δ* strain) shows a petite phenotype. The strain is demonstrating defects in the mitochondrial cytochrome complexes and are thus not capable to grow on non-fermentable carbon sources like glycerol and ethanol (Wiesenberger et al, 1992). The growth defect cannot be compensated by the second mitochondrial Mg^{2+} transporter, Lpe10, indicating that although the two proteins are 32 % identical at the amino acid level, but they cannot functionally substitute for each other (Gregan et al, 2001a). Furthermore, for Mrs2 it has been recently reported that it also forms hetero-oligomers with Lpe10 (Sponder et al, 2010). Thus, the *MRS2* deleted yeast strain is very useful for the functional analysis of other members of the 2-TM-GxN family of transporters.

1.4.2 Mammalian transport systems

Over the last several years considerable efforts have been made to characterize molecular mechanisms of the transporters and its components regarding, regulation of Mg^{2+} homeostasis in mammals. The 2-TM-GxN family has a number of members in lower eukaryotes like fungi; however, vertebrates distinctly own only the Mrs2 transporter located in the inner mitochondrial membrane. The human Mrs2 has been cloned and has functionally studied in yeast (Knoop et al, 2005; Zsurka et al, 2001). This indicates that proteins different from the CorA/Mrs2 family are responsible for Mg^{2+} transport in the remaining membranes of mammalian cells.

In 2003 a human homologue of the microbial MgtE was discovered and was termed SLC41A1 (for solute carrier family 41 member 1). Its recent functional characterization suggested it, to be involved in magnesium homeostasis (Kolisek et al, 2008). This protein also has homologues in *Homo sapiens* and in metazoans as well, representing a eukaryotic gene family (Kolisek et al, 2008; Wabakken et al, 2003). SLC41A1 possible implication in Mg^{2+} and other, divalent cation transport was further endorsed by voltage-clamp analysis of SLC41A1 and SLC41A2 expressed in *Xenopus laevis* oocytes. (Goytain & Quamme, 2005a; Goytain & Quamme, 2005b; Wabakken et al, 2003). Recently, it has been reported by Kolisek et al. (2008) that human SLC41A1 (hSLC41A1) acts as a magnesium transporter and is non sensitive to well-known magnesium channel blocker, cobalt (III) hexamine. They also demonstrated that hSLC41A1 localizes to the plasma membrane (Kolisek et al, 2008).

In the mammalian plasma membrane two magnesium channels, TRPM6 and TRPM7 are found. They belong to the TRPM (melastatin-related transient receptor potential) superfamily of ion channels (Callera et al, 2009). Both of them possess six predicted TM helices and host a unique kinase domain at the C-terminus, which may be responsible for the regulation of channel. (Ikari et al, 2008; Schmitz et al, 2003). TRPM7 (also known as LTRPC7) is also permeable for a number of other divalent cations as well. (Monteilh-Zoller et al, 2003; Nadler et al, 2001). TRPM7 is ubiquitously expressed among tissues and has been described to be necessary for cell viability, whereas TRPM6, predominantly expressed in intestinal epithelia and kidney tubules (Romani, 2007). It has been shown that these TRPMs have to be

involved in Mg^{2+} absorption and the whole body Mg^{2+} homeostasis. (Chubanov et al, 2004; Ryazanova et al, 2010; Schlingmann et al, 2002; Teramoto et al, 2005).

Goytain and Quamme discovered another two genes that encode a Mg^{2+} transporter, *ACDP2* and *MagT1*. The *MagT1* gene (Magnesium Transporter 1) encodes a Mg^{2+} transporter protein with no sequence homology to any known transporters (Goytain & Quamme, 2005c), again indicating that these transporters generally comprises unique types of proteins. It is expressed in a wide range of tissues, their levels of expression, both *MagT1* and *ACDP2* (Ancient Conserved Domain Protein 2) seem to be regulated in response to external Mg^{2+} concentrations (Goytain & Quamme, 2005c; Zhou & Clapham, 2009). When expressed in oocytes cells, *MagT1* is able to evoke large Mg^{2+} dependent currents. This transporter only transports Mg^{2+} ions and is thus quite specific. On the other hand, *ACDP2* exhibits voltage-dependent transporter characteristics with a broad spectrum of substrates, besides Mg^{2+} other divalent cations including Mn^{2+} , Co^{2+} , Sr^{2+} , Fe^{2+} , Ba^{2+} and Cu^{2+} can be transported by *ACDP2* (Goytain & Quamme, 2005a; Goytain & Quamme, 2005c). *MagT1* has five predicted TM helices.

MagT1 is capable to substitute for the yeast *Alr1* magnesium transporter (Quamme, 2010; Zhou & Clapham, 2009). All members of this family are widely distributed in all domain of life and share their characteristic conserved domain with the microbial *CorC* protein (Goytain & Quamme, 2005a; Goytain & Quamme, 2005c).

Another gene product, known as paracellin-1 (*PCLN-1*), is responsible for the total body Mg^{2+} homeostasis in mammalian cells (Simon et al, 1999). It is a member of the claudin family of tight-junction proteins mainly located in the thick ascending limb of Henle's loop and also in the distal nephron that control paracellular reabsorption in the kidney (Gunzel et al, 2009). The pore possibly formed by *PCLN-1* conducts Mg^{2+} fluxes by a complex mechanism. *PCLN-1* first interacts with apical Ca^{2+} activated Cl^{-} channels, taking into account Cl^{-} currents, which then regulate the Mg^{2+} concentration in the cells (Gunzel et al, 2009).

1.4.3 Plant transport systems

Recently, in plants, the homologues of CorA/Mrs2 have been discovered, as members of the large gene family and called them AtMRS2 or AtMGT, because of magnesium transport. At present, two different types of magnesium transport systems have been known in plants. (a) The vacuolar Mg^{2+}/H^{+} exchanger AtMHX (b) the 2-TM-GxN class of transporters, the first one is the *Arabidopsis thaliana* Mg^{2+} proton exchanger while the second is homologous to the yeast Mrs2/CorA class of transporters (Gebert et al, 2009; Schock et al, 2000; Shaul et al, 1999). Homologues of prokaryotic magnesium transport systems, e.g. MgtE and MgtA/B are not yet discovered in plants.

AtMHX (ATMRS2-11) transporters are quite unique in nature, its gene is similar to that of SCL8 family, encoding the Na^{+}/Ca^{2+} exchanger NCX1 (Na^{+}/Ca^{2+} exchanger 1) of the mammalian plasma membrane (Schmitz et al, 2003). Its homologues are also discovered in *Paramecium*, but their role in magnesium transport is not yet reported. It is localized in the tonoplast, mediates the electrogenic exchange of protons with Mg^{2+} and Zn^{2+} ions, and was predicted to contain eleven TM helices (Shaul et al, 1999). AtMHX proteins are expressed mainly in the xylem parenchyma cells of the plants (Shaul et al, 1999).

In 2000, the group of Volker Knoop and colleagues discovered the family of magnesium transporter in plants, and because of its ability to substitute with yeast Mrs2, they called them as AtMRS2 (Schock et al, 2000). In *Arabidopsis thaliana* and *Oryza sativa* 11 gene of AtMRS2 transport system are spread over five chromosomes, from AtMRS2 to AtMRS9 (Gebert et al, 2009). All these proteins were predicted to have a chloroplast leader peptide in their sequence. All the AtMRS2 genes were analysed in yeast, which shows that these genes significantly increased the rate of magnesium uptake in yeast (Li et al, 2001). Some of these transporters show higher similarity to a subclass of microbial 2-TM-GxN transporters, one of them being the zinc transporter (ZntB) from *Salmonella enterica* (Knoop et al, 2005). The conserved GMN motif of 2-TM-GxN family of magnesium transporting proteins is changed into GIN in ZntB (Worlock & Smith, 2002), which is also found in some plant homologues as well (Knoop et al, 2005). The ZntB proteins do not transport Mg^{2+} but mediate the efflux of Zn^{2+} from the bacterium (Tan et al,

2009). As was expected the structure of the soluble domain of ZntB resemble the CorA structure to high extent (Tan et al, 2009). Even so, according to Orit Shaul, very little is known about the magnesium transport systems in plants and in future most likely further transport systems might be discovered (Shaul, 2002).

By now many genes have been reported from plants, bacteria and animals encoding for proteins involved or mediating Mg^{2+} transport (Gardner, 2003). Considering the biological abundance and importance of Mg^{2+} , there is still a surprising gap of information regarding the proteins that transport Mg^{2+} , the mechanisms by which they do so, the regulation of their transport and their physiological roles within the cell. Many open questions concerning not only their biological and physiological functions, but also their structures and the capability and mechanism of Mg^{2+} transport remains. The low sequence homology of the eukaryotic Mrs2 transporters with the prokaryotic magnesium transporter Tm-CorA, or any other protein of known structure, makes it difficult to predict accurately their structure and function (Weghuber et al, 2006). In this thesis, I present the crystal structure of the N-terminal moiety of the yeast (*Saccharomyces cerevisiae*) mitochondrial magnesium transporter Mrs2 at the atomic resolution and its functional characterization.

2. AIM OF THE THESIS

Metal ions are essential elements in many cellular processes. Therefore, their concentrations in cells and organelles must be kept at appropriate levels. In fact, an impairment of transport systems has been implicated in a number of pathological conditions, collectively called channelopathies (Hubner & Jentsch, 2008). The expression of *MRS2* has been associated with the maintenance of proper steady-state concentrations of mitochondrial Mg^{2+} . Understanding the regulation of the magnesium transporter Mrs2 at a molecular level is very important for the comprehension of its function in mitochondrial Mg^{2+} homeostasis.

A mechanism of opening and closing of the prokaryotic magnesium transporter CorA has been proposed by the construction of a model based on the crystal structure of the inner soluble domain of CorA from *Thermotoga maritima* (Tm-CorA) and its comparison with the structure of Tm-CorA in its closed state (Payandeh et al, 2008; Payandeh & Pai, 2006). In the absence of intracellular magnesium, the Mg^{2+} ions bound between the monomers are released, which triggers structural changes in the N-terminal domain as well as in the membrane spanning region. These changes cause opening of the gates in the pore, and allow Mg^{2+} flux into the cytoplasm.

Low sequence homology of the N-terminal domain of Mrs2 with the prokaryotic magnesium transporter Tm-CorA or any other protein of known structure hampers accurate predictions of its structure and function. We, therefore, set out for a functional and structural analysis of the N-terminal domain of Mrs2 from *Saccharomyces cerevisiae* inner mitochondrial membrane, using a combination of these analyses with the goal to:

- Generate high resolution structural information on the eukaryotic Mg^{2+} transporter Mrs2 (from yeast), focusing on its N-terminal soluble domain.

- Relate structural analysis to Mrs2 function through biochemical, genetic and atomic absorption spectroscopy of selected mutants and wild-type protein.

Specific aims are:

- Structural analysis and comparison with structures of prokaryotic homologues.
- Identification of the divalent cation binding sites (DCS), and of the hydrophobic gate forming residues.
- Understanding the determinants of the oligomerisation of the N-terminal soluble domain of Mrs2.
- Validation and functional characterization of residues implicated in the putative magnesium binding site and in gating.
- Effect of mutations in the conserved GMN motif on ion transport and selectivity in Mrs2.
- Assessment of the role of the C-terminal extension of Mrs2 as the “basic sphincter”.

3. MATERIALS AND METHODS

3.1 Constructs and nomenclature

The constructs used for this study are shown in (Table 3.1). The residues are numbered according to the sequence of the Mrs2 with the N-terminal target peptide (32 amino acids). Constructs for Mrs2 were designed based on the homology modeling, limited proteolysis and spontaneous degradation. For expression in *E. coli* most of the constructs were cloned in vector pETM11 and few of them were cloned in pCS19 both with N- and C-terminal 6xHis-tag. While for expression in *Pichia pastoris* vector pPic3.5K was used, expressing the full-length and the one truncated at N-terminus.

Table 3.1: Construct name, designed and its experimental results

S.NO.	Amino Acid	Vector Used	Construct Name	Designed	Results
1	33-270	pETM13/ pETM13 GST	Mrs2 ₃₃₋₂₇₀	Bioinformatics	Aggregated
2	33-308	pTEM11	Mrs2 ₃₃₋₃₀₈	Bioinformatics	Struc.Solved
3	33-337	pTEM11/pCS19	Mrs2 ₃₃₋₃₃₇	Bioinformatics	Purified
4	33-470	pTEM11/pCS19	Mrs2 ₃₃₋₄₇₀	Bioinformatics	Purified
5	48-308	pTEM11/pETM20	Mrs2 ₄₈₋₃₀₈	Limited Proteolysis/Degradation	Struc.Solved
6	48-310	pTEM11	Mrs2 ₄₈₋₃₁₀	Limited Proteolysis/Degradation	Struc.Solved
7	48-312	pTEM11	Mrs2 ₄₈₋₃₁₂	Limited Proteolysis/Degradation	Struc.Solved
8	48-314	pTEM11	Mrs2 ₄₈₋₃₁₄	Limited Proteolysis/Degradation	Struc.Solved
9	48-316	pTEM11	Mrs2 ₄₈₋₃₁₆	Limited Proteolysis/Degradation	Struc.Solved
10	48-318	pTEM11	Mrs2 ₄₈₋₃₁₈	Limited Proteolysis/Degradation	Purified
11	48-320	pTEM11	Mrs2 ₄₈₋₃₂₀	Limited Proteolysis/Degradation	Purified
12	48-337	pTEM11/pCS19	Mrs2 ₄₈₋₃₃₇	Limited Proteolysis/Degradation	Purified
13	48-470	pTEM11/pCS19	Mrs2 ₄₈₋₄₇₀	Limited Proteolysis/Degradation	Purified
14	33-369	pETM11	Mrs2 ₃₃₋₃₆₉	Bioinformatics	Purified

3.2 DNA manipulation

3.2.1 DNA amplification PCR and colony PCR

The PCR reaction was prepared to a final volume of 50 μ l: 3.125 mM MgCl₂, 0.625 mM dNTP's, 6.25 units of *Taq* DNA Polymerase, 2.5x PCR buffer (10 mM Tris-HCl pH 8.0, 50 mM KCl, 0.08 % Nonidet P-40), 25 pmol of each oligonucleotide (forward/reverse) and 25 to 30 ng of DNA template. The cycles of PCR reactions were optimized according to the length of the target product under investigation (construct) and the melting temperature oligonucleotides (T_m ; Table 3.2).

To identify the positive clones similar PCR reaction was performed as described above, but the template used was a mixture containing a dilution of a colony in double distilled water. The template here prepared by diluting a single colony in 100 μ l of double distilled water. The mixture was heated to 95° C for 10 minutes, centrifuged and then used 1 μ l of the supernatant for the reaction.

Most of the constructs were cloned in the pETM expression system, which has fused tag at N-terminal of the expressed protein. These vectors are available with different tag like polyhistidine-tag (6x His-tag / 8x His-tag), green fluorescent protein (GFP), glutathione S-transferase-tag (GST), disulfide oxidoreductase A (DsbA), *E. coli* thioredoxin A (TrxA). These fused tag help in the protein purification, its identification and also in the solubilization of the cloned protein. The characteristics of the expression plasmid with their corresponding tags are listed in (Table 3.3). The restriction endonuclease reaction was followed by ligation reaction using the T4 DNA ligase enzyme and buffers of the Fermentas. The reaction was set up according to the supplier manual.

Table 3.2: Oligonucleotides and T_m (°C). Restriction sites are highlighted in red for NotI, in blue for NcoI, in bright Green for KpnI, lavender for BamHI and in black for HindIII.

Primer Name	OLIGONUCLEOTIDES (5' TO 3')	T _m (°C)
MRS2 Nco1 wo sig BD fw WTM1_ML rv	CTTTATTTTCAGGGCG CCATGGG C AAACAGTTAC TATCGTTGAA GCCCATT	65.3
	GTG CTC GAG TGC GGCCGC TTA CAA CAT TAA GGA ATT TCT ATT TGC GTC CAA	66.3
MRS2 Nco1 wo sig BD fw WTM1_LE	CTTTATTTTCAGGGCG CCATGGG C AAACAGTTAC TATCGTTGAA GCCCATT	65.3
	GTG CTC GAG TGC GGCCGC TTA CTC CAA CAA CAT TAA GGA ATT TCT ATT TGC	66
MRS2 Nco1 wo sig BD fw WTM1_LK	CTTTATTTTCAGGGCG CCATGGG C AAACAGTTAC TATCGTTGAA GCCCATT	65.3
	GTG CTC GAG TGC GGCCGC TTA GGT AAC CTC CAA CAA CAT TAA GGA ATT TCT	65.3
MRS2 Nco1 wo sig BD fw WTM1_VT	CTTTATTTTCAGGGCG CCATGGG C AAACAGTTAC TATCGTTGAA GCCCATT	65.3
	GTG CTC GAG TGC GGCCGC TTA GGT AAC TTT CAA CTC CAA CAA CAT TAA G	66
MRS2 Nco1 wo sig BD fw WTM1_IY	CTTTATTTTCAGGGCG CCATGGG C AAACAGTTAC TATCGTTGAA GCCCATT	65.3
	GTG CTC GAG TGC GGCCGC TTA GTA GAT GGT AAC TTT CAA CTC CAA CAA C	67
MRS2 Nco1 wo sig BD fw WTM1_TL	CTTTATTTTCAGGGCG CCATGGG C AAACAGTTAC TATCGTTGAA GCCCATT	65.3
	GTG CTC GAG TGC GGCCGC TTA CAA CGT GTA GAT GGT AAC TTT CAA CT	66.6
MRS2 Nco1 wo sig BD fw Mrs2 Not 1 wo sig with TM 1 rv	CTTTATTTTCAGGGCG CCATGGG C AAACAGTTAC TATCGTTGAA GCCCATT	65.3
	GTGCTCGAGT GCGGCCGC TTA CTTTAAATTCATACCATAGAATGCCGG	66
MRS2 Nco1 wo sig BD fw MRS2 Not1 with TM1,2 end	CTTTATTTTCAGGGCG CCATGGG C AAACAGTTAC TATCGTTGAA GCCCATT	65.3
	GTGCTCGAGT GCGGCCGC TTAATTTTTCTTGTCTTCTATCAACCATTTCAAA	65.3
MRS2 Nco1 wo sig BD fw MRS2 Not1 with TM1,2 run_rev	CTTTATTTTCAGGGCG CCATGGG C AAACAGTTAC TATCGTTGAA GCCCATT	65.3
	GTGCTCGAGT GCGGCCGC TTATAAAGAATTTAAATTTTTCTTGGTGATATAAAGGG	64
Mrs2 Nco1 wo sig alpha 4 fw Kpn1 wo sig alpha 4 rv	AA CCATGGG AGCTGACACATCCACTGCTG	59
	TAA GGTACC TTATTACTCTATAAGCATTTCGAAGTCC	56
InfusionMRS2 fw (BamHI) InfusionMRS2 rew (NotI)	TTATTTCGAAG GGATCC ACCATGGGGAATCGGCGTCTCTGGTACG	68.6
	ATTAATTC GCGGCCGC TCAATGATGATGATGATGGTATTTTTCTTGTCTTCTATCAACCATTTC	69
F1 NcoI(N) R1 BamHI(TM1)	CTTTATTTTCAGGGCG CCATGGG GAGCTGACACATCCACTGCTGCAAA	66
	GTGCTCGAGT GGATCC CTTTAAATTCATACCATAGAATGCCGGC	64
F1 NcoI(N) R3(438) BamHI(TM1, 2)	CTTTATTTTCAGGGCG CCATGGG GAGCTGACACATCCACTGCTGCAAA	66
	GTGCTCGAGT GGATCC ATTTTTCTTGTCTTCTATCAACCATTTCAAA	62
F2 NcoI(BD) R1 BamHI(TM1)	CTTTATTTTCAGGGCG CCATGGG GAAAACAGTTACTATCGTTGAAGCCC	65
	GTGCTCGAGT GGATCC CTTTAAATTCATACCATAGAATGCCGGC	64
F2 NcoI(BD) R3(438) BamHI(TM1, 2)	CTTTATTTTCAGGGCG CCATGGG GAAAACAGTTACTATCGTTGAAGCCC	65
	GTGCTCGAGT GGATCC ATTTTTCTTGTCTTCTATCAACCATTTCAAA	62
F1 BamHI(N) R1 HindIII(TM1)	CTTTATTTTCAGGGCG GGATCC ATGGCTGACACATCCACTGCTGCAAA	66
	GTGCTCGAGT AAGCTT TTTACTTTAAATTCATACCATAGAATGCCGGC	62
F1 BamHI(N) R2 HindIII(TM1,2)	CTTTATTTTCAGGGCG GGATCC ATGGCTGACACATCCACTGCTGCAAA	66
	GTGCTCGAGT AAGCTT TTTATCAATTTTTCTTGTCTTCTATCAACCATTTC	61
F2 BamHI(BD) R1 HindIII(TM1)	CTTTATTTTCAGGGCG GGATCC ATGAAACAGTTACTATCGTTGAAGCCC	65
	GTGCTCGAGT AAGCTT TACTTTAAATTCATACCATAGAATGCCGGC	62
F2 BamHI(BD) R2 HindIII(TM1,2)	CTTTATTTTCAGGGCG GGATCC ATGAAACAGTTACTATCGTTGAAGCCC	65
	GTGCTCGAGT AAGCTT TTTATCAATTTTTCTTGTCTTCTATCAACCATTTC	61
Mrs2 Nco1 wo sig with alpha 4 fw Mrs2 Kpn1 wo TM1	AA CCATGGG AGCTGACACATCCACTGCTG	59
	TAA GGTACC TTATTATTTCAACTCCAACAACATTAAG	54

3.2.1.1 Soluble domain constructs: Mrs2₃₃₋₂₇₀, Mrs2₃₃₋₃₀₈, Mrs2₄₈₋₃₀₈, Mrs2₄₈₋₃₁₀, Mrs2₄₈₋₃₁₂, Mrs2₄₈₋₃₁₄, Mrs2₄₈₋₃₁₆, Mrs2₄₈₋₃₁₈, Mrs2₄₈₋₃₂₀

Mrs2 target fragments were amplified by PCR using the full-length fragment cloned into pETM 11 as the template (Fig. 3.1). For all constructs specific oligonucleotides were designed including the restriction sites for Nco1 (forward) and Not1, Kpn1 (reverse) etc. (Table 3.2).

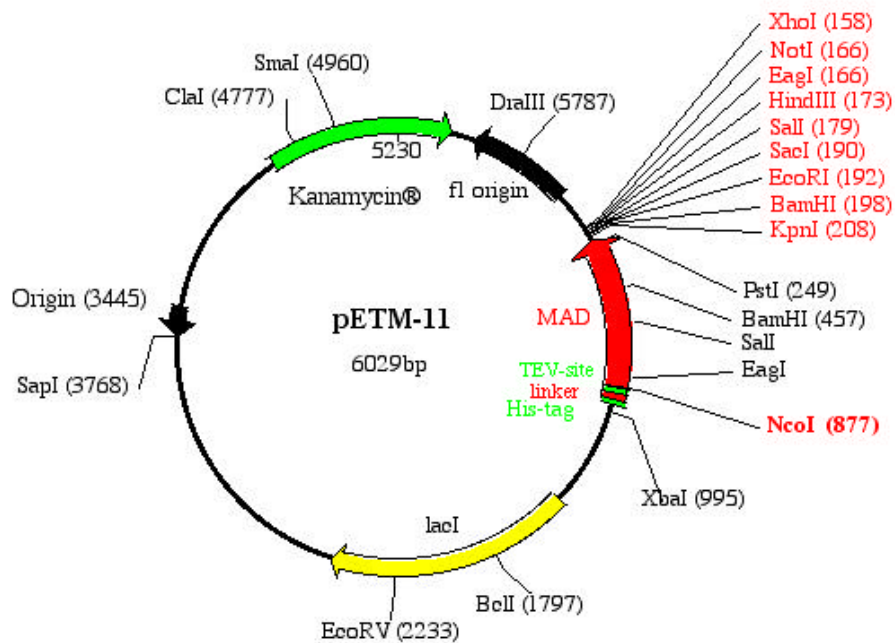


Fig. 3.1: Vector map of pETM-11 courtesy of EMBL

3.2.1.2 Full-length Mrs2

The full-length Mrs2 was amplified by PCR, using the full-length fragment cloned into pUC18 vector by the group of Prof. Schweyen (late) Austria as a template. Specific oligonucleotides were designed including the restriction sites for Nco1 (forward) and Not1 (reverse) (Table 3.2)

3.2.2 DNA agarose gel electrophoresis

All the DNA samples were analysed by DNA agarose gel electrophoresis in different concentrations ranging from 0.8 % (w/v) to 1.2 % (w/v) in 1x TAE buffer (10x TAE buffer = 400 mM Trizma, 40.7 % acetic acid, 500 mM EDTA pH 8.0) and 1 µl of SYBR Safe dye. The electrophoresis was carried out at 80-100 V for 30-40 mins and the DNA bands were visualized by ultraviolet (UV) light.

3.2.3 Restriction endonuclease reactions

All the expression plasmids and PCR fragments were subjected to restriction endonuclease enzymes reaction, the enzymes were selected according to their restriction sites. The plasmids and the amplified target DNA were digested by NcoI – NotI and KpnI in accordance with their restriction site (Table 3.2). Restriction enzymes and the relevant buffers used were from New England BioLabs and the reaction was performed according to the manual.

3.2.4 DNA purification

Both the linearized plasmids and PCR fragments after the restriction reactions were run on DNA agarose gel, and then purified by using the QIAGEN QIAquick Gel Extraction Kit according to the manual.

Table 3.3: Expression vectors and their respective fused tags

Plasmid cloning vector	Tag
pETM13	No tag
pETM11	N-ter 6x His-tag
pETM13 GST	N-ter 6x His-tag + GST-tag
pETM20	N-ter 6x His-tag + TrxA
pCS19	N-ter 6x His-tag
pCS19	C-ter 6x His-tag
pPIC3.5K	No tag

3.2.5 Transformation

The ligation mixture was transformed into a *E.coli* strain DH5 α (Table 3.4). The transformation process was carried out by heat shock procedure, in which 5 μ l mixture of ligation were added to 100 μ l of the DH5 α cells. Incubate for 15-20 mins on ice, heat shock at 42° C for 90 sec and then immediately place on ice for 5 mins. To this mixture 900 μ l of Luria Broth (LB, Sigma) were added, and then incubated at 37° C with 150 rpm for 1 h.

The same method was employed to transform positively selected plasmids into other different expression strains: BL21 (DE3) Star, *E. coli* BL21 (DE3), C-41 DE3, C-43 (DE3), BL21 (DE3) Rosetta pLysS, and BL21 (DE3) pLysS, (Table 3.4).

3.2.6 Selection of positive clones using antibiotics

The transformation mixture were plated on appropriate antibiotics containing, LB-agar medium (LB + 1.5 % agar): Kanamycin (50 μ g/ml), Carbenicillin (100 μ g/ml) or chloramphenicol (34 μ g/ml), based on the plasmid and the *E. coli* strain (Table 3.4), and incubated at 37° C. for 12 - 14 h.

3.2.7 Plasmid extraction in mini scale (miniprep)

The positive clones, which were identified by antibiotics and PCR, subjected to plasmid miniprep using a kit supplied by QIAGEN, following the protocol of the QIAGEN.

3.2.8 DNA sequencing

All the products of the miniprep were sent to DNA sequencing facilities at VBC-Biotech Service GmbH, Vienna, Austria and Agowa DNA Sequencing Erlin Germany, using a primer for of T7 promoter/terminator.

Table 3.4: *E. coli* strains their genetic background and the corresponding construct expressed

in the strain (Hanahan, 1983)

<i>E. coli</i> STRAINS	GENOTYPE	Construct Expressed
BL21 (DE3)	<i>E. coli</i> B F- ompT hsdSB(rB-mB-) gal dcm λ (DE3)	Mrs2 33-308,33-270,48-308,48-310,48-312,48- 314,48-316,48-318,48-320
BL21 (DE3) plyss	<i>E. coli</i> B F- ompT hsdSB(rB-mB-) gal dcm λ (DE3) plyss (CmR)	Mrs2 33-308,33-270,48-308,48-310,48-312,48- 314,48-316,48-318,48-320
DH5 α	supE44 Δ lacU169 (Φ 80 lacZ Δ M15) hsdR17 recA1 endA1 gyrA96 thi-1 relA1	Plasmid manipulation
BL21 (DE3) Star	<i>E. coli</i> B F- ompT hsdSB(rB-mB-) gal dcm λ (DE3) me131	Mrs2 33-308,33-270,48-308,48-310,48-312,48- 314,48-316,48-318,48-320,33-337,48-337
BL21 (DE3) Rosetta plyss	<i>E. coli</i> B F- ompT hsdSB(rB-mB-) gal dcm lacY1 λ (DE3) plyss pRARE2 (CmR)	Mrs2 33-308,33-270,48-308,48-310,48-312,48- 314,48-316,48-318,48-320
C-41 DE3	F ⁻ ompT gal dcm hsdSB(rB-mB-)(DE3)	Mrs2 33-337, 48-337, 33-470,48-470, 33-369
C-43 (DE3)	F ⁻ ompT gal dcm hsdSB(rB-mB-)(DE3)	Mrs2 33-337, 48-337, 33-470,48-470, 33-369

3.2.9 Cloning in *Pichia pastoris*

Mrs2 target fragments were amplified by PCR using the full-length fragment of Mrs2 cDNA as a template. Specific oligonucleotides were designed including the restriction sites for *Bam*H I (forward) and *Eco*R I (reverse) (Table 3.2).

The vectors pPIC3.5K was used for cloning in *Pichia pastoris*. Vector pPIC3.5K is 9004 bp, and created in such a way to find out *in vivo* manifold integrations of the gene in the *Pichia* genome. It has five distinct restriction sites in the cloning sites: *Not* I, *Bam*H I, *Eco*R I, *Avr* II *Sna*B I (Fig. 3.2). It needs ATG codon for initiation in a Kozak consensus sequence for correct expression of the gene (Invitrogen, 2002). The characteristics of the expression plasmid with their corresponding tags are listed above in (Table 3.3).

For cloning in *Pichia pastoris* the restriction endonuclease reaction was followed by submitting the target fragments over night to ligation reaction with the *T4* DNA ligase enzyme using buffer purchased from Invitrogen. The ligation mixture transformed to DH5 α , in the same method as described above, and then screened for positive clones (Cregg et al, 2000). The positive clones were then pursued by manipulation of the plasmid, sequenced the plasmid to conform the target sequence. The sequenced plasmid (one with the correct fragment) was later linearized at *AOX 1* with *Sac* I for insertion of the target fragment to *pichia* GS115 cells. Streak GS115 cells onto a YPD plate in such a way that an isolated, single colonies will grow, incubated the plate at 30° C, for one to two night, preparation of the spheroplast was done using protocol supplied by Invitrogen (p31-33) (Invitrogen). Concentrated 10 ug of linearized pPIC3.5K was added to 100ul of the spheroplast and incubated at room temperature for 10 min, the rest of the transformation protocol followed as provided by Invitrogen (P 34-35) (Invitrogen) manual. The qualitative screen with Geneticin resistance was performed to find out the multiple inserted colonies (Ausubel, 1994).

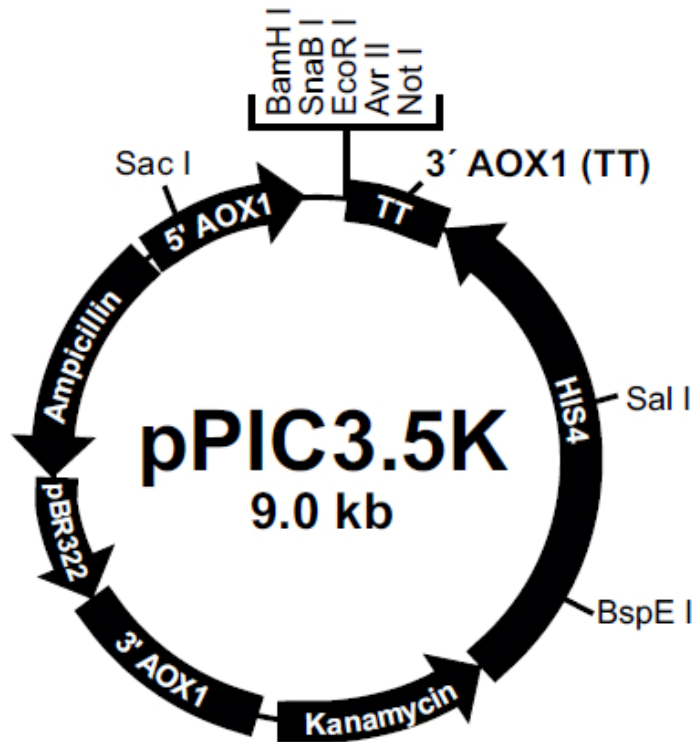


Fig. 3.2: Vector map of pPIC3.5K courtesy of Invitrogen™

3.3 Protein expression

3.3.1 Over-expression of recombinant proteins

After confirming the sequence identities of the cloned inserts, the plasmids were transformed into different expression strains and plated into LB-agar supplied containing an appropriate antibiotic. Took a single isolated colony and diluted in 10 ml LB pre-culture. The 10 ml pre-culture of the target protein grown over night at 37° C and 200 rev. min⁻¹, was diluted in fresh 1 liter LB having the appropriate antibiotics. For small scale over-expression experiments, 0.2 ml of pre-culture was diluted in 5 ml LB desired antibiotics. The fresh culture grew at 37° C and 130 rev min⁻¹ until it reached an optical density OD₆₀₀ between 0.6 and 0.8. The proteins were then induced by adding 0.5 mM isopropyl-β-D-1-thiogalactopyranoside (IPTG (Sigma)) and allowed to grow to a final OD₆₀₀ of 2.3 at 21° C or 37° C at 120 rev. min⁻¹. Protein induction lasted 3 h for experiments performed at 37° C or over night for experiments performed at 21° C. the expressed culture was harvested by centrifugation (6,000 g, 30 min, at 4° C).

The cells of the small scale over-expression experiments were lysed by using Bug buster protein expression kit (Novagen), according to the manual.

3.3.2 Purification of recombinant N-terminal soluble constructs

Mrs2₃₃₋₂₇₀, Mrs2₃₃₋₃₀₈ Mrs2₄₈₋₃₀₈, Mrs2₄₈₋₃₁₀, Mrs2₄₈₋₃₁₂, Mrs2₄₈₋₃₁₄, Mrs2₄₈₋₃₁₆, Mrs2₄₈₋₃₁₈, Mrs2₄₈₋₃₂₀ of Mrs2

To obtain pure protein the expressed cells were resuspended in sonication buffer 10-20 ml lysis buffer per liter of culture (50 mM Tris–HCl pH 8.0, 500 mM NaCl) supplemented with 1 mM phenylmethanesulfonylfluoride (PMSF), 5 mM β-mercaptoethanol (BME), 20 mM imidazole and 5 % glycerol, and lysed by sonication (disrupted for 10 min sonication on ice with 60 % maximum energy output (Bandelin Sonoplus)) and also by French press. The cell lysate was then centrifuged at 50,000 g, 30 min, at 4° C. The supernatant of the centrifuged lysate was submitted to three different protein purification steps, including NTA agarose column (Qiagen), ion exchange (Resource Q column) and size exclusion chromatography (SEC) (Khan et al, 2010).

The NTA agarose column (Qiagen) was pre-equilibrated in the buffer A (50 mM Tris–HCl pH 8.0, 500 mM NaCl, 1 mM PMSF, 5 mM BME, 20 mM imidazole and 5 % glycerol). The column was extensively washed before applying the sample with buffer A containing 20 mM imidazole. Previously, the NTA agarose column was charged with 100 mM NiSO₄ (Khan et al, 2010).

The supernatant of the cell lysate was loaded onto a NTA agarose column. After the supernatant had passed through the column, 6 column volumes of the buffer A was used to wash it. The protein was eluted with a linear gradient of buffer B (buffer A + 500 mM imidazole). The N-terminal His₆ tag was cleaved using TEV (see below Cleavage of His₆-tag by *Tobacco etch virus* (TEV) protease). The cleaved N-terminus and TEV were separated from the protein by reapplying the reaction mixture onto the Ni–NTA column(Khan et al, 2010).

The next protein purification step was the ion exchange chromatography using a Resource Q column (6 ml; GE Healthcare). The flow through of Ni-NTA was pooled and loaded onto a Resource Q column equilibrated with buffer A containing of 50 mM Tris-HCl pH 8.0, 5 mM BME, 20 mM NaCl and 1 mM PMSF and the protein was eluted either, a gradient of 20 – 1000 mM NaCl in 50 mM Tris-HCl pH 8.0, 5 mM BME and 1 mM PMSF or eluted with single step of 50 % of the above buffer (Khan et al, 2010). The protein eluted from the Resource Q column in a single peak at about 280 mM NaCl (Khan et al, 2010).

The last purification step was carried out on a HiLoad 26/60 Superdex 200 (GE Healthcare) gel-filtration column in 50 mM Tris-HCl pH 8.0 and 300 mM NaCl.

The purified protein was concentrated by reapplying it onto a Resource Q column (6 ml; GE Healthcare) as described above; it was concentrated to about 3 mg ml⁻¹(Khan et al, 2010).

3.3.2.1 Purification of constructs containing trans-membrane helices Mrs2₃₃₋₃₃₇, Mrs2₄₈₋₃₃₇, Mrs2₃₃₋₃₆₉, Mrs2₄₈₋₄₇₀, and full-length Mrs2₃₃₋₄₇₀ of Mrs2

The purification of transmembrane constructs Mrs2₃₃₋₃₃₇, Mrs2₄₈₋₃₃₇, Mrs2₃₃₋₃₆₉, Mrs2₄₈₋₄₇₀ and full-length construct Mrs2₃₃₋₄₇₀ of Mrs2 is considerably different from that of the N-terminal soluble domain. In order to obtain pure protein the induced cells were resuspended in 10 - 20 ml lysis buffer (50 mM Tris-HCl pH 8.0, 500 mM NaCl) per liter of culture, supplemented with 1 mM phenylmethanesulfonylfluoride (PMSF), 5 mM β-mercaptoethanol (BME) and 5 % glycerol. Cells were lysed by using French press at 18,000 Psi pressure, maintaining the temperature at 4°C. The resulting supernatant was centrifuged at 10,000 rpm for 1 hour. The pellet was discarded and the supernatant centrifuged at 45,000 rpm for 1 hour, discard the supernatant and collect the pellet (membrane). The pellet was then solubilised in membrane solubilising buffer containing 50 mM Tris-HCl pH 8.0, 500 mM NaCl, 20 mM imidazole supplemented with 1 mM PMSF, 5 BME, 10 % glycerol and 1 % *n*-

Dodecyl- β -D-maltosid (DDM) and stirred gently at 4°C for overnight. The membrane extracts were then centrifuged at 45,000 rpm for 1 hour.

The resulting supernatant from the centrifuged lysate was submitted to two different protein purification steps, including NTA agarose column (Qiagen) and size exclusion chromatography. The NTA agarose column (Qiagen) pre-equilibrated in the buffer A (50 mM Tris-HCl pH 8.0, 500 mM NaCl, 1 mM PMSF, 5 mM BME, 20 mM imidazole 10 % glycerol and 1 % DDM). The membrane extracted supernatant was loaded onto a NTA agarose. After the supernatant had passed through the column, 5 column volumes of the same buffer A was used to wash it. The protein was eluted with a linear gradient of buffer B (buffer A + 500 mM imidazole).

Subsequent purification was carried out on a HiLoad 26/60 Superdex 200 (GE Healthcare) gel-filtration column in 50 mM Tris-HCl pH 8.0 and 500 mM NaCl 10 % glycerol 1 mM PMSF and 0.2 % DDM.

3.3.3 Cleavage of His₆-tag by *Tobacco etch virus* (TEV) protease

The N-terminal His₆-tag was cleaved using an optimised amount of TEV (protease: protein mass ratio 1:70) for 12-16h in the dialysis bag, dialysing against 50 mM Tris-HCl pH 8.0 containing 300 mM NaCl, 1 mM dithiothreitol (DTT) and 1 mM PMSF at 4° C (Khan et al, 2010). To increase the cleavage reaction the TEV protease was refreshed after the first hour of the reaction. The reaction mixture was purified by reapplying onto Ni-NTA column as described above. The purity of the cleaved samples was analyzed by SDS-PAGE for all the constructs. The cleaved protein target was submitted for further purification steps as described above (Khan et al, 2010).

3.3.4 Protein dialysis

Dialysis of the soluble N-terminal domain constructs of Mrs2 was carried out in a dialysis membrane (Spectra/Por Dialysis Membrane Tubing), with a molecular weight cut off (MWCO) of 12 kDa (Spectrum laboratories Inc.), while the full-length (homopentamer) was dialysed using 30 kDa cut off against 3 liter of the desired

buffer at 4°C for overnight. To increase the dialysis speed the buffer were refresh after 1 h.

3.3.5 Protein concentration

The concentration of the full-length protein and the protein containing one transmembrane was performed by using 10, 30 or 50 kDa cut off (Millipore) membranes of Centriprep centrifugal filters devices with the regenerated cellulose. The centrifugation was done as advised by the manufacturers.

3.3.6 Sodium dodecyl sulfate polyacrylamide gel electrophoresis (SDS-PAGE)

The purity of the protein samples were analysed under denaturing conditions on a 12-15 % polyacrylamide gel depending on the molecular weight of the constructs under investigation, according to the protocol of Laemmli's (Laemmli, 1970). The protein bands were stained by Coomassie Brilliant Blue R-250 for 10 mints and then consequently destained by destaining solution.

3.3.7 Protein concentration determination

The concentration of protein was determined spectroscopically, measuring the protein absorbance by UV at 280 nm (OD_{280} ; Nanophotometer, IMPLLEN). Concentration of the protein was computed by an equation: protein concentration (mg/ml) = $OD_{280} \times \text{dilution factor} / \text{extinction coefficient (g/l)}$ and afterwards converted into mg/ml for all constructs. The extinction coefficient (ϵ) of the protein was determined by the ProtParam tool using the website (<http://www.expasy.ch/>) of ExPASy proteomics and primary sequence of each construct.

3.3.8 Protein storage

The purified protein in buffer containing 300 mM of NaCl and 50 mM of Tris-HCl pH 8.0 was flash frozen in liquid nitrogen and kept at -80° C for long storage purpose, while for short storage purpose the protein was kept at 4° C on ice.

3.3.9 Differential scanning fluorimetry (DSF) or Thermo Fluor

DSF was used for screening the optimal buffer conditions for protein stability. The dye binding affinity towards protein increase, when the protein unfolds, which leads to the increase fluorescence (Niesen et al, 2007). The protein solution was heated from 4° C to 95° C during the DSF experiment. The buffer condition at which the protein unfolds at the highest temperature (T_m) is considered the most stable condition (Ericsson et al, 2006).

A combination of different pH, ionic strength and glycerol were prepared in a 96 well plate (Table 3.5). The solution was performed in a final volume of 20 μ l, 10 μ l buffers, 4 μ l proteins (~1.5 mg/ml) and 6 μ l of SYPRO Orange dye (Invitrogen) (the dye used was 5x of the original 5000x as the absolute dye concentration was not registered). The experiment was performed on an instrument (Real-Time PCR) supplied with unique filters calibrated to the SYPRO Orange dye signals. The instrument contains Mx3005 Real-Time QPCR System from Stratagene, Mastercycler *eprealplex* from Eppendorf and from Bio-Rad the iQ5 multicolour Real-Time PCR Detection System.

Table 3.5: Buffer conditions used for optimization of protein

	1	2	3	4	5	6	7	8	9	10	11	12
A	KP pH 7.0 H ₂ O	Hepes pH 7.0 H ₂ O	AA pH 7.3 H ₂ O	SP pH 7.5 H ₂ O	Tris pH 7.5 H ₂ O	Id pH 8.0 H ₂ O	Hepes pH 8.0 H ₂ O	Tris pH 8.0 H ₂ O	Bicine pH 8.0 H ₂ O	Tris pH 8.5 H ₂ O	Bicine pH 9.0 H ₂ O	H ₂ O
B	KP pH 7.0 100mM NaCl	Hepes pH 7.0 100mM NaCl	AA pH 7.3 100mM NaCl	SP pH 7.5 100mM NaCl	Tris pH 7.5 100mM NaCl	Id pH 8.0 100mM NaCl	Hepes pH 8.0 100mM NaCl	Tris pH 8.0 100mM NaCl	Bicine pH 8.0 100mM NaCl	Tris pH 8.5 100mM NaCl	Bicine pH 9.0 100mM NaCl	H ₂ O 100mM NaCl
C	KP pH 7.0 500mM NaCl	Hepes pH 7.0 500mM NaCl	AA pH 7.3 500mM NaCl	SP pH 7.5 500mM NaCl	Tris pH 7.5 500mM NaCl	Id pH 8.0 500mM NaCl	Hepes pH 8.0 500mM NaCl	Tris pH 8.0 500mM NaCl	Bicine pH 8.0 500mM NaCl	Tris pH 8.5 500mM NaCl	Bicine pH 9.0 500mM NaCl	H ₂ O 500mM NaCl
D	KP pH 7.0 100mM KCl	Hepes pH 7.0 100mM KCl	AA pH 7.3 100mM KCl	SP pH 7.5 100mM KCl	Tris pH 7.5 100mM KCl	Id pH 8.0 100mM KCl	Hepes pH 8.0 100mM KCl	Tris pH 8.0 100mM KCl	Bicine pH 8.0 100mM KCl	Tris pH 8.5 100mM KCl	Bicine pH 9.0 100mM KCl	H ₂ O 100mM KCl
E	KP pH 7.0 500mM KCl	Hepes pH 7.0 500mM KCl	AA pH 7.3 500mM KCl	SP pH 7.5 500mM KCl	Tris pH 7.5 500mM KCl	Id pH 8.0 500mM KCl	Hepes pH 8.0 500mM KCl	Tris pH 8.0 500mM KCl	Bicine pH 8.0 500mM KCl	Tris pH 8.5 500mM KCl	Bicine pH 9.0 500mM KCl	H ₂ O 500mM KCl
F	KP pH 7.0 100mM (NH ₄) ₂ SO ₄	Hepes pH 7.0 100mM (NH ₄) ₂ SO ₄	AA pH 7.3 100mM (NH ₄) ₂ SO ₄	SP pH 7.5 100mM (NH ₄) ₂ SO ₄	Tris pH 7.5 100mM (NH ₄) ₂ SO ₄	Id pH 8.0 100mM (NH ₄) ₂ SO ₄	Hepes pH 8.0 100mM (NH ₄) ₂ SO ₄	Tris pH 8.0 100mM (NH ₄) ₂ SO ₄	Tris pH 8.5 100mM (NH ₄) ₂ SO ₄	Tris pH 8.5 100mM (NH ₄) ₂ SO ₄	Bicine pH 9.0 100mM (NH ₄) ₂ SO ₄	H ₂ O 100mM (NH ₄) ₂ SO ₄
G	KP pH 7.0 10%Gly	Hepes pH 7.0 10%Gly	AA pH 7.3 10%Gly	SP pH 7.5 10%Gly	Tris pH 7.5 10%Gly	Id pH 8.0 10%Gly	Hepes pH 8.0 10%Gly	Tris pH 8.0 10%Gly	Bicine pH 8.0 10%Gly	Tris pH 8.5 10%Gly	Bicine pH 9.0 10%Gly	H ₂ O 10%Gly
H	KP pH 7.0 20% Gly	Hepes pH 7.0 20% Gly	AA pH 7.3 20% Gly	SP pH 7.5 20% Gly	Tris pH 7.5 20%Gly	Id pH 8.0 20% Gly	Hepes pH 8.0 20%Gly	Tris pH 8.0 20% Gly	Bicine pH 8.0 20% Gly	Tris pH 8.5 20% Gly	Bicine pH 9.0 20% Gly	H ₂ O 20% Gly

Where as KP, AA, SP and Id stands for potassium phosphate, ammonium acetate, sodium phosphate and imidazole respectively

In order to find an optimal buffer condition for homo pentamerization of the soluble domain of Mrs2₄₈₋₃₀₈ DSF was employed. The protein thermal stability was assayed by varying a combination of pH, glycerol, PEG Smear and sucrose in the presence of 10mM NaCl (Table 3.6). The final reaction volume of 25 μ l contains: 12.5 μ l buffer, 5 μ l protein (1 - 0.5 mg/ml) and 7.5 μ l SYPRO Orange dye (Invitrogen) at a dilution of 5x.

Table 3.6: 96 Buffer conditions used for screening of optimal condition for homo pentamerization

	1	2	3	4	5	6	7	8	9	10	11
A	KP pH 7.0 0.25% PEG 6K	Hepes pH 7.0 0.25% PEG 6K	AA pH 7.3 0.25% PEG 6K	SP pH 7.5 0.25% PEG 6K	Tris pH 7.5 0.25% PEG 6K	Hepes pH 8.0 0.25% PEG 6K	Tris pH 8.0 0.25% PEG 6K	Bicine pH 8.0 0.25% PEG 6K	Tris pH 8.5 0.25% PEG 6K	CHES pH 9.4 0.25% PEG 6K	CAPS pH 10.5 0.25% PEG 6K
B	KP pH 7.0 0.5% PEG 4K	Hepes pH 7.0 0.5% PEG 4K	AA pH 7.3 0.5% PEG 4K	SP pH 7.5 0.5% PEG 4K	Tris pH 7.5 0.5% PEG 4K	Hepes pH 8.0 0.5% PEG 4K	Tris pH 8.0 0.5% PEG 4K	Bicine pH 8.0 0.5% PEG 4K	Tris pH 8.5 0.5% PEG 4K	CHES pH 9.4 0.5% PEG 4K	CAPS pH 10.5 0.5% PEG 4K
C	KP pH 7.0 1% PEG	Hepes pH 7.0 1% PEI 600K	AA pH 7.3 1% PEG	SP pH 7.5 1% PEG	Tris pH 7.5 1% PEG	Hepes pH 8.0 1% PEG	Tris pH 8.0 1% PEG	Bicine pH 8.0 1% PEG	Tris pH 8.5 1% PEG	CHES pH 9.4 1% PEG	CAPS pH 10.5 1% PEG
D	KP pH 7.0 2% sucrose	Hepes pH 7.0 2% sucrose	AA pH 7.3 2% sucrose	SP pH 7.5 2% sucrose	Tris pH 7.5 2% sucrose	Hepes pH 8.0 2% sucrose	Tris pH 8.0 2% sucrose	Bicine pH 8.0 2% sucrose	Tris pH 8.5 2% sucrose	CHES pH 9.4 2% sucrose	CAPS pH 10.5 2% sucrose
E	KP pH 7.0 0.5% PEG6K	Hepes pH 7.0 0.5% PEG6K	AA pH 7.3 0.5% PEG6K	SP pH 7.5 0.5% PEG6K	Tris pH 7.5 0.5% PEG6K	Hepes pH 8.0 0.5% PEG6K	Tris pH 8.0 0.5% PEG6K	Bicine pH 8.0 0.5% PEG6K	Tris pH 8.5 0.5% PEG6K	CHES pH 9.4 0.5% PEG6K	CAPS pH 10.5 0.5% PEG6K
F	KP pH 7.0 1% PEG 4K	Hepes pH 7.0 1% PEG 4K	AA pH 7.3 1% PEG 4K	SP pH 7.5 1% PEG 4K	Tris pH 7.5 1% PEG 4K	Hepes pH 8.0 1% PEG 4K	Tris pH 8.0 1% PEG 4K	Bicine pH 8.0 1% PEG 4K	Tris pH 8.5 1% PEG 4K	CHES pH 9.4 1% PEG 4K	CAPS pH 10.5 1% PEG 4K
G	KP pH 7.0 2% PEG	Hepes pH 7.0 2% PEG	AA pH 7.3 2% PEG	SP pH 7.5 2% PEG	Tris pH 7.5 2% PEG	Hepes pH 8.0 2% PEG	Tris pH 8.0 2% PEG	Bicine pH 8.0 2% PEG	Tris pH 8.5 2% PEG	CHES pH 9.4 2% PEG	CAPS pH 10.5 2% PEG
H	KP pH 7.0 4% sucrose	Hepes pH 7.0 4% sucrose	AA pH 7.3 4% sucrose	SP pH 7.5 4% sucrose	Tris pH 7.5 4% sucrose	Hepes pH 8.0 4% sucrose	Tris pH 8.0 4% sucrose	Bicine pH 8.0 4% sucrose	Tris pH 8.5 4% sucrose	CHES pH 9.4 4% sucrose	CAPS pH 10.5 4% sucrose

Where as KP , AA and SP stands for potassium phosphate, ammonium acetate and sodium phosphate respectively

3.3.10 Dynamic light scattering (DLS)

DLS also known as Quasi-Elastic Light Scattering (QELS) is a technique most often used to measure the size of small molecules in solution. It is a well established technique measuring the size of molecules and particles below 1 nanometer (Chayen et al, 2004). The molecules in Brownian motion cause fluctuation in the scattered light intensity according to their composition. Protein solution in different oligomerization states (aggregates, oligomers, dimers, monomers, etc.), scatter light in different intensities evaluated by a detector positioned at a 90° angle to the incident laser light (Banachowicz, 2006; Cecere et al, 2003; Jamieson A & Mc, 1979). Sample dispersity can be estimated according to its population (Borgstahl, 2007). It is widely believed that monodisperse (polydispersity below 30 %) samples are more likely to crystallize (Carvalho et al, 2009; D'Arcy, 1994).

DLS was routinely employed to evaluate the polydispersity of the protein solutions prior to setting up the crystallization trials. DLS measurements were performed at 22° C as well as 4° C using the DynaPro-801 instrument (protein Solution Inc.) with 100 - 150 acquisitions taken each at 1 sec. intervals. The Dynamics V6 software (Protein Solutions Inc.) was employed for analysis of the recorded data.

3.3.11 Protein reductive methylation

To obtain diffraction-quality crystals is a major bottleneck in the macromolecular crystallography. Protein reductive methylation is a chemical method to modify the crystallization properties of protein (Fan & Joachimiak, 2010; Kim et al, 2008; Rypniewski et al, 1993). Protein reductive methylation generates changes in the surfaces charges of the protein that could likely enhance the crystal packing of the macromolecules during crystallization (Fan & Joachimiak, 2010). The change in surfaces charge occur as a result of primary free amino groups found in lysine residues or in the N-terminal of the protein being changed to tertiary or secondary amino groups (Fig. 3.3).

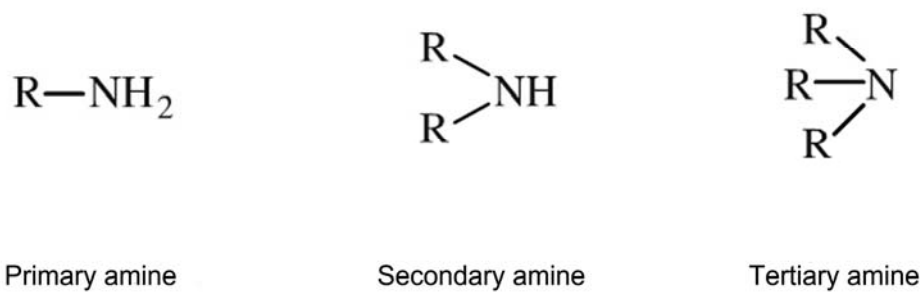


Fig. 3.3: Three different amino groups:

Primary (found in lysine or the N-terminal of proteins), secondary and tertiary amine.

Originally, the lysine methylation protocol was established by Rypniewski WR and modified by Thomas S Walter and coworkers (Rypniewski et al, 1993; Walter et al, 2006). Prior to lysine methylation all samples were purified and subsequently dialyzed against the desired methylation buffer (100 mM HEPES pH 7.5, 300 mM NaCl). The methylated samples were re-purified by size exclusion chromatography using the appropriate buffer.

3.3.12 Limited proteolysis

Limited proteolysis was employed to design stable constructs of N-terminal soluble domain of Mrs2. It is most significant for designing constructs of protein fragments that can fold autonomously and thus behaves as an individual protein domains (Fontana et al, 2004). Infect, Neurath (1980) proposed that proteolysis is anticipated at the whippy regions between different protein domains (Fontana et al, 2004; Neurath, 1980). Proteolytic reaction usually occurs at loops, which are accessible to solvents, and at flexible regions, which include disordered or denatured N- and C-termini plus uncovered loops or regions between different globular domains (Gao et al, 2005).

The N-terminal soluble domain construct of the Mrs2 (Mrs2₄₈₋₃₀₈, 2.5 mg/l), in 300 mM NaCl and 50 mM Tris-HCl pH 8.0, was incubated in presence of trypsin, chymotrypsin and protease K at different temperature 4°, 25° and 37° C. The reaction was stopped at different time intervals from 1 to 60 mints. The digested sample was run on 15 % SDS-PAGE. The band from SDS-PAGE was cut out and

dissolved in distilled water by heating gently. In-gel digestion of the protein was performed by trypsin overnight and then analyzed by MALDI MSMS.

3.3.14 Circular dichroism (CD)

CD was performed in the near UV region to gain information about the secondary and tertiary structure of the Mrs2 protein using construct Mrs2₄₈₋₂₇₆. CD measurement was performed on spectrometer instrument (Applied Photophysics PiStar-180), using quartz cell (Hella) of 1 mm path length. CD signals between 190 nm and 240 nm were measured for N-terminal soluble domain of Mrs2₄₈₋₂₇₆ in 20 mM HEPES pH 7.5, 100 mM NaCl. Data was collected at 25° C, with a wave length change of 1 nm.

3.3.15 Mrs2₄₈₋₃₀₈ soaking and co-crystallization

In order to check the magnesium or cobalt binding site within Mrs2 transporter, diffraction-quality crystals of Mrs2₄₈₋₂₇₆ were soaked in magnesium chloride, magnesium nitrate, or cobalt chloride solution of different molarities. The cryo-solution was prepared by increasing the ethylene glycol to 30 % (v/v) and 56 mM sodium/potassium phosphate pH 6.3. The concentration of magnesium and cobalt salt used ranged from 1 mM to 100 mM (final concentration) and different soaking times from 30 sec to one week.

The co-crystallization was done by adding 1 to 5 mM of magnesium salt to protein sample (2.8 mg/ml), incubated at 4° C for 30 min, and then centrifuged at 20,000 rpm, for 20 min at 4° C. The magnesium incubated sample was immediately submitted to crystallization trials.

MANUSCRIPT 1

Crystallization and preliminary X-ray diffraction analysis of the N-terminal domain of Mrs2, a magnesium ion transporter from yeast inner mitochondrial membrane

**Muhammad Bashir Khan, Björn Sjöblom, Rudolf J. Schweyen
and Kristina Djinović-Carugo**

Crystallization and preliminary X-ray diffraction analysis of the N-terminal domain of Mrs2, a magnesium ion transporter from yeast inner mitochondrial membrane

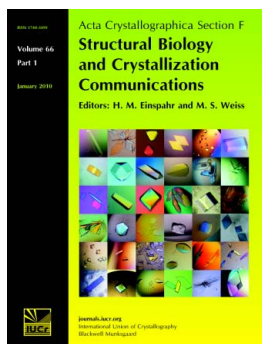
Muhammad Bashir Khan, Björn Sjöblom, Rudolf J. Schweyen and Kristina Djinović-Carugo

Acta Cryst. (2010). **F66**, 658–661

Copyright © International Union of Crystallography

Author(s) of this paper may load this reprint on their own web site or institutional repository provided that this cover page is retained. Reproduction of this article or its storage in electronic databases other than as specified above is not permitted without prior permission in writing from the IUCr.

For further information see <http://journals.iucr.org/services/authorrights.html>



Acta Crystallographica Section F: Structural Biology and Crystallization Communications is a rapid all-electronic journal, which provides a home for short communications on the crystallization and structure of biological macromolecules. It includes four categories of publication: protein structure communications; nucleic acid structure communications; structural genomics communications; and crystallization communications. Structures determined through structural genomics initiatives or from iterative studies such as those used in the pharmaceutical industry are particularly welcomed. *Section F* is essential for all those interested in structural biology including molecular biologists, biochemists, crystallization specialists, structural biologists, biophysicists, pharmacologists and other life scientists.

Crystallography Journals **Online** is available from journals.iucr.org

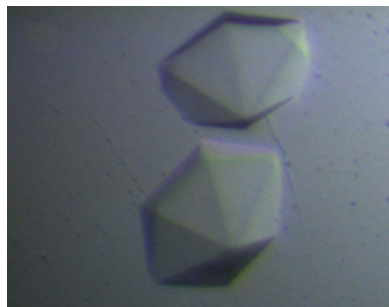
Muhammad Bashir Khan,^a Björn Sjöblom,^a Rudolf J. Schweyen^{b†} and Kristina Djinović-Carugo^{a,c*}

^aDepartment for Structural and Computational Biology, Max F. Perutz Laboratories, University of Vienna, Vienna, Austria, ^bDepartment of Microbiology, Immunobiology and Genetics, Max F. Perutz Laboratories, University of Vienna, Vienna, Austria, and ^cDepartment of Biochemistry, Faculty of Chemistry and Chemical Technology, University of Ljubljana, Ljubljana, Slovenia

† Deceased February 2009.

Correspondence e-mail:
kristina.djinovic@univie.ac.at

Received 18 February 2010
Accepted 31 March 2010



© 2010 International Union of Crystallography
All rights reserved

Crystallization and preliminary X-ray diffraction analysis of the N-terminal domain of Mrs2, a magnesium ion transporter from yeast inner mitochondrial membrane

Mrs2 transporters are distantly related to the major bacterial Mg²⁺ transporter CorA and to Alr1, which is found in the plasma membranes of lower eukaryotes. Common features of all Mrs2 proteins are the presence of an N-terminal soluble domain followed by two adjacent transmembrane helices (TM1 and TM2) near the C-terminus and of the highly conserved F/Y-G-M-N sequence motif at the end of TM1. The inner mitochondrial domain of the Mrs2 from *Saccharomyces cerevisiae* was overexpressed, purified and crystallized in two different crystal forms corresponding to an orthorhombic and a hexagonal space group. The crystals diffracted X-rays to 1.83 and 4.16 Å resolution, respectively. Matthews volume calculations suggested the presence of one molecule per asymmetric unit in the orthorhombic crystal form and of five or six molecules per asymmetric unit in the hexagonal crystal form. The phase problem was solved for the orthorhombic form by a single-wavelength anomalous dispersion experiment exploiting the sulfur anomalous signal.

1. Introduction

Mg²⁺ is the most abundant divalent cation in cells and organelles (Diwan, 1987). It plays important roles in stabilizing macromolecules and in binding to nucleotides and acts as a cofactor of many enzymes. By regulating the activities of ion channels and transporters, Mg²⁺ also influences cell volume and signalling processes (Ikari *et al.*, 2008; Mobasher *et al.*, 1998).

Mrs2 transporters form the major mitochondrial Mg²⁺-uptake system in yeast, plants and mammals (Zsurka *et al.*, 2001; Kolisek *et al.*, 2003; Li *et al.*, 2001; Schock *et al.*, 2000) and are essential for mitochondrial biogenesis (Walker *et al.*, 1982). Mrs2 transporters are distantly related to the major bacterial Mg²⁺ transporter CorA and to Alr1, which is located in the plasma membrane of lower eukaryotes. The amino-acid sequence identity between the N-terminal domains of CorA from *Thermotoga maritima* and Mrs2 from *Saccharomyces cerevisiae* is 11%. The members of the Alr1 subfamily appear to be restricted to lower eukaryotes, where they form the major Mg²⁺-uptake system of the plasma membrane. Expression of Alr1 is essential for the growth of yeast cells, except when kept in media with nonphysiologically high Mg²⁺ concentrations (Graschopf *et al.*, 2001). On the other hand, the cellular uptake of Mg²⁺ in mammals is mediated by proteins unrelated to the CorA–Mrs2–Alr1 superfamily that belong to the mammalian melastatin-related transient receptor potential (TRPM) family of cation channels (TRPM6 and TRPM7; Voets *et al.*, 2004; Schmitz *et al.*, 2005).

Common features of all of these proteins are the presence of two adjacent transmembrane helices (TM1 and TM2) near the C-terminus and of the highly conserved F/Y-G-M-N sequence motif at the C-terminus of TM1 (Bui *et al.*, 1999; Gardner, 2003; Knoop *et al.*, 2005; Lunin *et al.*, 2006). The N-terminus is characterized by a large cytoplasmic domain which forms a funnel and has been shown to constitute an allosteric regulatory module that can be engineered to promote an activated or closed state (Payandeh *et al.*, 2008).

Despite low amino-acid sequence identity, secondary-structure features appear to be conserved in the N-terminal and transmembrane portions of all members of the CorA–Mrs2–Alr1 superfamily (Lunin *et al.*, 2006), while they display notable differences in the

region C-terminal to TM2 (Gardner, 2003). Moreover, some of these transporters can partially replace each other, which strongly supports the notion that they are orthologues (Bui *et al.*, 1999; Lunin *et al.*, 2006; Li *et al.*, 2001; R. Schweyen, unpublished work).

Mrs2 is located in the inner mitochondrial membrane, while Alr1 is inserted into the cytoplasmic membrane. The orientation of these transporters in their cognate membranes is such that both the long sequence N-terminal to TM1 and the sequences C-terminal to TM2 are oriented towards the mitochondrial matrix and the cytoplasm in Mrs2 and Alr1, respectively. Only a short loop connecting the TM helices is oriented towards the space between the two mitochondrial membranes and outside in Mrs2 and Alr1, respectively (Baumann *et al.*, 2002; Bui *et al.*, 1999; Wachek *et al.*, 2006). In their cognate membranes yeast Mrs2 and Alr1 have been shown to form homooligomers, while the bacterial transporter CorA was found to be in a pentameric state (Kolisek *et al.*, 2003; Wachek *et al.*, 2006; Warren *et al.*, 2004; Weghuber *et al.*, 2006).

Here, we report the crystallization and X-ray diffraction analysis of the N-terminal domain of Mrs2, the Mg^{2+} transporter from yeast inner mitochondrial membrane.

2. Materials and methods

2.1. Cloning and expression

The gene encoding the mitochondrial magnesium transporter Mrs2 (YOR334W) from *S. cerevisiae* was used to amplify the mitochondrial matrix domain of Mrs2 (Mrs2_{16–276}; $M_r = 30\ 124$) by polymerase chain reaction (PCR) using *Taq* DNA polymerase with the forward primer 5'-CTTTATTTTCAGGGCGCCATGGGCAAACAGTTACTATC-GTTGAAGCCCATT-3' and the reverse primer 5'-GTGCTCGAGT-GCGGCCGCTTATAAGGAATTTCTATTTGCGTCCAATATGAT-3', which were designed based on the nucleotide sequence of the Mrs2 gene. The PCR product was digested with *Nco*I and *Not*I (the recognition sites are shown in bold in the primers used) and cloned into the vector pETM-11 (EMBL Hamburg) with a tobacco etch virus (TEV) cleavable N-terminal His₆ tag MKHHHHHHHPMSDYDIPT-TENLYFQGA. The DNA insert cloned in pETM-11 was sequenced to confirm the fidelity of DNA amplification.

The recombinant protein was overexpressed in BL-21 Star (DE3) *Escherichia coli* transformants grown in LB medium containing kanamycin (0.025 mg ml⁻¹) at 310 K with shaking at 200 rev min⁻¹; the cells were induced at an OD₆₀₀ of 0.6 with 0.5 mM isopropyl β -D-

1-thiogalactopyranoside (IPTG) and allowed to grow to a final OD₆₀₀ of 2.3 at 294 K. The cells were harvested by centrifugation (6000g, 30 min), resuspended in sonication buffer (50 mM Tris-HCl pH 8.0, 500 mM NaCl) supplemented with 1 mM phenylmethanesulfonyl-fluoride (PMSF), 5 mM β -mercaptoethanol (BME), 20 mM imidazole and 5% glycerol, and lysed by sonication.

2.2. Purification

After sonication of the cells, the crude extract was centrifuged at 50 000g for 30 min and the supernatant was loaded onto a 5 ml Ni-NTA agarose column (Qiagen) pre-equilibrated in buffer A (50 mM Tris-HCl pH 8.0, 500 mM NaCl, 1 mM PMSF, 5 mM BME, 20 mM imidazole and 5% glycerol). The column was extensively washed with buffer A containing 20 mM imidazole. The protein was eluted with a linear gradient of buffer B containing 500 mM imidazole. The N-terminal His₆ tag was cleaved using TEV (protease:protein mass ratio 1:70) for 12 h during dialysis against 50 mM Tris-HCl pH 8.0 containing 300 mM NaCl, 1 mM dithiothreitol (DTT) and 1 mM PMSF. The cleaved N-terminus and TEV were separated from the protein after TEV cleavage by again applying the reaction mixture onto the Ni-NTA column. The flowthrough was pooled and loaded onto a Resource Q column (6 ml; GE Healthcare) equilibrated with buffer A consisting of 50 mM Tris-HCl pH 8.0, 20 mM NaCl, 5 mM BME and 1 mM PMSF and the protein was eluted using a gradient of 20–1000 mM NaCl in 50 mM Tris-HCl pH 8.0, 5 mM BME and 1 mM PMSF. The protein eluted from the Resource Q column in a single peak at 280 mM NaCl. Further purification was carried out on a HiLoad 26/60 Superdex 200 (GE Healthcare) gel-filtration column in 50 mM Tris-HCl pH 8.0 and 300 mM NaCl. The protein eluted in a single peak at an elution volume of 218 ml, corresponding to a molecular weight of 30 kDa, which is compatible with the monomer of Mrs2_{16–276}. The purified protein was concentrated by reapplying it onto a Resource Q column (6 ml; GE Healthcare) as described above; it was concentrated to about 3 mg ml⁻¹ for crystallization screening. These procedures reproducibly yielded 6 mg protein from 1 l of bacterial culture.

The purity of the protein solution used in the crystallization experiments was checked by SDS-PAGE analysis and showed a single band with an apparent molecular weight of about 30 kDa (Fig. 1a).

Dynamic light scattering was used to assess the monodispersity of the protein solution: a monomodal distribution with a polydispersity of 5% was observed and the gyration radius was estimated to be 4.2 nm, suggesting that the protein solution was homogenous and monomeric. Circular-dichroism spectroscopy in the far-ultraviolet wavelength range showed that the protein was rich in α -helical content.

2.3. Crystallization

Initial screening for crystallization conditions was performed using Crystal Screens 1 and 2, PEG/Ion Screen, Index, Natrix, SaltRX, Cryo 1 and 2, JCSG, PACT and MembFac kits from Hampton Research. A nanodrop crystallization robot (Phoenix RE, Matrix Technologies) was employed for screening using the sitting-drop vapour-diffusion method at 295 K, mixing equal volumes (0.2 μ l) of protein solution (3 mg ml⁻¹ in anion-exchange buffer) and reservoir solution. Crystals of Mrs2_{16–276} were initially obtained from Cryo 1 and 2 condition No. 59, consisting of 0.1 M sodium/potassium phosphate pH 6.2, 25% (v/v) 1,2-propanediol, 10% (v/v) glycerol, and condition No. 22, composed of 0.1 M sodium/potassium phosphate pH 6.2, 40% (v/v) ethylene glycol. For optimization of crystallization

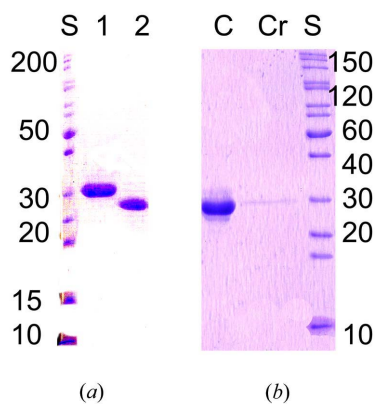


Figure 1
SDS-PAGE gels of TEV cleavage of Mrs2_{16–276} and of dissolved Mrs2_{16–276} crystals (form A). (a) Lane 1, before His₆-tag cleavage; lane 2, after His₆-tag cleavage with TEV; lane S, molecular-weight standards (kDa). (b) Lane C, control; lane Cr, dissolved crystals; lane S, molecular-weight standards (kDa).

conditions, 1 μl protein solution (3 mg ml⁻¹ in anion-exchange buffer) was mixed with 1 μl mother liquor for vapour-diffusion experiments against 0.5 ml reservoir solution. After further optimization of the crystallization conditions, the best crystals were obtained using 22% (v/v) ethylene glycol, 56 mM sodium/potassium phosphate pH 6.3. The crystals (form *A*) appeared overnight and grew to maximum dimensions of about 0.5 \times 0.2 \times 0.2 mm within 2–3 d (Fig. 2*a*). Small crystals of Mrs2_{16–276} (form *B*) were also obtained in the presence of 1.7 M NaCl, 70 mM imidazole pH 7.8 at 295 K (Fig. 2*b*). However, these crystals did not diffract to high resolution.

The crystals (form *A*) were dissolved in deionized water at room temperature. SDS–PAGE was performed on 12.5% polyacrylamide. The protein bands of dissolved crystals were identified by comparing their mobility with those of protein standard molecular-weight markers and purified Mrs2_{16–276} (Fig. 1*b*).

2.4. X-ray diffraction

All Mrs2_{16–276} X-ray diffraction data sets were collected at 100 K in a cold nitrogen stream using either an in-house Bruker Microstar

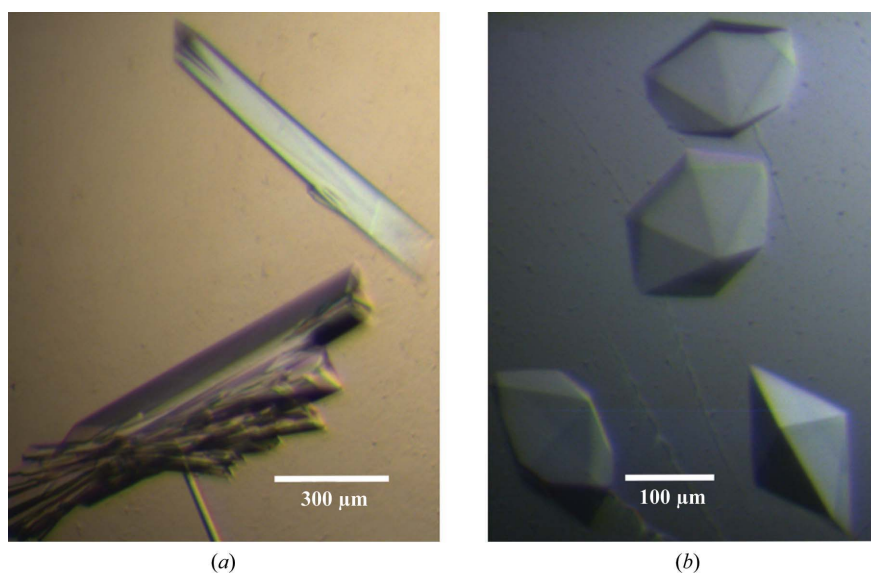


Figure 2
The two different forms of Mrs2_{16–276} crystals. (*a*) Crystals of Mrs2_{16–276} grown in 22% (v/v) ethylene glycol, 56 mM sodium/potassium phosphate pH 6.3 (form *A*). (*b*) Crystals of Mrs2_{16–276} grown in 1.7 M NaCl, 70 mM imidazole pH 7.8 (form *B*).

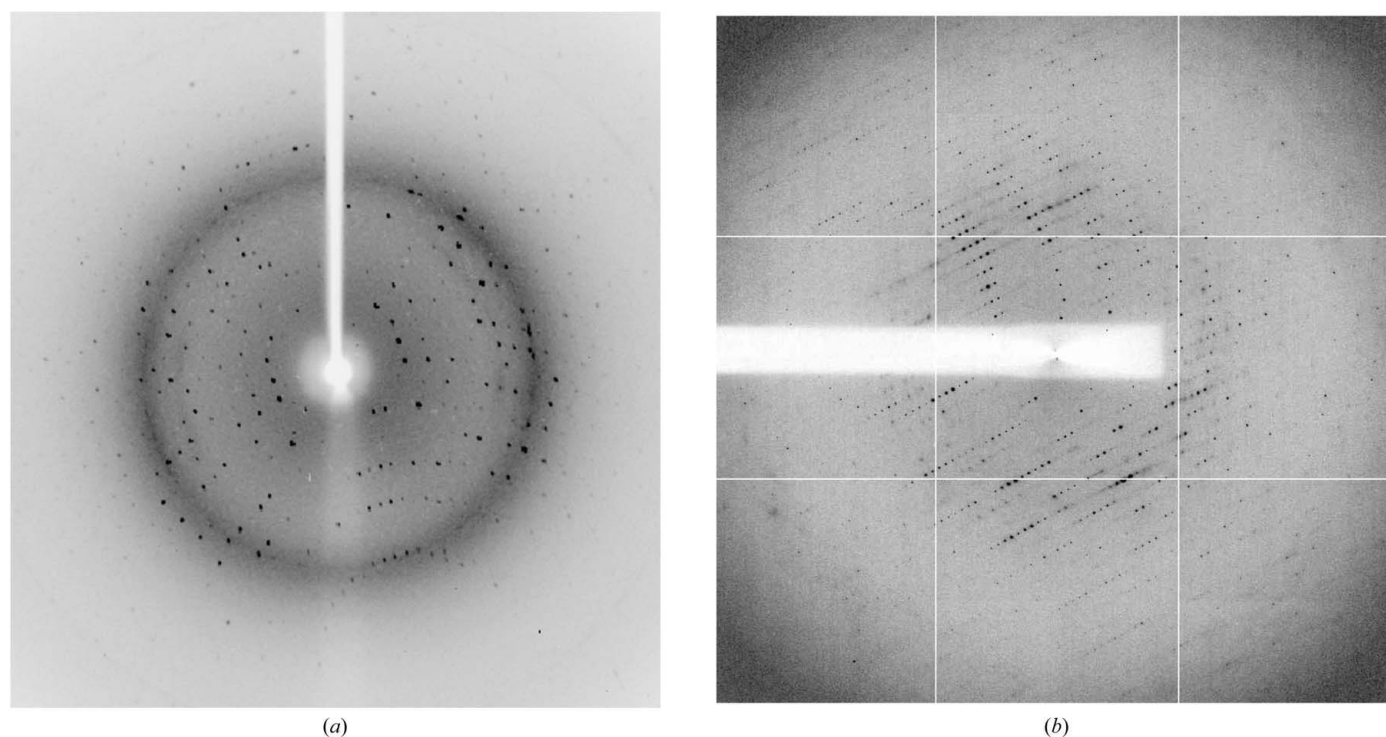


Figure 3
Diffraction patterns of Mrs2_{16–276} crystals. (*a*) Diffraction pattern of form *A* Mrs2_{16–276} crystals. The resolution is ~ 1.8 Å at the edge. (*b*) Diffraction pattern of form *B* Mrs2_{16–276} crystals. The resolution is ~ 3.4 Å at the edge.

Table 1

Data-collection statistics for the N-terminal domain of Mrs2.

Values in parentheses are for the outermost resolution shell. No $\sigma(I)$ cutoff was used in the data-integration process.

	Form A (home source)	Form B (ESRF ID14-1)
Wavelength (Å)	1.54178	0.933
Temperature (K)	100	100
Space group	$P2_12_12_1$	$P6_422$ or $P6_222$
Unit-cell parameters (Å, °)	$a = 54.66, b = 67.70,$ $c = 85.30,$ $\alpha = \beta = \gamma = 90$	$a = b = 230.00, c = 114.47,$ $\alpha = \beta = 90, \gamma = 120$
Resolution (Å)	36.89–1.83 (1.90–1.83)	50–3.60 (4.25–4.16)
Measured reflections	3977702	365747
Unique reflections	48844	25957
Completeness (%)	99 (92)	96 (90)
Redundancy	80 (13)	27 (28)
Anomalous completeness (%)	92.5 (83.0)	N/A
No. of subunits in asymmetric unit	1	5 or 6
Phasing power	0.311 (0.069)	N/A
Figure of merit (centric/acentric)	0.08586/0.21770	N/A
$R_{\text{p.i.m.}}^\dagger$ (%)	0.80 (23.0)	N/A
$R_{\text{merge}}^\ddagger$ (%)	8.5 (88.4)	9.6 (65.9)
R_{meas}^\S (%)	N/A	9.8 (67.0)
$\langle I/\sigma(I) \rangle$	40.2 (1.9)	31.7 (6.5)

$^\dagger R_{\text{p.i.m.}} = \sum_{hkl} [1/(N-1)]^{1/2} \sum_i |I_i(hkl) - \langle I(hkl) \rangle| / \sum_{hkl} \sum_i I_i(hkl)$, where $I_i(hkl)$ and $\langle I(hkl) \rangle$ are the i th and the mean measurements of the intensity of reflection hkl and N is the redundancy. $^\ddagger R_{\text{merge}} = \sum_{hkl} \sum_i |I_i(hkl) - \langle I(hkl) \rangle| / \sum_{hkl} \sum_i I_i(hkl)$. $^\S R_{\text{meas}} = \sum_{hkl} [N/(N-1)]^{1/2} \sum_i |I_i(hkl) - \langle I(hkl) \rangle| / \sum_{hkl} \sum_i I_i(hkl)$.

rotating-anode generator equipped with a Platinum 135 CCD detector and a 300 μm collimator or the ID14-1 beamline at ESRF equipped with an ADSC Q210 CCD detector, using a beam size of 100 \times 100 μm . Prior to cryocooling in a nitrogen stream, the form *A* crystals of Mrs2_{16–276} were transferred into a cryoprotectant solution containing 30% (v/v) ethylene glycol, 56 mM sodium/potassium phosphate pH 6.3, while the form *B* crystals were transferred into a cryoprotectant solution containing 19% glycerol, 1.7 M NaCl, 70 mM imidazole pH 7.8. The form *A* crystals of Mrs2_{16–276} diffracted to 1.83 Å resolution on an in-house source (Fig. 3a) and belonged to space group $P2_12_12_1$ (unit-cell parameters $a = 54.66, b = 67.70, c = 85.30$ Å), with the asymmetric unit containing one molecule. This is consistent with a Matthews coefficient of 2.32 Å³ Da⁻¹ and a solvent content of 47.0%. The form *B* crystals of Mrs2_{16–276} diffracted to 4.16 Å resolution at ESRF (Fig. 3b) and belonged to space group $P6_222$ or $P6_422$ (unit-cell parameters $a = b = 230.00, c = 114.47$ Å), with the asymmetric unit being likely to contain five or six molecules, corresponding to a Matthews coefficient of 2.84 Å³ Da⁻¹ and a solvent content of 56.7%.

The data-collection statistics are summarized in Table 1. Crystallographic data collected in-house were processed (integrated and scaled) with the *PROTEUM2* software suite (Bruker AXS Inc.), while the synchrotron data sets were processed using *XDS* (Kabsch, 2010).

2.5. Solution of the phase problem

The structure could not be solved by molecular replacement using the known CorA structure as a search model (Lunin *et al.*, 2006), but was instead solved by the single-wavelength anomalous dispersion method (SAD) using the Mrs2 native S atoms for phasing. A highly redundant (average multiplicity of 80) data set with high anomalous completeness (92.5%; 83.0% in the outermost shell) was obtained from a form *A* crystal using the in-house X-ray source with a 1.54 Å

wavelength (Table 1). The diffraction data were cut to 2.5 Å resolution to determine the sulfur substructure using *SHELXD* (Sheldrick, 2008). All 11 S-atom sites were found, corresponding to the five cysteine and six methionine residues present in the protein. Subsequent heavy-atom refinement and density modification was performed using *autoSHARP* (Vonnrhein *et al.*, 2007). The sulfur SAD phases obtained from *autoSHARP* produced an electron-density map which was traced using *ARP/wARP* (Morris *et al.*, 2003; Joosten *et al.*, 2008) and automatically fitted 243 of the 261 amino-acid residues in three different chains (R_{work} and R_{free} of 0.21 and 0.30, respectively) into the density. Structure determination is currently in progress using the diffraction data extending to 1.83 Å resolution.

We acknowledge the ESRF, Grenoble for provision of synchrotron radiation. MBK is the recipient of a PhD fellowship from FWF (P20141). This work was partially supported by WWTF (LS05021) and the University of Vienna.

References

- Baumann, F., Neupert, W. & Herrmann, J. M. (2002). *J. Biol. Chem.* **277**, 21405–21413.
- Bui, D. M., Gregan, J., Jarosch, E., Ragnini, A. & Schweyen, R. J. (1999). *J. Biol. Chem.* **274**, 20438–20443.
- Diwan, J. J. (1987). *Biochim. Biophys. Acta*, **895**, 155–165.
- Gardner, R. C. (2003). *Curr. Opin. Plant Biol.* **6**, 263–267.
- Graschopf, A., Stadler, J. A., Hoellerer, M. K., Eder, S., Sieghardt, M., Kohlwein, S. D. & Schweyen, R. J. (2001). *J. Biol. Chem.* **276**, 16216–16222.
- Ikari, A., Okude, C., Sawada, H., Yamazaki, Y., Sugatani, J. & Miwa, M. (2008). *Biochem. Biophys. Res. Commun.* **369**, 1129–1133.
- Joosten, K., Cohen, S. X., Emsley, P., Mooij, W., Lamzin, V. S. & Perrakis, A. (2008). *Acta Cryst. D* **64**, 416–424.
- Kabsch, V. (2010). *Acta Cryst. D* **66**, 125–132.
- Knoop, V., Groth-Maloney, M., Gebert, M., Eifler, K. & Weyand, K. (2005). *Mol. Genet. Genomics*, **274**, 205–216.
- Kolisek, M., Zsurka, G., Samaj, J., Weghuber, J., Schweyen, R. J. & Schweigel, M. (2003). *EMBO J.* **22**, 1235–1244.
- Li, L., Tutone, A. F., Drummond, R. S., Gardner, R. C. & Luan, S. (2001). *Plant Cell*, **13**, 2761–2775.
- Lunin, V. V., Dobrovetsky, E., Khutoreskaya, G., Zhang, R., Joachimiak, A., Doyle, D. A., Bochkarev, A., Maguire, M. E., Edwards, A. M. & Koth, C. M. (2006). *Nature (London)*, **440**, 833–837.
- Mobasheri, A., Mobasheri, R., Francis, M. J., Trujillo, E., Alvarez de la Rosa, D. & Martin-Vasallo, P. (1998). *Histol. Histopathol.* **13**, 893–910.
- Morris, R. J., Perrakis, A. & Lamzin, V. S. (2003). *Methods Enzymol.* **374**, 229–244.
- Payandeh, J., Li, C., Ramjeesingh, M., Poduch, E., Bear, C. E. & Pai, E. F. (2008). *J. Biol. Chem.* **283**, 11721–11733.
- Schmitz, C., Dorovkov, M. V., Zhao, X., Davenport, B. J., Ryazanov, A. G. & Perraud, A. L. (2005). *J. Biol. Chem.* **280**, 37763–37771.
- Schock, I., Gregan, J., Steinhäuser, S., Schweyen, R., Brennicke, A. & Knoop, V. (2000). *Plant J.* **24**, 489–501.
- Sheldrick, G. M. (2008). *Acta Cryst. A* **64**, 112–122.
- Voets, T., Nilius, B., Hoefs, S., van der Kemp, A. W., Droogmans, G., Bindels, R. J. & Hoenderop, J. G. (2004). *J. Biol. Chem.* **279**, 19–25.
- Vonnrhein, C., Blanc, E., Roversi, P. & Bricogne, G. (2007). *Methods Mol. Biol.* **364**, 215–230.
- Wachek, M., Aichinger, M. C., Stadler, J. A., Schweyen, R. J. & Graschopf, A. (2006). *FEBS J.* **273**, 4236–4249.
- Walker, G. M., Birch Andersen, A., Hamburger, K. & Kramhoft, B. (1982). *Carlsberg Res. Commun.* **47**, 205–214.
- Warren, M. A., Kucharski, L. M., Veenstra, A., Shi, L., Grulich, P. F. & Maguire, M. E. (2004). *J. Bacteriol.* **186**, 4605–4612.
- Weghuber, J., Dieterich, F., Froschauer, E. M., Svidova, S. & Schweyen, R. J. (2006). *FEBS J.* **273**, 1198–1209.
- Zsurka, G., Gregan, J. & Schweyen, R. J. (2001). *Genomics*, **72**, 158–168.

MANUSCRIPT 2

Structural and Functional Characterization of the N-Terminal
Moiety of Yeast Mg^{2+} Transporter Mrs2

Muhammad Bashir Khan, Gerhard Sponder, Björn Sjöblom,
Soňa Svidová, Rudolf J. Schweyen, Oliviero Carugo, Kristina
Djinović-Carugo

To be submitted to *PNAS*.

Structural and Functional Characterization of the N-Terminal Moiety of Yeast Mg²⁺ Transporter Mrs2

Muhammad Bashir Khan¹, Gerhard Sponder², Björn Sjöblom¹, Soňa Svidová², Rudolf J. Schweyen^{2†}, Oliviero Carugo³, and Kristina Djinović-Carugo^{1,4,*}

¹Department for Structural and Computational Biology, Max F. Perutz Laboratories, University of Vienna, Vienna, Austria

²Department of Microbiology, Immunobiology and Genetics, Max F. Perutz Laboratories, University of Vienna, Vienna, Austria

³Department of Chemistry, University of Pavia, Pavia, Italy

⁴Department of Biochemistry, Faculty of Chemistry and Chemical Technology, University of Ljubljana, Ljubljana, Slovenia

*Correspondence e-mail: kristina.djinovic@univie.ac.at

† Deceased in February 2009

ABSTRACT

Eukaryotic Mrs2 transporters are distantly related to the major bacterial Mg²⁺ transporter CorA and the eukaryotic Alr1, located in the plasma membranes of lower eukaryotes. All Mrs2 proteins are functional pentamers composed of large soluble N-terminal domains and 2 adjacent transmembrane helices, followed by a variable C-terminal region. Here we report a functional and structural analysis of the N-terminal domain of Mrs2 from the inner mitochondrial membrane of *Saccharomyces cerevisiae* by crystallography, genetics, biochemistry and fluorescence. By analytical gel filtration and dynamic light scattering, the N-terminal domain of Mrs2 forms a homopentamer in low-salt solutions. Structural analysis showed that the fold of the N-terminal domain bears differences compared with the prokaryotic CorA counterpart, and suggested residues that form hydrophobic gates and the putative magnesium sensing site. Functional analysis of the candidate gating mutants in isolated mitochondria confirmed the involvement of the identified amino acids in gating. We further functionally examined the exceptionally long C-terminus of *S. cerevisiae* Mrs2, in particular, a positively charged stretch in the C-terminal region concerning its function in the transporter regulation.

Keywords: amino-terminal domain / crystallography / eukaryotic magnesium transporter / hydrophobic gates / Mrs2

INTRODUCTION

Magnesium ion, Mg^{2+} , is essential for many biochemical processes and remains the only major biological ion whose mechanism of transport is still not fully understood. It is present at 15–25 mM in prokaryotic and mammalian cells (Ikari et al, 2008; Lunin et al, 2006; Mobasheri et al, 1998). Mg^{2+} mediates the stabilization of macromolecules during binding to nucleotides and is a cofactor for many enzymes. By regulating the activities of ion channels and transporters, Mg^{2+} also influences cell volume and signalling processes (Ikari et al, 2008; Mobasheri et al, 1998). In the cytosol, the majority of Mg^{2+} is bound to adenosine-5'-triphosphate (ATP) and other phosphonucleotides. In all cells, Mg^{2+} is an essential structural element for ribosomes and membranes. In prokaryotes, Mg^{2+} is an important regulatory signal that is essential for virulence (Eshaghi et al, 2006; Garcia Vescovi et al, 1996; Lunin et al, 2006; Papp-Wallace et al, 2008).

Balancing Mg^{2+} levels is vital for normal cellular function. Homeostasis is maintained by a delicate balance of transport activities across the plasma and organelle membranes. The CorA family mediates Mg^{2+} uptake in most prokaryotes and is the most extensively studied set of magnesium transporters. 3 crystal structures (at 2.9, 3.7, and 3.9 Å resolution) (Eshaghi et al, 2006; Lunin et al, 2006; Payandeh & Pai, 2006) of *Thermatoga maritima* CorA (Tm-CorA) and the structure of the soluble cytoplasmic domain of the *Vibrio parahaemolyticus* zinc transporter ZntB (Vp-ZntB) (at 1.9 Å resolution) have revealed homopentameric assemblies (Tan et al, 2009). Full-length Tm-CorA has 2 transmembrane α -helices (TM1, TM2) per monomer and a large intracellular N-terminal moiety.

Conversely, the structures of the cytoplasmic domain of Tm-CorA (1.85 Å) (Lunin et al, 2006) and *Archaeoglobus fulgidus* CorA (Af-CorA) (2.9 Å) show dimeric arrangement of the CorA subunits, which might be attributed to crystal packing effects (Payandeh & Pai, 2006).

Mrs2 transporters constitute the major mitochondrial Mg^{2+} uptake system in yeast, plants, and mammals (Kolisek et al, 2003; Li et al, 2001; Schock et al, 2000; Zsurka et al, 2001) and are essential for mitochondrial biogenesis (Walker et al, 1982). Human mitochondrial Mrs2 promotes multidrug resistance in gastric cancer cells by regulating p27, cyclin D1 expression, and cytochrome C release (Tiao et al, 2009). Mrs2 transporters are distantly related to the major bacterial Mg^{2+} transport system CorA. The amino acid sequence identity and similarity between the N-terminal domains of Tm-CorA and *Saccharomyces cerevisiae* Mrs2 are 11% and 40%, respectively, compared with 15% and 31%, respectively, for the entire sequences.

Mrs2 transporters are also related to the Alr1 subfamily, which is restricted to lower eukaryotes where it forms the principal Mg^{2+} uptake system in the plasma membrane. Alr1 is essential for the growth of yeast cells, except if cultured in media with non-physiological, high Mg^{2+} concentrations (Kolisek et al, 2003). Some of these transporters can partially functionally replace each other, which strongly suggests that they are homologues (Bui et al, 1999; Kehres & Maguire, 2002; Li et al, 2001; Zsurka et al, 2001).

The CorA, Mrs2, and Alr1 families harbour 2 adjacent transmembrane helices (TM1, TM2) at the C-terminus and a highly conserved G-M-N motif at the end of TM1. The N-terminus of Tm-CorA has a large cytoplasmic domain that forms a funnel in the functional pentamer. Two divalent cation sensing (DCS) sites that regulate the opening and closing of the transporter have been mapped to the N-terminal domain of CorA (Eshaghi et al, 2006; Lunin et al, 2006; Payandeh et al, 2008; Payandeh & Pai, 2006).

Despite the low sequence identity between members of the CorA-Mrs2-Alr1 superfamily, the structures of their N-terminal domains and transmembrane regions are partially conserved. In contrast, based on their sequences, the C-

terminal regions that follow TM2 are expected to differ significantly. Although the sequences of the CorA-Mrs2-Alr1 superfamily are extremely divergent, they appear to exploit the membrane potential in driving Mg^{2+} uptake (Froschauer et al, 2004; Kolisek et al, 2003).

The cation selectivity of CorA and Mrs2 is attributed to their signature motifs (CorA: YGMNFxxMPEL, Mrs2: xGMNxxxFIEE) (Kehres et al, 1998; Worlock & Smith, 2002), as also suggested for the ZntB zinc transporter family (GxxG[I,V]NxGGxP) (Tan et al, 2009). The motif lies at the end of the TM1 α -helix at the outer surface of the membrane, and it tends to be disordered in crystal structures (Lunin et al, 2006; Payandeh & Pai, 2006). It has been recently reported by Yu Xia et al. that Tm-CorA preferentially transports Co^{2+} and not Mg^{2+} (Xia et al, 2011).

Mg^{2+} gating mechanisms through the transmembrane region were proposed based on Tm-CorA structures. Together with the successive negatively charged loop, the G-M-N motif has been implicated in the binding and dehydration of magnesium hexaaqua ions (Eshaghi et al, 2006; Lunin et al, 2006; Payandeh & Pai, 2006). Residue Asn314 of the G-M-N motif at the external entrance to the pore and a pair of hydrophobic rings that are formed by Met291 and Leu294 were hypothesized to be involved the gating of the channel (Lunin et al, 2006).

Mechanisms by which the conductance of the bacterial transporter Tm-CorA is regulated has been proposed (Eshaghi et al, 2006; Lunin et al, 2006; Payandeh et al, 2008; Payandeh & Pai, 2006). In the absence of sufficient intracellular Mg^{2+} levels, Mg^{2+} ions that are bound between monomers are released, and the N-terminal domains of the protomers move as a rigid body, whereas the willow helices (2 antiparallel helices at the N-terminus) rearrange with respect to each other and relative to the stalk helix (the pore-forming helix). These actions create a torque along the stalk helix. The torque propagates to the

hydrophobic gates (Met291 and Leu294) and possibly activates the periplasmic gate residue Asn314 through interaction of the cytoplasmic N-terminus (acidic residues) and the positively charged C-terminal basic sphincter. This activation impinges on the Asn314 residue through movement of TM2 and the MPEL motif (in the loop that connects TM1 and TM2), allowing Mg^{2+} ion to flow through (Lunin et al, 2006; Payandeh et al, 2008).

Many genes that encode proteins that mediate Mg^{2+} transport have been reported in plants, bacteria, and animals (Gardner, 2003). Nevertheless, there are limited data on their biological and physiological functions, structures, and capabilities and mechanisms of Mg^{2+} transport. The low sequence homology between eukaryotic Mrs2 transporters and the prokaryotic magnesium transporter Tm-CorA, or any other protein with a known structure, renders it difficult to predict structure and function of Mrs2 accurately.

Here, we report the crystal structure of the N-terminal domain of the yeast (*Saccharomyces cerevisiae*) mitochondrial magnesium transporter Mrs2 at 1.28 Å resolution and characterize selected residues that are critical for magnesium transport. This structure can be used to study regulatory metal sites, conformational changes during regulation and transport, and the residues that mediate the formation of hydrophobic gates and to evaluate the hallmarks of this transporter family.

RESULTS AND DISCUSSION

Ionic strength modulates oligomeric state of Mrs2₄₈₋₃₀₈

Based on our study (Khan et al, 2010), we designed a stable Mrs2 construct (48–308), denoted Mrs2₄₈₋₃₀₈ (this construct was termed Mrs2₁₆₋₂₇₆ in our previous publication, wherein the mitochondrial targeting sequence was not included in the numbering), which included the entire soluble, N-terminal matrix domain of Mrs2. The optimal buffers conditions were found by using Thermofluor-based essay

(Supplementary Figure 5). By analytical size exclusion chromatography, Mrs2₄₈₋₃₀₈ behaves as a monomer in high-ionic-strength buffers and as a homopentamer in low-ionic-strength buffers (Supplementary Figure 1). The circular dichroism (CD) spectrum of Mrs2₄₈₋₃₀₈ showed minima at 208 and 219 nm, typical for a protein that is rich in α -helices (Supplementary Figure 2).

Dynamic light scattering (DLS) was used to assess the monodispersity of the protein in solution: a monomodal distribution with a polydispersity of 5% was observed, and the gyration radius was estimated to be 4.2 nm in high-ionic-strength buffers. Under low-ionic-strength conditions, the protein solution exhibited polydispersity of about 25% and a radius of gyration of 14 nm, which are consistent with the analytical size exclusion chromatography findings. These data suggest that our construct is autonomously folded into the native conformation in solution and that the protein solution is monomeric at high ionic strengths and pentameric at low ionic strengths.

Overall structure of Mrs2₄₈₋₃₀₈ versus those of prokaryotic magnesium and zinc transporters

A monomer of Mrs2₄₈₋₃₀₈ was crystallized in the orthorhombic space group P2₁2₁2₁, and its structure was solved by experimental phasing, exploiting the anomalous signals of sulphur (Khan et al, 2010). The overall organizations of prokaryotic (Tm-CorA) and eukaryotic (Mrs2₄₈₋₃₀₈) magnesium transporters are thus similar (Figure 1C and D). Each subunit can be divided into an N-terminal alpha/beta domain that is followed by an alpha domain. Whereas the former is a compact alpha-beta-alpha sandwich, the latter contains a triple coiled-coil, the end of which enters the membrane with a TM helix (Figure 1C).

Although the coiled-coil domains in Tm-CorA and Mrs2₄₈₋₃₀₈ are nearly identical, the N-terminal domains differ (Figure 1C and D). The central beta sheet is formed by 7 strands in Tm-CorA versus 6 strands in Mrs2₄₈₋₃₀₈. Whereas the last 4 strands (termed C1–C4 in the Figure 1D) are topologically identical in both

proteins and form a series of 3 beta hairpins, the first 2 beta strands differ topologically. The alpha helix that follows the N2 strand, and the entire N3 strand are missing in Mrs2₄₈₋₃₀₈, rendering the eukaryotic protein smaller than its prokaryotic counterpart. Although this disparity appears to have arisen due to deletion during molecular evolution, we cannot reject other hypotheses. However, it is clear that any structural alignments of these structural moieties will be misleading, because Tm-CorA and Mrs2 adopt different folds.

The relatively long $\alpha 5$ and $\alpha 6$ helices, which extend toward the membrane, are called 'willow' helices in Tm-CorA, "as they hang down like the branches of a weeping willow tree" and harbor many glutamic and aspartic acid residues in the tip region (Lunin et al, 2006). For Mrs2₄₈₋₃₀₈, $\alpha 5$ and $\alpha 6$, corresponding to the willow helices of Tm-CorA, contain 3 acidic residues compared with 10 in Tm-CorA. In Tm-CorA, there is also an extended loop between C2 and C3 that protrudes like the willow helices toward the membrane surface. The tip of this loop in Tm-CorA has a very high density of aspartic and glutamic acid residues (Maguire, 2006). In contrast, the C2 and C3 strands of Mrs2₄₈₋₃₀₈ are shorter, and the loop that intercalates between them does not protrude toward the willow helices or harbor any acidic residues (Figure 1C and D).

To determine the structural neighbours of Mrs2₄₈₋₃₀₈, we used the web-based Dali server (Holm & Sander, 1996), which identified the following structures that had Z-scores greater than 9: (i) *Thermotoga maritima* divalent metal ion transporter Tm-CorA (PDB code 2IUB); (ii) *Vibrio parahaemolyticus* RIMD cytoplasmic domain of zinc transporter Vp-ZntB (PDB code 3CK6); (iii) *Dictyostelium discoideum* STAT protein, (PDB code 1UUS); and (iv) *Escherichia coli* Pore-forming toxins (PDB code 2WCD). The latter two hits clearly have molecular functions different from Mrs2 and CorA. All of these structures have low sequence similarity with *S. cerevisiae* Mrs2, and only the metal ion transporter Tm-CorA was identified in a BLAST search (Altschul et al, 1990) against the Mrs2 sequence.

Despite the low sequence homology Mrs2₄₈₋₃₀₈, Tm-CorA, and Vp-ZntB are structurally similar with regard to overall architecture and also perform similar functions. Nevertheless, the protomer and pentamer structures cannot be superimposed easily, because the relative orientations of the $\alpha/\beta/\alpha$ and helical subdomains, as well as the folds, are different. Mrs2₄₈₋₃₀₈ and the soluble domain of Tm-CorA (PDB code 2IUB) can be superimposed with an RMSD value of 2.85 Å (for C α , 179 of 256 residues aligned, with a sequence identity of 16%) (Supplementary Figure 3A). Separately, the subdomains of Mrs2₄₈₋₃₀₈, Vp-ZntB and Tm-CorA ($\alpha/\beta/\alpha$ and helical) align with different RMSD values.

The $\alpha/\beta/\alpha$ subdomains of Mrs2₄₈₋₃₀₈ and Tm-CorA can be superimposed over the C α atoms with an RMSD value of 2.96 Å (for C α , 69 of 117 residues aligned, with a sequence identity of 8%) (Supplementary Figure 3C). Similarly, the corresponding helical subdomains can be aligned with an RMSD value of 2.62 Å (for C α , 112 of 131 residues aligned, with a sequence identity of 13%) (Supplementary Figure 3E).

Mrs2₄₈₋₃₀₈ and Vp-ZntB (PDB code 3CK6) can be superimposed with an RMSD value of 2.61 Å (for C α , 158 of 237 residues aligned, with a sequence identity of 14%) (Supplementary Figure 3B). Conversely, the $\alpha/\beta/\alpha$ subdomains of Mrs2₄₈₋₃₀₈ and Vp-ZntB can be superimposed with an RMSD value of 2.75 Å (for C α , 57 of 116 residues aligned, with a sequence identity of 5%) (Supplementary Figure 3D), and the helical subdomains can be aligned with an RMSD value of 2.22 Å (for C α , of 110 of 121 residues aligned, with a sequence identity of 8%) (Supplementary Figure 3F). These changes in orientation between the 2 sub-domains may be due to different levels of funnel opening in the 3 different ion transporters.

The soluble domains of Tm-CorA (PDB code 2IUB) and Vp-ZntB (PDB code 3CK6) can be superimposed with an RMSD value of 1.89 Å (for C α , 199 of

237 residues aligned, with a sequence identity of 19%). Separately, the soluble domains $\alpha/\beta/\alpha$ aligned with an RMSD of 1.93 Å (for C α , 92 of 116 residues aligned, with a sequence identity of 9%), whereas the helical domain was superimposed with an RMSD value of 1.71 Å (for C α , 112 of 121 residues aligned, with a sequence identity of 19%).

These data clearly demonstrate that the prokaryotic proteins Tm-CorA and Vp-TntB are structurally more similar to each other than to the eukaryotic protein Mrs2₄₈₋₃₀₈. Vp-ZntB also contains a mixed 7-stranded beta-sheet that is clearly similar to that of Tm-CorA but differs from the 6-stranded sheet of Mrs2₄₈₋₃₀₈. Moreover, we hypothesize that the structural variability between the 3 proteins is related to the different states (open/closed) of the ion channel/transporter, which are reflected in the reorientation of the coiled-coil moiety (see below) and influenced by cation concentrations.

A structure-based sequence alignment (SBSA) (manually corrected) between Mrs2₄₈₋₃₀₈ and Tm-CorA together with the analysis of the Mrs2 pentamer model identified important residues involved in the formation of hydrophobic gates and in propagation of magnesium across the ion conduction pathway in Mrs2-type transporters (Figure 1B).

Model of Mrs2₄₈₋₃₀₈ funnel

To generate a model of the pentameric funnel from the monomeric Mrs2₄₈₋₃₀₈ structure, we superimposed Mrs2₄₈₋₃₀₈ onto the helical domains of Tm-CorA and Vp-ZntB. The maximum diameter of the funnel, based on Tm-CorA, is 106 Å, and the residues at the C-terminus of the stalk helix (forming the wall of the funnel) clash at the tips (Figure 2C and D). This phenomenon might be attributed to the structure of Tm-CorA, which has been reported in a closed conformation, whereas monomeric Mrs2₄₈₋₃₀₈ is more relaxed and might reflect an open conformation of the transporter.

In a functional pentamer, each protomer makes contacts with 2 adjacent molecules. Our structural analysis of the Mrs2₄₈₋₃₀₈ funnel model, based on the Tm-CorA structure, shows 5 hydrogen bonding interactions and 1 salt bridge. The residues involved in the formation of the salt bridge are Glu295 of one protomer and Lys291 of an adjacent protomer. These interacting residues belong to the α 7 stalk helix of a subunit, the α 7 stalk helix of the adjacent subunit, and the tip of the α 5 and α 6 willow helices.

Conversely, the funnel model that is based on Vp-ZntB has a maximum diameter of 102 Å and reveals no clash of the C-termini - further evidence that the Vp-ZntB is likely in an open conformation. A structural analysis of the funnel model of Mrs2₄₈₋₃₀₈ shows that the interface between the α 7 stalk helix of a protomer and the α 5 and α 6 willow helices of an adjacent protomer, comprises 2 hydrogen bonds and 1 salt bridge. The residues involved in the formation of the salt bridge are Lys221 of a protomer and Glu205 of an adjacent protomer.

In contrast, there are 8 hydrogen bonds and 8 salt bridges in the funnel domain of the Vp-ZntB (PDB code 3CK6) transporter and 16 hydrogen bonds and 15 salt bridges in Tm-CorA (PDB code 2BBJ). Although the stereochemistry of the interface of the Mrs2₄₈₋₃₀₈ funnel was not optimized, the presence of remarkably fewer hydrogen bonds and salt bridges compared with Tm-CorA and Vp-ZntB might explain the higher sensitivity of Mrs2₄₈₋₃₀₈ to elevated salt concentrations.

An analysis of the electrostatic surface potential of the structure of Mrs2₄₈₋₃₀₈ showed that the α 7 helices, forming the inner wall of the pentameric funnel, are lined along their lengths with negatively charged or hydroxyl-bearing residues (Figure 2A and B). Such an arrangement exists in other monovalent cation (KcsA) and divalent cation (CorA, ZntB) channels and were proposed to constitute an electrostatic sink that increases local ion concentrations (Roux & MacKinnon, 1999).

Putative magnesium-sensing sites in Mrs2

Two divalent cation binding sites have been identified at the protomer-protomer interface in the funnel of Tm-CorA (Eshaghi et al, 2006; Lunin et al, 2006; Payandeh et al, 2008; Payandeh & Pai, 2006) - termed “divalent cation sensor” (DCS) sites. Whereas the first binds cations directly through the 2 carboxylates of Asp89 and Asp253, the second, comprising Glu88, Asp175, Asp253, and His257, binds them indirectly by coordinating hydrated metal cations. According to a model of the regulation of Tm-CorA, a torque is generated at the bottom of the stalk helix ($\alpha 7$) by releasing bound magnesium from magnesium-binding sites and propagates toward the hydrophobic gate (Eshaghi et al, 2006; Lunin et al, 2006; Payandeh et al, 2008; Payandeh & Pai, 2006).

Based on a structural comparison between Tm-CorA and our model of the Mrs2₄₈₋₃₀₈ funnel, we identified the candidate amino acid residues that could form a DCS site in Mrs2 that corresponds to DSC1 of Tm-CorA: Asp97 from one subunit and Glu270 from an adjacent subunit (Figure 2C and D, Figure 4D). By sequence alignment of eukaryotic Mrs2 homologues, Asp97 and Glu270 are highly conserved throughout the entire family, and equivalent residues exist in the prokaryotic CorA family (Figure 1B). In Mrs2₄₈₋₃₀₈, Glu270 lies in the N-terminus of $\alpha 7$, corresponding to Asp253 in Tm-CorA (Figure 4A and C); Asp97 is located in the $\alpha 3$ helix, corresponding to Asp89 of Tm-CorA (Figure 4A and B). In this structural analysis, we could not confidently identify the residues that constitute the second DCS site.

In the initial crystallization conditions no magnesium was present, but we obtained crystals with 1.5 mM magnesium chloride and 1.5 mM cobalt chloride. Native crystals were soaked in the presence of magnesium chloride, cobalt and nickel chloride and structurally analyzed. The structures of Mrs2₄₈₋₃₀₈ in magnesium, cobalt, and nickel-soaked crystals and magnesium and cobalt co-crystals did not reveal bound metal ions and were essentially identical to the

native crystal structure in the absence of exogenous divalent cations. The addition of magnesium in the crystal environment did not change the structure of the native protein. The absence of cations bound to the monomeric Mrs2₄₈₋₃₀₈ is in agreement with the notion that the DCSs are composed of ligands from adjacent subunits in the pentamer implying that a single subunit cannot bind divalent ions with high affinity.

Effect of metal ions on protease susceptibility of pentameric Mrs2₄₈₋₃₀₈

Payandeh et al. showed that cations in the protomer interface stabilize Tm-CorA but are not required to maintain its pentameric state (Payandeh & Pai, 2006). Furthermore, they demonstrated that Tm-CorA becomes resistant to trypsin in a divalent cation-dependent manner, wherein the presence of ions renders the conformation trypsin-resistant, presumably reflecting the closed state of the channel. To determine whether Mrs2₄₈₋₃₀₈ undergoes conformational changes in function of divalent cations, we performed the protease susceptibility assay in the presence and absence of magnesium and cobalt ions.

Prior to this experiment, Mrs2₄₈₋₃₀₈ was dialyzed against a low-ionic-strength buffer to induce the formation of functional pentamers and incubated with various concentrations of magnesium, cobalt, EDTA and trypsin. In the presence of EDTA, the protein was protected from protease digestion. Conversely, only high concentrations of cobalt rendered Mrs2₄₈₋₃₀₈ less susceptible to trypsin cleavage, whereas the presence of magnesium did not, irrespective of incubation time (Fig. 3). The reactions were performed at 4°C and 37°C for 4 and 15 hours.

These results demonstrate that Mrs2 adopts 2 distinct conformations in a magnesium-dependent manner, wherein the closed conformation (in the presence of magnesium) appears to be more susceptible to protease cleavage compared with the open conformation (in the presence of EDTA). This differential

susceptibility compared with Tm-CorA implicates distinct conformations and distinct conformational changes in the N-terminal domains of the 2 types of transporters. Differences between the folds of the 2 domains might explain the varying responses and patterns with regard to protease susceptibility.

Hydrophobic gates in Mrs2

In Tm-CorA Met291 and Leu294 form the main hydrophobic gate by creating a strong energetic barrier to ion permeation (Lunin et al, 2006; Svidova et al, 2010). The gate residues in Tm-CorA are positioned at the membrane/cytoplasmic interface, with Met291 being cytoplasmic and Leu294 membrane embedded (Lunin et al, 2006).

Because no 3-dimensional structure of full-length Mrs2 is available, we generated the Mrs2 pentamer, including the transmembrane helices, starting from the funnel model and extended the sequence in the alignment and in the model (by homology modelling) to the C-terminal TM1 and TM2 α -helices. Inspection of sequence alignment (Figure 1B) showed that eukaryotic magnesium transporters consistently display a three amino acid insertion after position corresponding to Met291 in prokaryotic transporters, extending in this way the helix α 7.

In searching for gating residues in Mrs2 corresponding to Met291 and Leu294 in Tm-CorA, we imposed 2 criteria: (i) involvement in formation of a constriction in the pore; (ii) mitochondrial matrix location for the first gating residue and membrane embedded location for the second position.

By analysis of the pentameric Mrs2 model, the narrowest constriction of the pore lay at residue Met309 (Figure 4F), corresponding to the hydrophobic gate residue Met291 in Tm-CorA (Figure 4E). By TMpred analysis (Online server Prediction of Transmembrane Regions and Orientation http://www.ch.embnet.org/software/TMPRED_form.html) of the primary sequence

of *S. cerevisiae* Mrs2, the first transmembrane helix comprises residues Val315 to Leu336, while Met309 is predicted to be located in the matrix. Further, by sequence alignment of members of the eukaryotic Mrs2 family, Met309 is highly conserved (Figure 1B), and we named it Gate 1.

The second narrowest opening, which we termed Gate 2, occurred at Val315, corresponding to Leu294 in Tm-CorA (Figure 4E and F). TMpred analysis predicts Val315 to be in a transmembrane helix. Sequence alignment of eukaryotic Mrs2 homologues revealed that Val315 is less conserved than Met309, with the bulkier phenylalanine and smaller valine present in some sequences (Figure 1B).

Functional analysis of selected mutants

To validate the function of the candidate residues that were identified in our structural analysis to be involved in magnesium sensing and the formation of hydrophobic gates, we performed a functional and mutational analysis of these residues. Further, we examined the role of positively charged residues at the C-terminus in transport activity and regulation of Mrs2.

DCS mutants

According to our structural analysis, Asp89 and Asp253, which form the primary cation-sensing site in Tm-CorA, in Mrs2 correspond to Asp97 and Glu270 in Mrs2. In Tm-Cor, mutations in the first DCS site alter the transport of Mg²⁺ by Tm-CorA (Payandeh et al, 2008).

To assay the function of Asp97 in the regulation of the transporter, we performed site-directed mutagenesis, changing Asp97 to Ala, Phe, and Trp. We intentionally did not choose a positively charged mutation, because Payandeh et al reported that salt bridge across the first DCS site can partially maintain TmCorA in a closed or inactive conformation (Payandeh et al, 2008). The resulting mutants expressed in *S. cerevisiae*, did not exhibit notable growth

defects on non-fermentable carbon sources (Figure 5A). Accordingly, no significant differences in Mg^{2+} uptake between wild-type Mrs2 and the mutant proteins in isolated mitochondria were observed (Figure 5B).

Based on the high conservation of Asp97 throughout the Mrs2 subfamily, the lack of effect is noteworthy and implies that the sensing of magnesium, which is exerted by several residues in the two DCS sites cannot be abrogated by a mutation of a single residue in Mrs2. Large hydrophobic residues at the Asp97 location were predicted to disrupt metal binding as well as to perturb domain closure or packing within the funnel. The weak effect of bulky amino acid residue on growth on non-fermentable carbon sources may be explained by local structural rearrangements, allowing for the conformational changes upon transporter closure.

Gating mutants

The candidate Gate 1 and 2 residues (Met309 and Val315) were mutated to 3 amino acids with disparate properties with regard to size and charge - the small glycine, the negatively charged glutamic acid, and the bulky phenylalanine. The effects of these mutations were monitored by growth complementation assays and using mag-fura-2 measurements of Mg^{2+} influx into mitochondria.

Deletion of *MRS2* causes a growth defect on non-fermentable carbon sources and abolishes Mg^{2+} influx into mitochondria (Kolisek et al, 2003; Wiesenberger et al, 1992). Strain DBY747 *mrs2* Δ was transformed with the high-copy number vector YEp351 or with the centromeric plasmid YCp22, harbouring the mutated *MRS2* variants, and as controls, the wild-type *MRS2* and the empty vector. In growth tests, all 3 mutations at Met309 location impaired growth on non-fermentable carbon sources, indicating that they had a considerable effect on magnesium homeostasis in mitochondria. The Met309Gly mutant had the most dramatic effect (Figure 6A, B).

The greatest decrease in magnesium uptake was observed in the Met309Phe variant (Figure 6B), which is attributed to its bulky side chain, narrowing the pore at this position. The Met309Gly mutant effected the highest degree of dysregulation with regard to the gating of the channel. The exchange of Met309 for Gly resulted in a considerably stronger influx compared with the wild-type protein and significantly elevated the final steady-state magnesium concentrations (Figure 6B). Particularly strong uptake was observed after the initial addition of magnesium, and plateau levels were less pronounced compared with the wild-type control (Figure 6B). The transporter was able to close the ion conduction pathway to a limited extent (Figure 6B), suggesting that in the Met309Gly mutant, the pore is wide and cannot close properly due to the absence of the glycine side chain. An effect similar to that of Met309Gly mutant was observed for Met309Glu, which displayed higher final steady-state magnesium levels compared with wild-type (Figure 6B). This effect was most likely caused by its charge, in the pentamer forming a negatively charged ring that could elicit more robust transport due to increased electrostatic attraction of the magnesium ion.

Substitution of Gate 2 residue Val315 to Glu and Phe had no significant effects on growth on non-fermentable carbon sources (Figure 7A). Consistent with this result, Mg^{2+} uptake was less affected by mutations compared with Gate 1 mutants at position 309. Mg^{2+} uptake by the Glu mutant was comparable with that of wild-type Mrs2. The bulky Phe residue was well tolerated and did not impair ion conduction to such an extent that led to a substantial reductions in magnesium uptake (Figure 7B). This is not surprising, as this residue is found at position 315 also in some naturally occurring sequences, suggesting that a bulkier residue can be accommodated at this location (Figure 1B). As expected, the Val315Gly mutation reduced growth (Figure 7A), which was though less pronounced than in the Met309Gly mutant (Figure 6A). Based on the mag-fura-2 measurements, this effect was caused by greater magnesium uptake due to a widening of the channel at this position (Figure 7B).

Taken together the above observations confirm the residue Met309 as Gate 1, equivalent to Met291 in Tm-CorA, but leave some uncertainty as to Val315 residue being Gate 2. The less pronounced constriction together with natural amino acid variability at this location may be the basis for good tolerance of the mutations. Nevertheless, it needs to be kept in mind that the homology models have their limitations, in particular, when it comes to accommodation of insertions or deletions. Based on the amino acid sequence alignment (Figure 1B) highly conserved Leu313 could be an alternative candidate for Gate 2, although it is not positioned inside the pore in the homology model.

Function of the Mrs2 C-terminus

Tm-CorA has a highly conserved, positively charged sequence at the C-terminus, comprising a series of lysine residues, termed the basic sphincter. It lies in the cytoplasmic neck at the hydrophobic gate of the pore and was proposed to be important for transporter function (Lunin et al, 2006). The basic sphincter was proposed to draw negative charges away from the middle of the pore, preventing passage of the charged Mg^{2+} cations (Eshaghi et al, 2006; Lunin et al, 2006; Weghuber et al, 2006). The combination of the positive potential field of the ring of lysine residues in the basic sphincter and the hydrophobic barrier of the gate creates a formidable impediment to the passage of positively charged Mg^{2+} ions in the closed state. In the open state, the negatively charged willow helices pull the positive charge of the basic sphincter away from the central axis of the pore, allowing the passage of magnesium (Eshaghi et al, 2006; Lunin et al, 2006; Payandeh & Pai, 2006).

Members of the Mrs2 subfamily have C-termini that vary in length, nearly absent of conserved primary sequence motifs. The only conserved feature is a surplus of positively charged residues (Supplementary Table 1). On average, 20% of residues in the C-terminus of the Mrs2 family have a positive charge, which may collectively have the same function as the basic sphincter in Tm-

CorA. A C-terminal moiety of Mrs2 directly following TM2 contains a segment that has characteristics of an amphipathic helix that might function as an internal targeting signal that mediates an N_{in} - C_{in} topology (Baumann et al, 2002).

Yeast Mrs2 has a 107-amino-acid-long C-terminal sequence and a positively charged KRRRK stretch (402–406) that is not conserved in the Mrs2 family. This positively charged sequence was deleted in a previous study, reducing Mg^{2+} uptake when expressed from a low-copy vector. In contrast, overexpression of this mutant nearly restored Mg^{2+} uptake to wild-type levels (Weghuber et al, 2006). To obtain greater insight into the function of the KRRRK stretch, we reversed the charge of this sequence by introducing negatively charged Glu residues at these positions. The resulting mutant permitted good growth on non-fermentable carbon sources, expressed from the centromeric plasmid YCp22 or when overexpressed (Figure 8A). Mg^{2+} uptake capacity was moderately increased in this mutant.

To further investigate the function of the C-terminus, we removed the C-terminal region of Mrs2 after residue Thr376. Notably, truncation of the entire C-terminus impeded the growth of cells on non-fermentable carbon sources (Figure 8A), consistent with the strong reduction in Mg^{2+} transport, based on mag-fura-2 measurements in isolated mitochondria (Figure 8B).

Taken together, the small nonconserved positively charged stretch (KRRRK, 402-406) does not appear to be critical for Mrs2 function. These findings imply that the introduction of a highly negatively charged cluster that encloses the ion conduction pathway generates a more active transporter without impairing its regulation (Figure 8B). Conversely, complete truncation of the C-terminus (deletion of 94 residues at the C-terminus), impairs transport, suggesting that the electrostatic potential that results from the overall surplus of positively charged residues in the C-terminus of Mrs2 has a similar function as the basic sphincter in Tm-CorA.

Conclusions

This study provides the first molecular view of the N-terminal moiety of a eukaryotic magnesium transporter, Mrs2 from *S. cerevisiae*. Together with structure-based mutagenesis and functional analysis *in vivo*, the study provides insight into gating and regulation of Mrs2. The study identified candidate residues implicated in divalent cation binding, residues involved in formation of the hydrophobic gate, and showed that the entire C-terminal region acts as the basic sphincter. Our observations suggest a higher degree of regulation of the Mrs2 transporter compared with CorA; ie, the high inside negative membrane potential of mitochondria attracts the positively charged Mg^{2+} ion and requires fine and stringent control of transport at more than one site of the ion conduction pathway to ensure normal mitochondrial function.

MATERIALS AND METHODS

Preparation of Protein

Details on cloning and purification were reported earlier (Khan et al, 2010). The mitochondrial matrix domain of *Saccharomyces cerevisiae* was cloned from genomic DNA into pETM-11 vector (EMBL Hamburg) with a tobacco etch virus (TEV) cleavable N-terminal His₆-tag. The recombinant protein was over expressed in BL-21 star (DE3) at 21 °C, in the presence of 0.025 mg/ml of kanamycin and induced by 0.5 mM isopropyl β-D-thiogalactopyranoside (IPTG). Cells were sonicated in a suitable buffer. The supernatant after centrifugation was applied onto a 5 ml Ni-NTA agarose column (Qiagen). The N-terminal His₆-tag was cleaved using TEV. After the TEV cleavage, the protein was reapplied on a Ni-NTA column, followed by Resource Q column, and HiLoad 26/60 Superdex 200 (GE Healthcare) size exclusion chromatography.

Protein purity and monodispersity controls

The purity of the protein solution used for the crystallization experiments was evaluated by SDS-PAGE analysis and showed a single band of apparent

molecular weight of about 30 kDa. Dynamic light scattering (DLS) was used to assess the monodispersity of the protein solution: a monomodal distribution with a polydispersity of 5% was observed and the gyration radius was estimated to be 4.2 nm, suggesting that the protein solution was homogenous and monomeric. Circular dichroism (CD) spectroscopy in the far ultraviolet wavelength range showed that the protein is rich in alpha helical content.

Analytical gel filtration chromatography

Analytical gel filtration chromatography on Mrs2₄₈₋₃₀₈ was performed at 4 °C, using the construct eluted as a monomer from Superdex 200 10/300 column (Amersham Biosciences), after dialyzing the protein against low ionic salt and run on an analytical gel filtration 200 10/300 column in 15 mM Tris-HCl (pH 8.0), 15mM NaCl. The protein eluted as a pentamer.

Crystallization

Details on crystallization conditions were reported earlier (Khan et al, 2010). Initial crystallization screening conditions obtained from the sparse matrix screen from MembFac kits and Hampton Research were optimized by hanging drop at 22 °C. Magnesium and cobalt-soaked crystals were obtained by soaking the native crystal with 1-5 mM magnesium chloride and 5 mM cobalt chloride in the crystallization drops. Co-crystals with magnesium or cobalt were grown by vapor diffusion at 22 °C in a solution containing 2.8 mg/ml protein, 22% v/v ethylene glycol 56 mM Na/K phosphate pH 6.3, 1.5 mM magnesium chloride, or cobalt chloride. Crystals were flash-frozen in a solution containing 30% v/v ethylene glycol 56 mM Na/K phosphate pH 6.3 and mounted on loops at 100 K prior to data collection.

Data collection, structure solution and refinement

Mrs2₄₈₋₃₀₈ X-ray diffraction data sets were collected at 100 K in a cold nitrogen stream using various beamlines at ESRF or Microstar rotating anode at 1.54 Å.

The crystals of Mrs2₄₈₋₃₀₈ diffracted to 1.83 Å resolution on an in-house source and to 1.28 Å at ESRF. Detail of the data collection, statistics and processing were reported earlier (Khan et al, 2010). Crystallographic data collected in-house were processed (integrated and scaled) with the Proteum2 software suite (Bruker AXS Inc.), while the synchrotron data sets were processed using XDS (Kabsch, 1988). The structure of Mrs2₄₈₋₃₀₈ was solved, using a highly redundant data set collected on an in-house source by the single-wavelength anomalous dispersion method (SAD) exploiting the Mrs2 native sulphur (S) atoms for phasing using SHELXD (Uson & Sheldrick, 1999). After finding the S atoms, heavy atom refinement and density modification were performed using autoSHARP (Vonrhein et al, 2007). The electron density map obtained from autoSHARP was traced by ARP/wARP (Joosten et al, 2008; Morris et al, 2003), which fitted 243 out of 261 amino acid residues in three different chains with $R_{work}/R_{free} = 0.21/0.30$. The structure refinement yielded final R_{work} and R_{free} values of 0.193 and 0.243, respectively. This model contains 258 amino-acid residues and 432 water molecules. Two complete data sets at 1.42 Å and 1.28 Å were collected at ESRF ID14-1, processed individually using XDS. The data sets were then scaled together using SCALA. The structure from S-SAD data was further refined against the merged 1.28 Å data sets using REFMAC5 and phenix. The final model contains 261 amino acid and 392 water and five ethylene glycol molecules with a R_{work} and R_{free} of 0.169 and 0.204 respectively. Details on the refinement statistics are shown in Table 1.

Miscellaneous

The SBSA were made by SHEBA (Structural Homology by Environment-Based Alignment) (Jung & Lee, 2000). For the SBSA, the structures Mrs2₄₈₋₃₀₈ and Tm-CorA were first aligned by SHEBA. The two aligned sequences were then aligned with randomly selected sequences of ten eukaryotic and ten prokaryotic magnesium channels using the profile alignment features of ClustalX2 (Larkin et al, 2007).

Manual adjustments were applied to further improve alignments. Sequence identity and conservation were determined using the Lalign web-server (Pearson, 1991) and ESPript (Gouet et al, 2003), respectively. Protein Homology/analogy Recognition Engine (phyre) (<http://www.sbg.bio.ic.ac.uk/~phyre>) was used for homology modeling of the transmembrane portion of Mrs2 (Kelley & Sternberg, 2009).

Protease susceptibility assay

For 50 ml reaction volumes, stock solutions were prepared to obtain the final concentration desired upon dilution: 39 ml of protein (2.5 mg/ml), 1 µl of trypsin (10 mg/ml; Sigma), and 10 µl of 0-100 mM of metal solution. Reaction solutions were mixed and equilibrated at 4°C for 20 min. Trypsin was then added, and reactions were incubated at 4° or 37°C for the desired times. After adding 50 ml of SDS-PAGE sample buffer, samples were boiled and run immediately on 15% SDS-PAGE gels. In order to rule out the possibility of trypsin inhibition, controls were performed on the test protein bovine serum albumin (BSA) over the full range of conditions.

Yeast strains, growth media and genetic procedures

S. cerevisiae strain DBY747 and the isogenic deletion strain *mrs2Δ* have been described previously (Bui et al, 1999; Wiesenberger et al, 1992). Yeast cells were grown in YPD (1% yeast extract, 2% peptone, 2% glucose) to stationary phase. For growth tests on solid media, yeast cells were grown in YPD over

night, washed with dH₂O and spotted in ten-fold dilutions on YPD or YPG (1% yeast extract, 2% peptone, 3% glycerol) and incubated at 28°C for 2 (YPD) or 6 days (YPG).

Plasmid constructs

The plasmid Yep351-*MRS2*-HA (Bui 1999) was used as the template in overlap extension PCR. For mutagenesis of Met309, Val315, and the putative sensing site Asp following mutagenic forward and reverse primers were used (changed nucleotides are in bold):

MRS2 M309E fw: 5'-CGCAAATAGGAATTCCTTAGAGTTGTTGGAGTTGAAAGTTACC-3'
MRS2 M309E rev: 5'-GGTAACTTTCAACTCCAACA**ACTC**TAAGGAATTCCTATTTGCG-3'
MRS2 M309F fw: 5'-CGCAAATAGGAATTCCTTATTCCTTGTGGAGTTGAAAGTTACC-3'
MRS2 M309F rev: 5'-GGTAACTTTCAACTCCAACA**GAATAAGGAATTC**CTATTTGCG-3'
MRS2 M309G fw: 5'-CGCAAATAGGAATTCCTTAGGATTGTTGGAGTTGAAAGTTACC-3'
MRS2 M309Grev: 5'-GGTAACTTTCAACTCCAACA**ATCCTAAGGAATTC**CTATTTGCG-3'

MRS2 V315E fw:
 5'-CGCAAATAGGAATTCCTTAATGTTGTTGGAGAGGAAAGTTACCATCTACACGTTGGG-3'
MRS2 V315E rev:
 5'-CCCAACGTGTAGATGGTAACTTT**CCTC**TCCAACAACATTAAGGAATTCCTATTTGCG-3'
MRS2 V315F fw:
 5'-CGCAAATAGGAATTCCTTAATGTTGTTGGATT**CG**GAAAGTTACCATCTACACGTTGGG-3'
MRS2 V315F rev:
 5'-CCCAACGTGTAGATGGTAACTTT**CGAAT**TCCAACAACATTAAGGAATTCCTATTTGCG-3'
MRS2 V315G fw:
 5'-CGCAAATAGGAATTCCTTAATGTTGTTGGAG**GG**GAAAGTTACCATCTACACGTTGGG-3'
MRS2 V315G rev:
 5'-CCCAACGTGTAGATGGTAACTTT**CCTC**TCCAACAACATTAAGGAATTCCTATTTGCG-3'

MRS2 D97A fw: 5'-CATTCCCTTTTCCCGAGAGCGCTGAGGAAAATAGATAACTCC-3'
MRS2 D79A rev: 5'-GGAGTTATCTATTTT**CCTCAGCGCTC**TCTCGGGAAAAGGGAATG-3'
MRS2 D97F fw: 5'-CATTCCCTTTTCCCGAGATTTCTGAGGAAAATAGATAACTCC-3'
MRS2 D97F rev: 5'-GGAGTTATCTATTTT**CCTCAGAAATC**TCTCGGGAAAAGGGAATG-3'
MRS2 D97 Wfw: 5'-CATTCCCTTTTCCCGAGATGGCTGAGGAAAATAGATAACTCC-3'
MRS2 D97 Wrev: 5'-GGAGTTATCTATTTT**CCTCAGCCAT**TCTCGGGAAAAGGGAATG-3'

The above mentioned mutagenic primers were used in combination with the forward primer MRS2Mcsfw: 5'-CGATTAAGTTGGGTAACGCCAGGG-3' and

the reverse primer MRS2Mcsrev: 5'-GCACGACAGGTTTCCCGACTGGAAAGC-3.

Verification of positive clones was performed by restriction analysis of the introduced EcoRI (Met309 and Val315) or Aval (Asp97) sites (underlined). All restriction sites were introduced by silent mutations. No additional mutations were found by sequencing of the complete ORF.

PCR fragments were digested with XbaI and SmaI and cloned in the vector Yep351-MRS2-HA and YCp22-MRS2-HA digested with the same enzyme combination. To create the C-terminal truncation of *MRS2*, the primer MRS2Mcsfw and the reverse primer MRS2 CutCterm rev: GCGCGCGTCGACCGGTCATCTTTGTCAC were used. The XbaI/SmaI digested PCR fragment was cloned in vector Yep351 and YCp22. For the substitution of the positive amino acid stretch by negatively charged amino acid residues in the KRRRK/E mutant the mutagenic primers MRS2 KRRRK/E fw: 5'-GCGTCTATTGCCCTGACAAATAAACTAGAAGAGGAAGAGGAATGGTGGAAGTCAACCAAGCAGCGG-3' and MRS2 KRRRK/E rev: 5'-CCGCTGCTTGTTGACTTCCACCATTCCTCTTCCTCTTCTAGTTTATTTGTCAGGCAATAGACGC-3' were used with the above mentioned primers in overlap extension PCR. Positive clones were verified by the introduced HincII restriction site (underlined).

Isolation of mitochondria and measurement of $[Mg^{2+}]_m$ by spectrofluorimetry

Isolation of mitochondria and the ratiometric determination of intramitochondrial Mg^{2+} concentrations ($[Mg^{2+}]_m$) dependent on various external concentrations ($[Mg^{2+}]_e$) were performed as reported previously (Kolisek et al, 2003).

ACKNOWLEDGMENTS

We acknowledge the ESRF, Grenoble for the provision of synchrotron radiation. MBK, GS, SS were recipients of a PhD fellowship from FWF (P20141) and from WWTF (LS05021). MBK was partially supported by the University of Vienna funds. We also acknowledge The BIN-III initiative of the Austrian GEN-AU for financial support. The coordinates of the Mrs₂₄₈₋₃₀₈ have been deposited in Protein Data Bank (PDB) under the accession code 3RKG.

CONFLICT OF INTEREST

The authors declare that they have no conflict of interest.

REFERENCES

Altschul SF, Gish W, Miller W, Myers EW, Lipman DJ (1990) Basic local alignment search tool. *J Mol Biol* **215**: 403-410

Baumann F, Neupert W, Herrmann JM (2002) Insertion of bitopic membrane proteins into the inner membrane of mitochondria involves an export step from the matrix. *J Biol Chem* **277**: 21405-21413

Bui DM, Gregan J, Jarosch E, Ragnini A, Schweyen RJ (1999) The bacterial magnesium transporter CorA can functionally substitute for its putative homologue Mrs2p in the yeast inner mitochondrial membrane. *J Biol Chem* **274**: 20438-20443

Eshaghi S, Niegowski D, Kohl A, Martinez Molina D, Lesley SA, Nordlund P (2006) Crystal structure of a divalent metal ion transporter CorA at 2.9 angstrom resolution. *Science* **313**: 354-357

Froschauer EM, Kolisek M, Dieterich F, Schweigel M, Schweyen RJ (2004) Fluorescence measurements of free [Mg²⁺] by use of mag-fura 2 in *Salmonella enterica*. *FEMS Microbiol Lett* **237**: 49-55

Garcia Vescovi E, Soncini FC, Groisman EA (1996) Mg²⁺ as an extracellular signal: environmental regulation of *Salmonella* virulence. *Cell* **84**: 165-174

Gardner RC (2003) Genes for magnesium transport. *Curr Opin Plant Biol* **6**: 263-267

Holm L, Sander C (1996) Mapping the protein universe. *Science* **273**: 595-603

Ikari A, Okude C, Sawada H, Yamazaki Y, Sugatani J, Miwa M (2008) TRPM6 expression and cell proliferation are up-regulated by phosphorylation of ERK1/2 in renal epithelial cells. *Biochem Biophys Res Commun* **369**: 1129-1133

Joosten K, Cohen SX, Emsley P, Mooij W, Lamzin VS, Perrakis A (2008) A knowledge-driven approach for crystallographic protein model completion. *Acta Crystallogr D Biol Crystallogr* **64**: 416-424

Jung J, Lee B (2000) Protein structure alignment using environmental profiles. *Protein Eng* **13**: 535-543

Kabsch W (1988) Automatic-Indexing of Rotation Diffraction Patterns. *Journal of Applied Crystallography* **21**: 67-71

Kehres DG, Lawyer CH, Maguire ME (1998) The CorA magnesium transporter gene family. *Microb Comp Genomics* **3**: 151-169

Kehres DG, Maguire ME (2002) Structure, properties and regulation of magnesium transport proteins. *Biometals* **15**: 261-270

Kelley LA, Sternberg MJ (2009) Protein structure prediction on the Web: a case study using the Phyre server. *Nat Protoc* **4**: 363-371

Khan MB, Sjoblom B, Schweyen RJ, Djinovic-Carugo K (2010) Crystallization and preliminary X-ray diffraction analysis of the N-terminal domain of Mrs2, a magnesium ion transporter from yeast inner mitochondrial membrane. *Acta Crystallogr Sect F Struct Biol Cryst Commun* **66**: 658-661

Kolisek M, Zsurka G, Samaj J, Weghuber J, Schweyen RJ, Schweigel M (2003) Mrs2p is an essential component of the major electrophoretic Mg²⁺ influx system in mitochondria. *EMBO J* **22**: 1235-1244

Larkin MA, Blackshields G, Brown NP, Chenna R, McGettigan PA, McWilliam H, Valentin F, Wallace IM, Wilm A, Lopez R, Thompson JD, Gibson TJ, Higgins DG (2007) Clustal W and Clustal X version 2.0. *Bioinformatics* **23**: 2947-2948

Li L, Tutone AF, Drummond RS, Gardner RC, Luan S (2001) A novel family of magnesium transport genes in Arabidopsis. *Plant Cell* **13**: 2761-2775

Lunin VV, Dobrovetsky E, Khutoreskaya G, Zhang R, Joachimiak A, Doyle DA, Bochkarev A, Maguire ME, Edwards AM, Koth CM (2006) Crystal structure of the CorA Mg²⁺ transporter. *Nature* **440**: 833-837

Maguire ME (2006) The structure of CorA: a Mg(2+)-selective channel. *Curr Opin Struct Biol* **16**: 432-438

Mobasher A, Mobasher R, Francis MJ, Trujillo E, Alvarez de la Rosa D, Martin-Vasallo P (1998) Ion transport in chondrocytes: membrane transporters involved in intracellular ion homeostasis and the regulation of cell volume, free [Ca²⁺] and pH. *Histol Histopathol* **13**: 893-910

Morris RJ, Perrakis A, Lamzin VS (2003) ARP/wARP and automatic interpretation of protein electron density maps. *Methods Enzymol* **374**: 229-244

Papp-Wallace KM, Nartea M, Kehres DG, Porwollik S, McClelland M, Libby SJ, Fang FC, Maguire ME (2008) The CorA Mg²⁺ channel is required for the virulence of Salmonella enterica serovar typhimurium. *J Bacteriol* **190**: 6517-6523

Payandeh J, Li C, Ramjeesingh M, Poduch E, Bear CE, Pai EF (2008) Probing structure-function relationships and gating mechanisms in the CorA Mg²⁺ transport system. *J Biol Chem* **283**: 11721-11733

Payandeh J, Pai EF (2006) A structural basis for Mg²⁺ homeostasis and the CorA translocation cycle. *EMBO J* **25**: 3762-3773

Pearson WR (1991) Searching protein sequence libraries: comparison of the sensitivity and selectivity of the Smith-Waterman and FASTA algorithms. *Genomics* **11**: 635-650

Roux B, MacKinnon R (1999) The cavity and pore helices in the KcsA K⁺ channel: electrostatic stabilization of monovalent cations. *Science* **285**: 100-102

Schock I, Gregan J, Steinhauser S, Schweyen R, Brennicke A, Knoop V (2000) A member of a novel Arabidopsis thaliana gene family of candidate Mg²⁺ ion transporters complements a yeast mitochondrial group II intron-splicing mutant. *Plant J* **24**: 489-501

Svidova S, Sponder G, Schweyen RJ, Djinić-Carugo K (2010) Functional analysis of the conserved hydrophobic gate region of the magnesium transporter CorA. *Biochim Biophys Acta* **1808**: 1587–1591

Tan K, Sather A, Robertson JL, Moy S, Roux B, Joachimiak A (2009) Structure and electrostatic property of cytoplasmic domain of ZntB transporter. *Protein Sci* **18**: 2043-2052

Tiao MM, Lin TK, Liou CW, Wang PW, Chen JB, Kuo FY, Huang CC, Chou YM, Chuang JH (2009) Early transcriptional deregulation of hepatic mitochondrial biogenesis and its consequent effects on murine cholestatic liver injury. *Apoptosis* **14**: 890-899

Uson I, Sheldrick GM (1999) Advances in direct methods for protein crystallography. *Curr Opin Struct Biol* **9**: 643-648

Vonrhein C, Blanc E, Roversi P, Bricogne G (2007) Automated structure solution with autoSHARP. *Methods Mol Biol* **364**: 215-230

Walker GM, Birch Andersen A, Hamburger K, Kramhoft B (1982) Magnesium-Induced Mitochondrial Polymorphism and Changes in Respiratory Metabolism in the Fission Yeast, Schizosaccharomyces Pombe. *Carlsberg Research Communications* **47**: 205-214

Weghuber J, Dieterich F, Froschauer EM, Svidova S, Schweyen RJ (2006) Mutational analysis of functional domains in Mrs2p, the mitochondrial Mg²⁺ channel protein of Saccharomyces cerevisiae. *FEBS J* **273**: 1198-1209

Wiesenberger G, Waldherr M, Schweyen RJ (1992) The nuclear gene MRS2 is essential for the excision of group II introns from yeast mitochondrial transcripts in vivo. *J Biol Chem* **267**: 6963-6969

Worlock AJ, Smith RL (2002) ZntB is a novel Zn²⁺ transporter in *Salmonella enterica* serovar Typhimurium. *J Bacteriol* **184**: 4369-4373

Xia Y, Lundback A-K, Sahaf N, Nordlund G, Brzezinski P, Eshaghi S (2011) Co²⁺ selectivity of *Thermotoga maritima* CorA and its inability to regulate Mg²⁺ homeostasis present a new class of CorA proteins. *Journal of Biological Chemistry*

Zsurka G, Gregan J, Schweyen RJ (2001) The human mitochondrial Mrs2 protein functionally substitutes for its yeast homologue, a candidate magnesium transporter. *Genomics* **72**: 158-168

FIGURE LEGENDS

Figure 1 Structure-based sequence alignment of Mrs2₄₈₋₃₀₈ and its closest structural homologue Tm-CorA. (A) A schematic view of the domain structure of Mrs2 (B) Structure-based sequence alignment of Mrs2₄₈₋₃₀₈ and Tm-CorA (PDB code [2IUUB](#)). The first two sequences belonging to the structures of Mrs2₄₈₋₃₀₈ and Tm-CorA are followed by ten sequences of eukaryotic Mrs2 and ten sequences of prokaryotic CorA transporters from different species. Identical residues between Mrs2 and Tm-CorA transporters are in red. The gaps due to residues omitted from the sequence alignment are represented by two solid black lines. The sequences of the two phyla are separated by horizontal black solid line. The sequence identity between the prokaryotic species used in the alignment is about 53% while between eukaryotic species is about 52%. The conserved signature sequence GMN is boxed. Residues of the putative magnesium binding site in eukaryotes, i.e. Asp97 and Glu270, are boxed and are denoted by + and × symbols. The prokaryotic magnesium binding site formed by Asp89 and Asp253 is boxed and denoted by = and # symbols in the sequence alignment. The residue involved in the formation of an Asp ring is boxed and represented by * symbol. The residues involved in the hydrophobic gate formation, i.e. Met309, Val315 in case of Mrs2 transporter and Met291, Leu294 in case of Tm-CorA transporter are boxed and are denoted by G1 and G2 in the sequence alignment (representing Gate 1 and Gate 2), respectively. The secondary structure derived from Mrs2₄₈₋₃₀₈ is shown above the sequence. The residues embedded in the first transmembrane (TM1) are represented by black solid (C) The structures of the soluble moiety of Tm-CorA and Mrs2 contain a C-terminal triple coiled-coil (magenta), which continues into the membrane (not shown), and an N-terminal alpha/beta/alpha domain (green). (D) The N-terminal domains of Tm-CorA and Mrs2₄₈₋₃₀₈ are different. While the last four beta strands (C1-C4, yellow) are topologically identical, there are three N-terminal beta strands in Tm-CorA and two in Mrs2 (N1 and N2, magenta) and three in Tm-

CorA (N1-N3, magenta). The helix, which is intercalated between the second and the third strand, of Tm-CorA is missing in Mrs2₄₈₋₃₀₈.

Figure 2 Structural features of Mrs2₄₈₋₃₀₈ and the proposed funnel model. (A) Mrs2₄₈₋₃₀₈ is represented as ribbon and the side chains of the negatively charged or hydroxyl bearing residues of helix α 7, making the inner side of the pore, are represented as stick. (B) Electrostatic surface potential analysis of Mrs2, generated by APBS. Views are from the helix forming the inner wall of the funnel (*red*, negatively charged; *blue*, positively charged; *white*, uncharged). The red arrow shows the gradual increase of negative charge from top to bottom (C) Side view of the pentamer funnel model of the inner soluble domain of Mrs2 based on Tm-CorA from *Thermotoga maritima*. (D) Bottom view of the pentamer funnel model, highlighting the putative magnesium binding site (red). All structural figures were created with Pymol (<http://www.pymol.org/>).

Figure 3 Protease susceptibility assay. Trypsin susceptibility of Mrs2₄₈₋₃₀₈ after 4 h (right) and 15 h (left). Reactions were performed as described in Experimental Procedures. Control samples (C) for the different experimental conditions and the molecular weight ladder (S) are shown. The different tested conditions in the protease susceptibility assay are: (1) 20 mM EDTA, (2) 5 mM EDTA, (3) 5 mM Mg²⁺ (or 5 mM Co²⁺), (4) 20 mM Mg²⁺ (or 20 mM Co²⁺).

Figure 4 Putative magnesium binding site in Mrs2₄₈₋₃₀₈ and the hydrophobic gate residues in Mrs2 and Tm-CorA. (A) Superposition of Mrs2₄₈₋₃₀₈ (blue) and Tm-CorA (cyan) soluble domains showing the magnesium binding site of Tm-CorA and the putative magnesium binding site of Mrs2₄₈₋₃₀₈. The colored boxes (panels B and C) show the residues involved in magnesium sensing. (B) The magnesium binding residue Asp89 of Tm-CorA and the corresponding putative magnesium binding residue Asp97 of Mrs2₄₈₋₃₀₈. (C) The magnesium binding residue Asp253 of Tm-CorA and the corresponding putative magnesium binding residue Glu270 of Mrs2₄₈₋₃₀₈. (D) Putative magnesium binding pocket featuring

Asp97 from one monomer (blue) and Glu270 from an adjacent subunit (cyan) in a proposed functional funnel model. (E) Top view of CorA (PDB code 2IUB) showing the hydrophobic gate residues Met291 and Leu294 (red). (F) Top view of the model of Mrs2 transporter showing the putative hydrophobic Gate 1 residues Met309 and Gate 2 residues Val315 (red).

Figure 5 Mutation of Asp97 of a putative Mg²⁺ binding site in Mrs2 does not influence the regulation of the transporter. (A) Growth phenotypes of *Saccharomyces cerevisiae* strain DBY747 *mrs2Δ* expressing *MRS2* variants harbouring mutations in the D97 site from high-copy number vector YEp351 or low copy vector YCp22. Serial dilutions of yeast cultures were spotted on fermentable (YPD) or non-fermentable (YPG) plates and incubated at 28°C for 3 or 6 days, respectively. (B) [Mg²⁺]_e-dependent changes in [Mg²⁺]_m in DBY 747 *mrs2Δ* mitochondria expressing *MRS2* or the mutant variants were determined. Representative curve traces of four individual measurements are shown.

Figure 6 Mutations in the hydrophobic Gate 1 (M309) of Mrs2 impairs growth on non-fermentable carbon sources and alters the transport activity of the channel. (A) Growth phenotypes of *Saccharomyces cerevisiae* strain DBY747 *mrs2Δ* expressing wild-type *MRS2* and the corresponding *MRS2* mutant variants from high-copy number vector YEp351 or low copy vector YCp22. Serial dilutions of the different strains were spotted on fermentable (YPD) and non-fermentable (YPG) substrates and grown for three or six days, respectively. (B) [Mg²⁺]_e-dependent changes in [Mg²⁺]_m in mitochondria of *mrs2Δ* cells, and cells expressing WT *MRS2* or the mutant variants. Isolated mitochondria were loaded with the Mg²⁺-sensitive dye mag-fura-2 and changes in the intramitochondrial free Mg²⁺ concentration upon addition of Mg²⁺ to the nominally Mg²⁺-free buffer, as indicated in the figure, were determined. Representative recordings of four individual measurements are shown.

Figure 7 Characterization of mutants in the hydrophobic gate 2 of Mrs2. (A) Serial dilutions of DBY747 WT and DBY747 *mrs2* Δ cells transformed with the vectors Yep351 and YCp22 expressing *MRS2* or different mutant variants for V315 were spotted on fermentable (YPD) or non-fermentable (YPG) plates and incubated at 28°C for 3 or 6 days, respectively. (B) $[Mg^{2+}]_e$ -dependent changes in $[Mg^{2+}]_m$ in mitochondria of DBY 747 *mrs2* Δ cells expressing WT *MRS2* or mutant variants of V315. Representative curve traces of three individual measurements are shown.

Figure 8 Characterization of the Mrs2 C-terminus. (A) Phenotypes associated with charge reversion of the KRRRK stretch and truncation of the C-terminus after Thr376. Serial dilutions of yeast cultures were spotted on fermentable (YPD) or non-fermentable (YPG) plates and incubated at 28°C for 3 or 6 days, respectively. (B) $[Mg^{2+}]_e$ -dependent changes in $[Mg^{2+}]_m$ in DBY 747 *mrs2* Δ mitochondria expressing the KRRRK/E mutant or the *MRS2* variant with a C-terminal truncation. Representative curve traces of four individual measurements are shown.

Figure 1 Structure-based sequence alignment of Mrs2₄₈₋₃₀₈ and its closest structural homologue Tm-CorA.

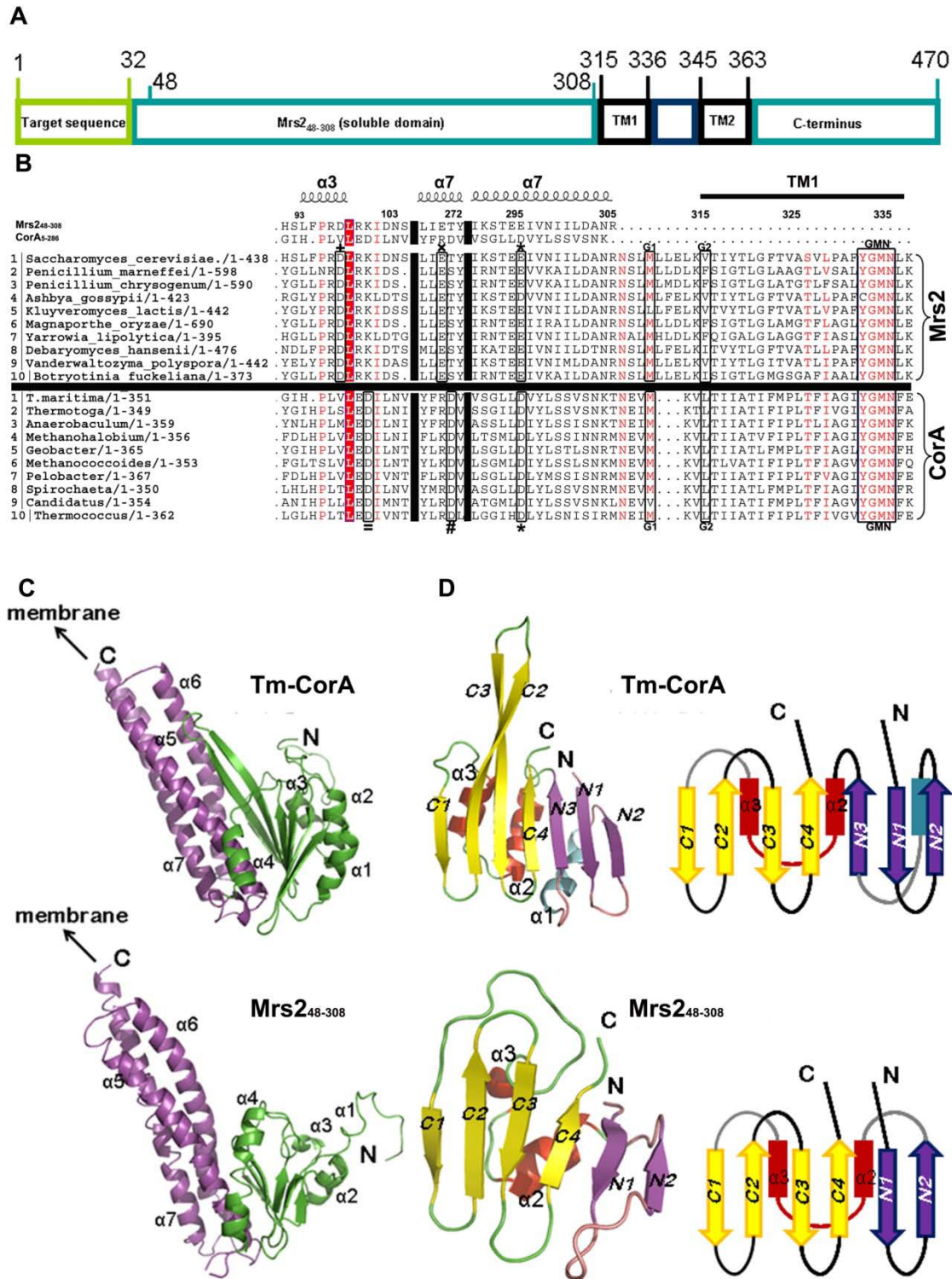


Figure 2 Structural features and proposed funnel model.

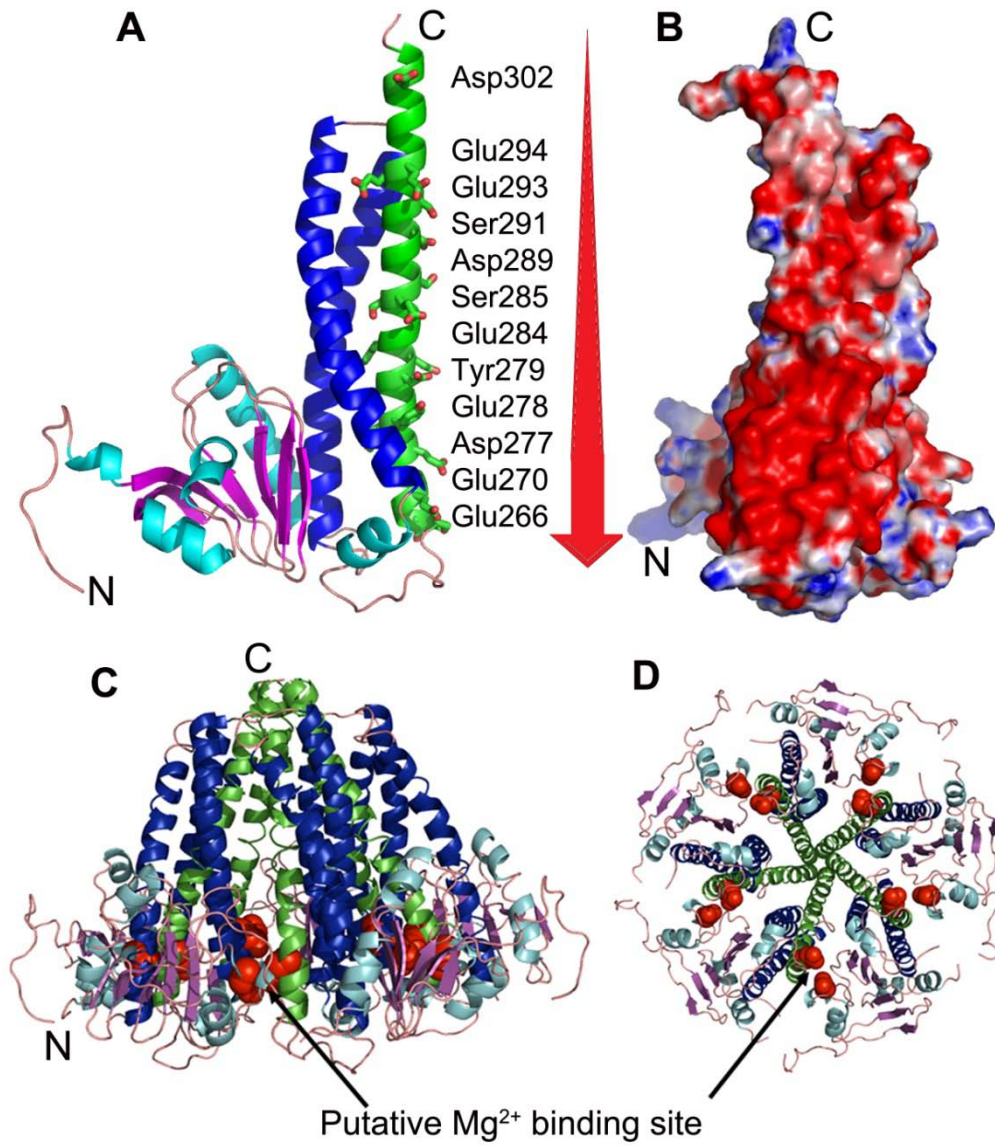


Figure 3 Protease susceptibility assay.

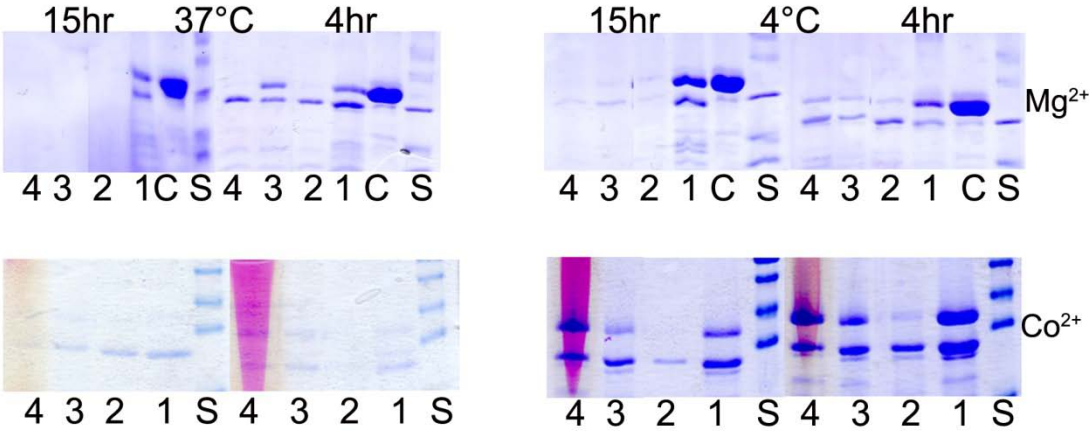


Figure 4 Magnesium binding site in Mrs2₄₈₋₃₀₈ and hydrophobic gate residues in Mrs2 and Tm-CorA.

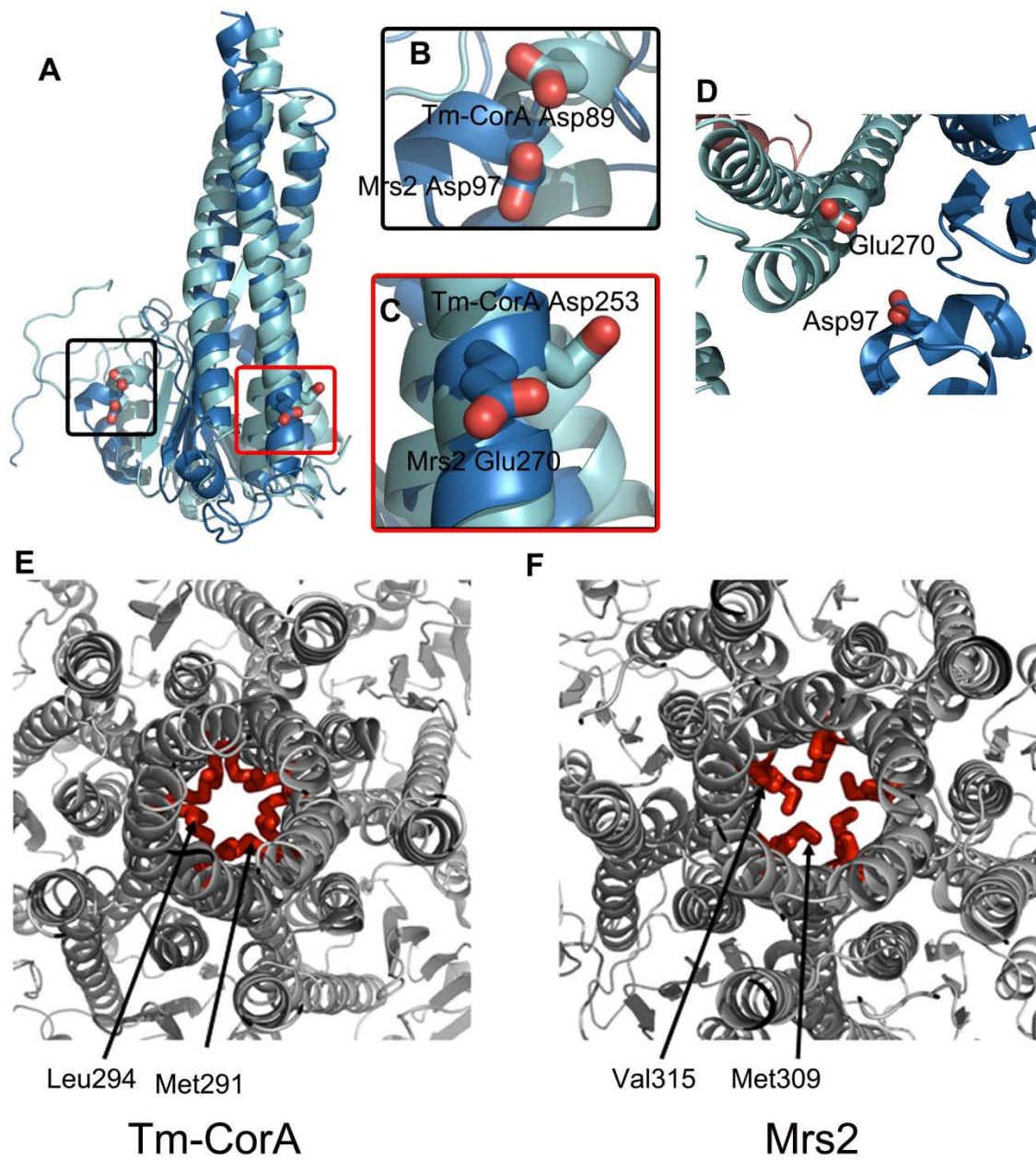


Figure 5 Mutation of Asp97 in putative Mg²⁺ binding site in Mrs2.

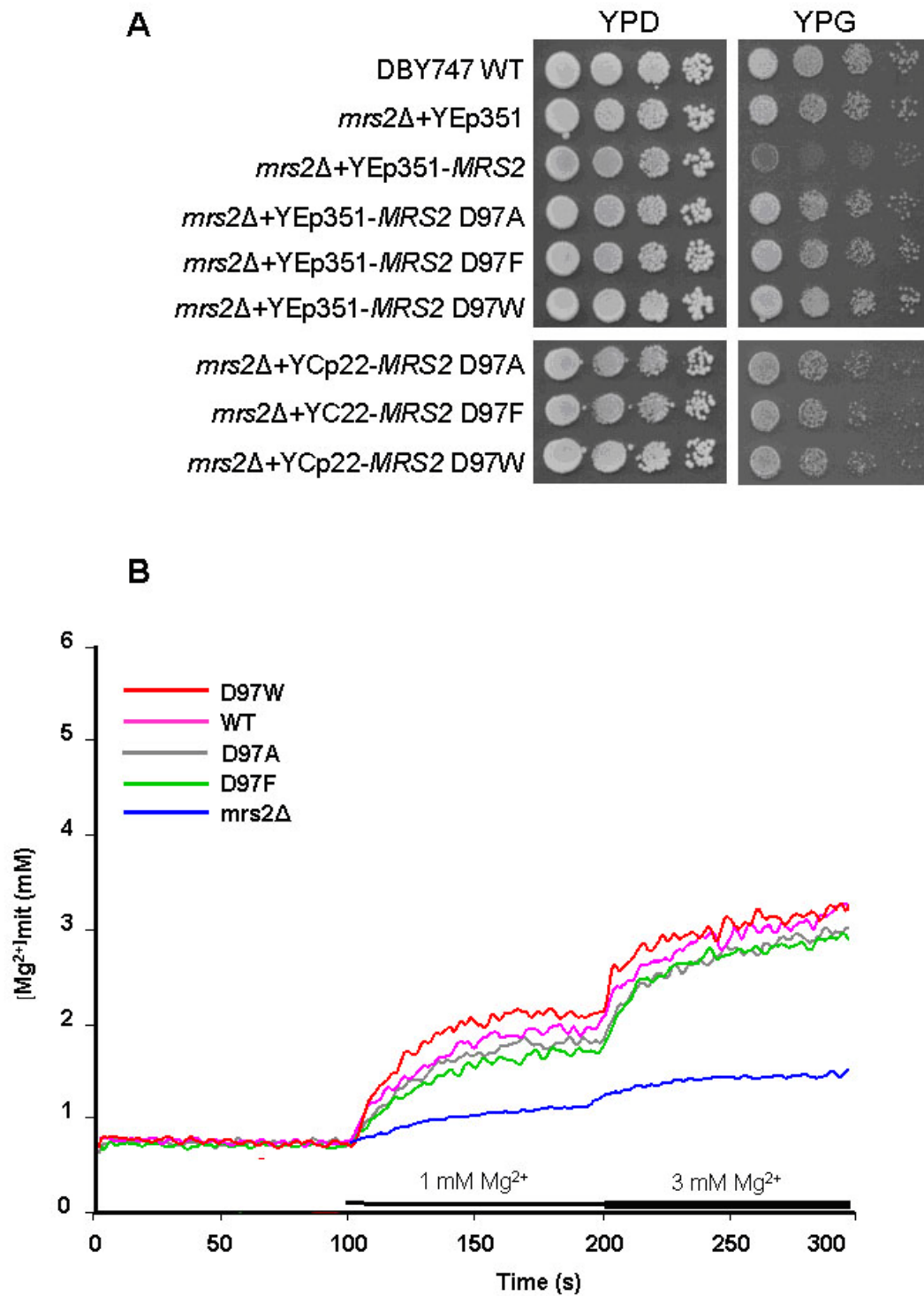


Figure 6 Mutations in the hydrophobic Gate 1 (Met309) of Mrs2.

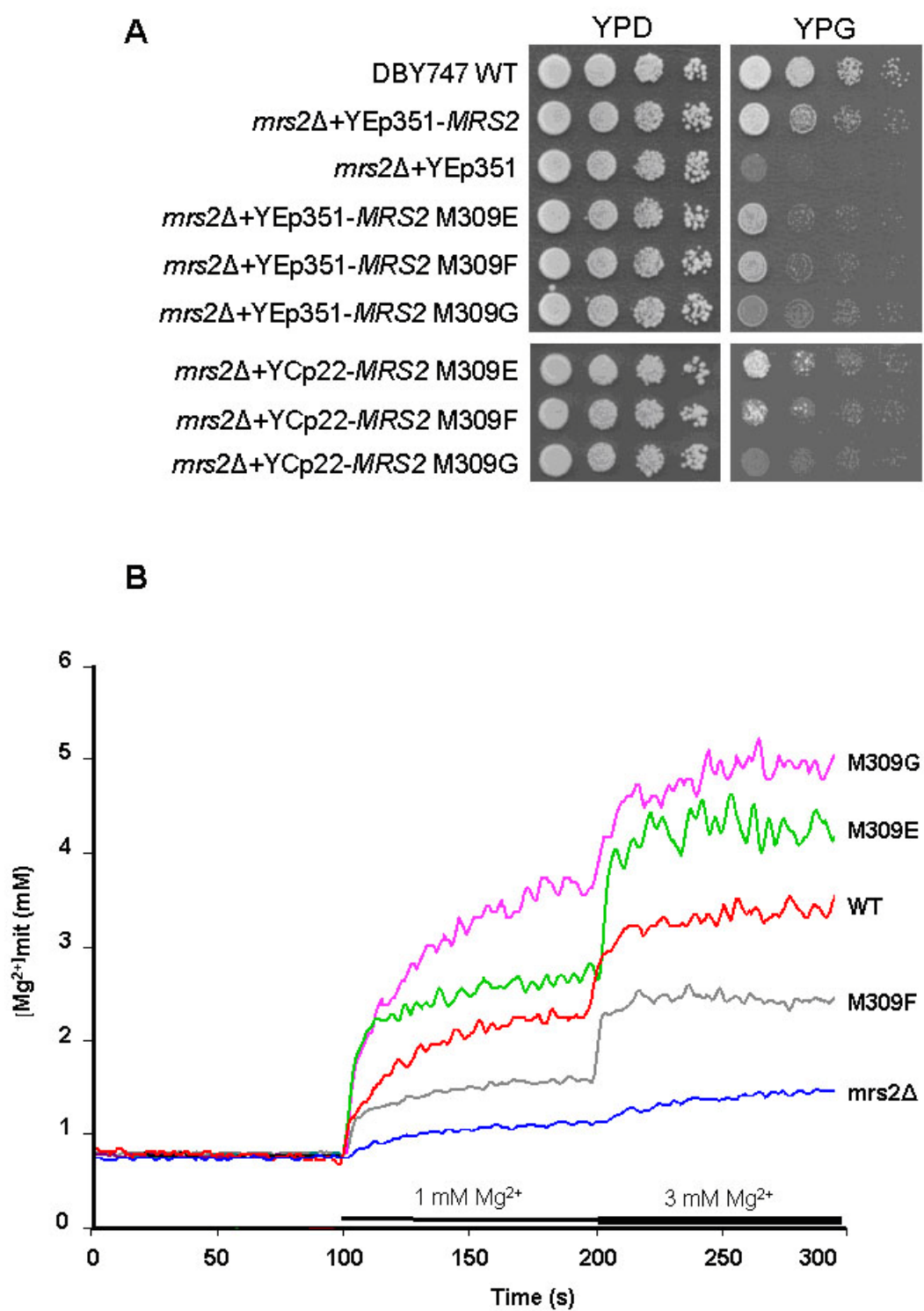


Figure 7 Characterization of mutants in the hydrophobic Gate 2 of Mrs2.

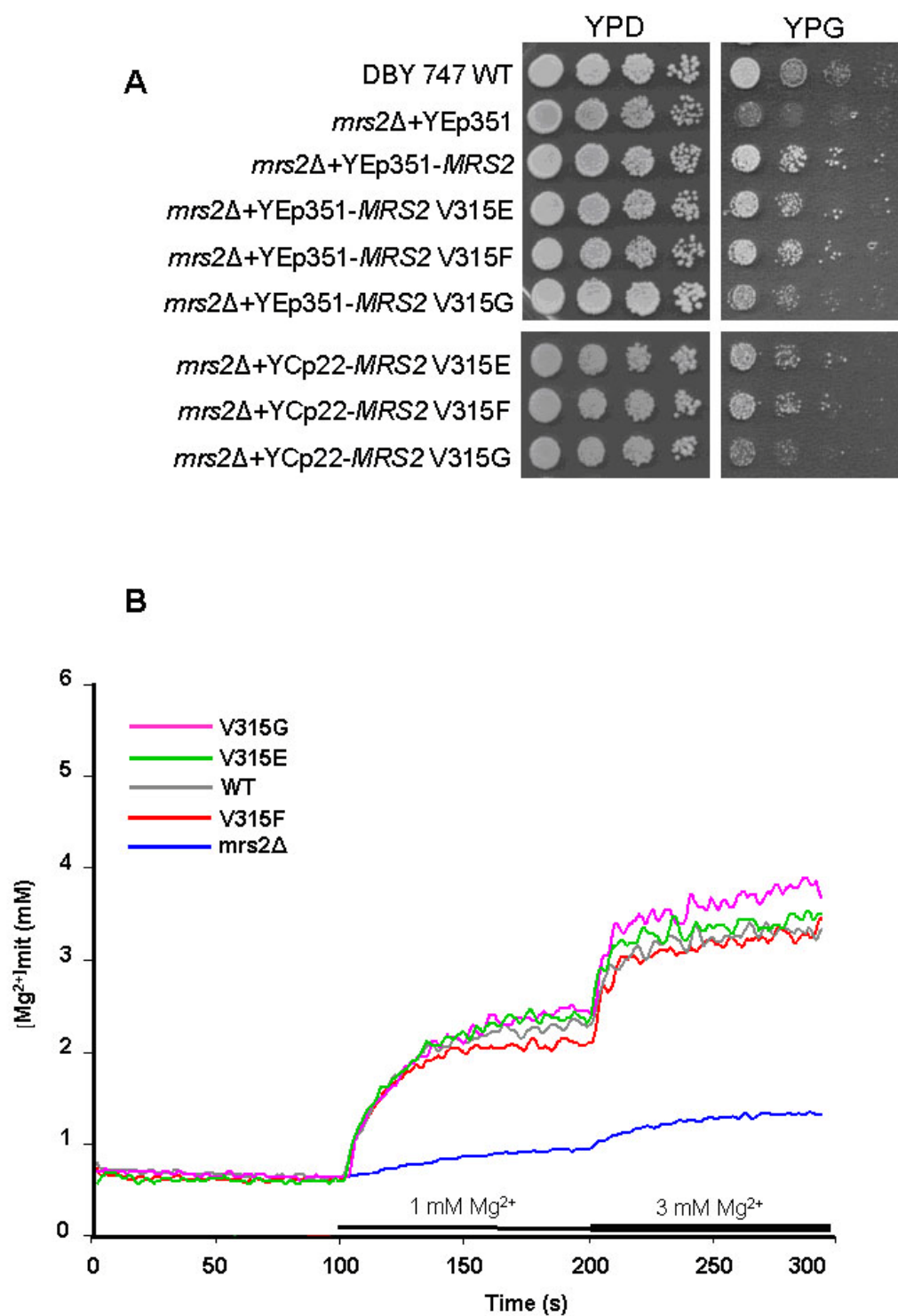


Figure 8: Characterization of the Mrs2 C-terminus.

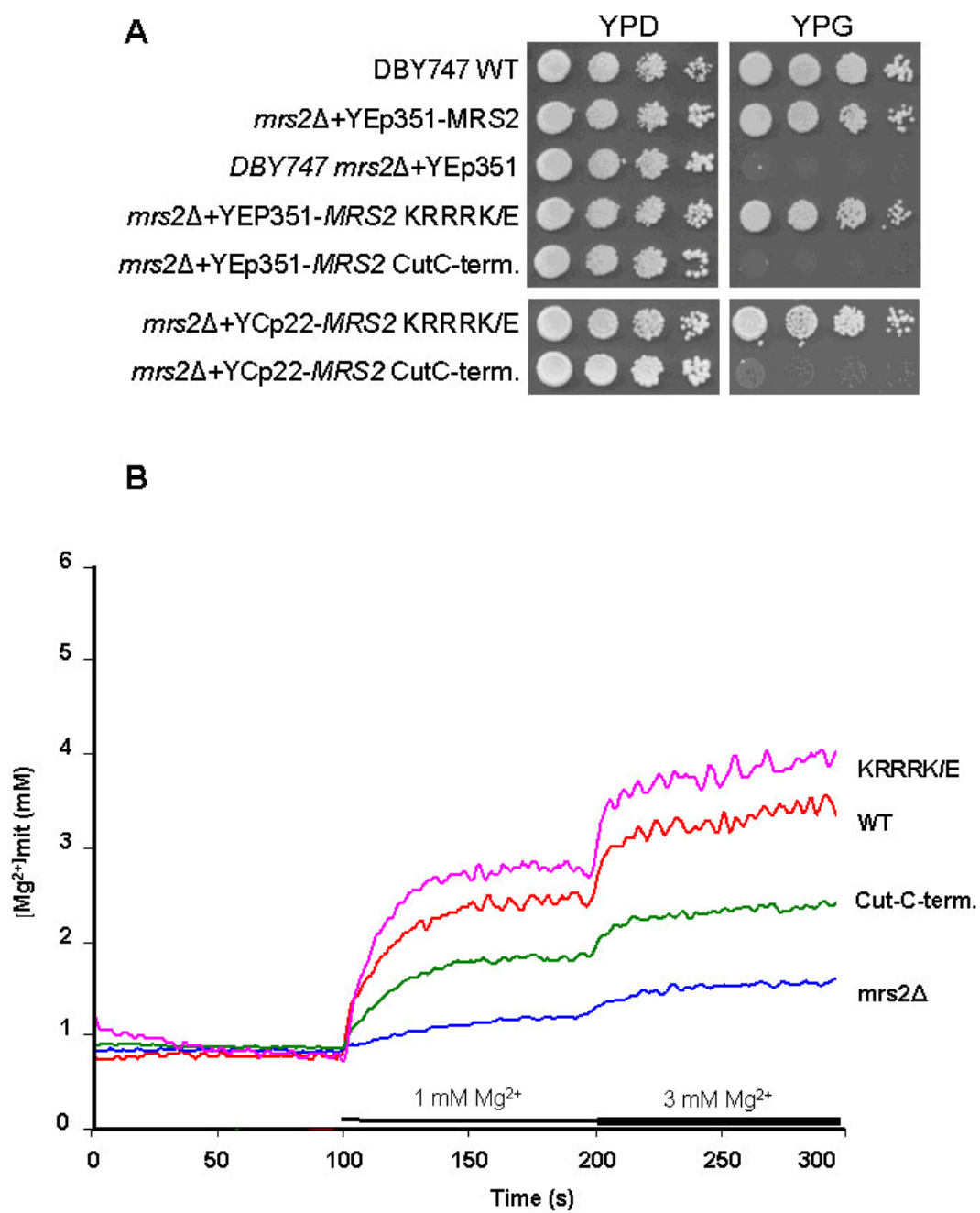


TABLE 1.
Data collection and refinement statistics

	Data set 1	Data set 2
DATA COLLECTION		
Source	Home source	ID14-1 (ESRF)
Wavelength (Å)	1.541	0.933
Resolution (Å)	36.89–1.83 (1.90–1.83) ^a	50.0–1.28 (1.35 - 1.28)
Space group	P2 ₁ 2 ₁ 2 ₁	P2 ₁ 2 ₁ 2 ₁
Unit cell (Å)	a = 54.66, b = 61.70, c = 85.30	a = 54.88 = 61.88, c = 85.45
Molecules / a.u.	1	1
Unique reflections	48844	69621 (4235)
Completeness (%)	99 (92)	92.1 (79.0)
R _{meas} ^b		0.069 (1.172)
R _{pim} ^c	0.80 (23.0)	
R _{anom}	0.0316	
Multiplicity	80 (13)	12.0 (6.2)
I/sig(I)	40.2 (1.9)	19.9 (1.83)
PHASING		
No. of sites	11	
Phasing power ^d	0.311 (0.069)	
Figure of merit	0.841	
REFINEMENT		
R _{cryst} ^e / R _{free} ^f	0.193/0.244	0.169/0.204
No. Reflections used for R _{free}	1289	7312
R.m.s.d. bonds (Å)	0.0124	0.004
R.m.s.d. angles (°)	1.33	0.91
B protein (Å ²)	29.6	15.1

^a Values in parentheses are for the highest resolution shell.

$$R_{meas} = \frac{\sum_h \sqrt{\frac{n_h}{n_h - 1}} \sum_i^{n_h} |\hat{I}_h - I_{h,i}|}{\sum_h \sum_i^{n_h} I_{h,i}} \quad \text{with} \quad \hat{I}_h = \frac{1}{n_h} \sum_i^{n_h} I_{h,i}$$

$$R_{pim} = \sum_{hkl} \sqrt{\frac{1}{N-1}} \sum_i |I_i(hkl) - \overline{I(hkl)}| / \sum_{hkl} \sum_i I_i(hkl)$$

Where I (hkl) is the mean intensity of multiple I_i (hkl) observations of the symmetry-related reflections, N is the redundancy, n_h is the multiplicity, \hat{I}_h is the average intensity and I_{h,i} is the observed intensity.

^dAnomalous phasing power: $(\sum |F_H(\text{imag})|^2 / \sum |\Delta F_{\pm PH}(\text{obs}) - |\Delta F_{\pm PH}(\text{calc})||^2)^{1/2}$ where $\Delta F_{\pm PH}$ is the structure factor difference between Bijvoet pairs and F_H(imag) is the imaginary component of the calculated structure factor contribution by the anomalously scattering atoms.

^eR_{cryst} = $\sum |F_o - F_c| / \sum F_o$

^fR_{free} is the cross-validation R_{factor} computed for the test set of reflections (5 %) which are omitted in the refinement process.

Supplementary Information

Supplementary Figure 1

Analytical size exclusion chromatography (ASEC) of Mrs2₄₈₋₃₀₈. (A) ASEC studies showed that Mrs2₄₈₋₃₀₈ behaves as a homo-pentamer in low ionic strength buffers (10 mM Tris-HCl, 10 mM NaCl) and (B) as a monomer in high ionic strength buffers (50 mM Tris-HCl, 300 mM NaCl). The corresponding peaks are visualized by SDS-PAGE. The column was pre-calibrated with standard molecular weight markers.

Supplementary Figure 2

Circular dichroism spectra of Mrs2₄₈₋₃₀₈. The mean residual ellipticity of Mrs2₄₈₋₃₀₈ at 1 mg/ml was monitored from 240 to 190 nm. Three scans were performed on individual sample and subsequently averaged. The data were reconstructed and the difference between the reconstructed and the experimental data was determined. The circular dichroism (CD) spectrum of Mrs2₄₈₋₃₀₈ showed the minima at 208 and 219 nm, a characteristic for a protein rich in α -helices.

Supplementary Figure 3

Superposition of Mrs2₄₈₋₃₀₈ on the soluble domains of Tm-CorA and ZntB.

(A) Superposition of the complete soluble domain of Mrs2₄₈₋₃₀₈ (red) on the soluble domain of Tm-CorA (PDB code 2IUB) with an RMSD of 2.85 Å and mscore of 70 %. (B) Superposition of the complete soluble domain of Mrs2₄₈₋₃₀₈ (red) on the soluble domain of ZntB (PDB code 3CK6) (green) with an RMSD of 2.61 Å and mscore of 67 %. (C) Superposition of $\alpha/\beta/\alpha$ subdomains of Mrs2₄₈₋₃₀₈ (red) and Tm-CorA (yellow) with an RMSD of 2.96 Å and mscore of 59 %. (D) Superposition of $\alpha/\beta/\alpha$ subdomains of Mrs2₄₈₋₃₀₈ (red) and ZntB (green) with an RMSD of 2.75 Å and mscore of 49 %. (E) Superposition of helical subdomains of Mrs2₄₈₋₃₀₈ and Tm-CorA with an RMSD of 2.62 Å and mscore of 85 %. (F) Superposition of helical subdomains of Mrs2₄₈₋₃₀₈ and ZntB with an RMSD of 2.71

Å and mscore of 91 %. Superpositions were made with a program SHEBA (Jung & Lee, 2000).

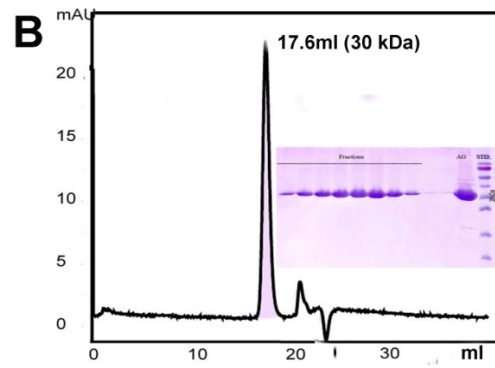
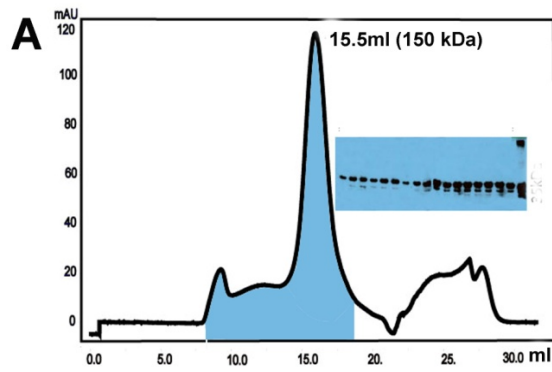
Supplementary Figure 4

Western Blot analysis of the expression levels of *MRS2* and the different *MRS2* mutant variants. Isolated mitochondria of *mrs2Δ* cells transformed with an empty plasmid or high copy number vector Yep351 expressing *MRS2*-HA or the mutant variants were separated by SDS/PAGE and proteins were visualized by immunoblotting with an antiserum against the HA tag. Porin was used as a loading control.

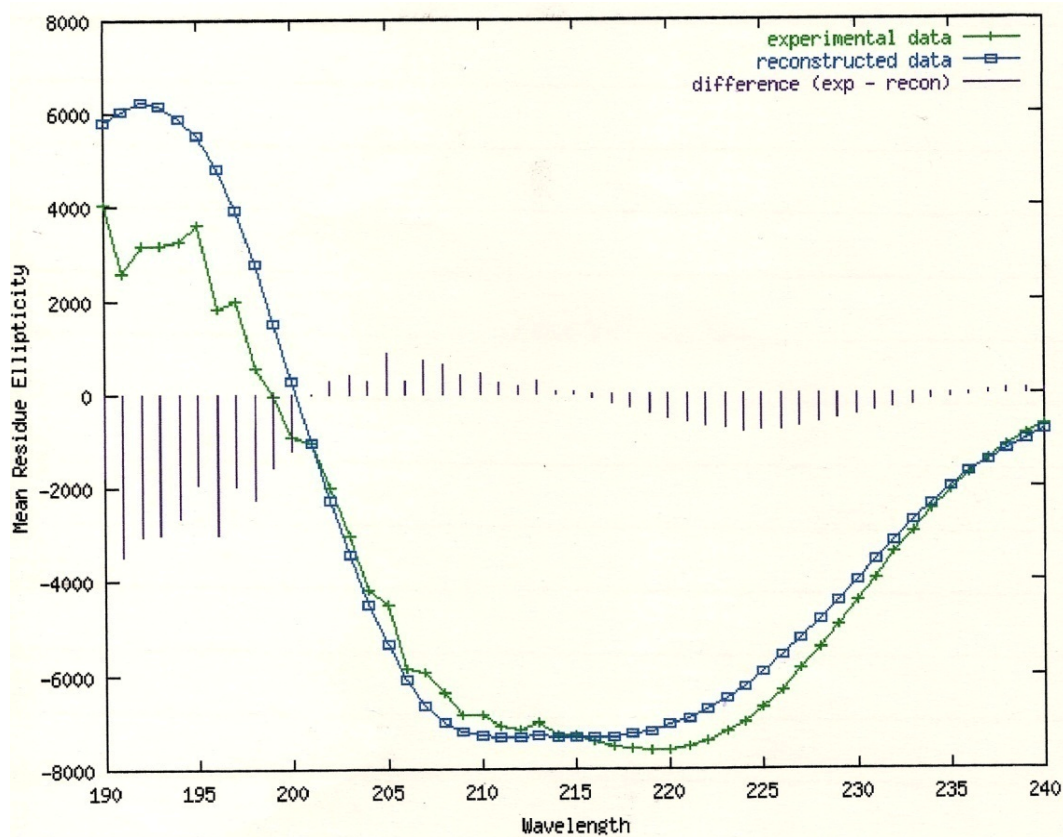
Supplementary Figure 5

Thermofluor-based stability optimization of *Mrs2*₄₈₋₃₀₈ (A) Thermal shift assay of protein *Mrs2*₄₈₋₃₀₈ in the initial condition, 50 mM Tris-HCl and 200 mM NaCl. (B) Thermal shift assay of protein *Mrs2*₄₈₋₃₀₈ in 50 mM Tris-HCl and 500 mM NaCl. The melting temperature T_m is determined at the inflection point of the melting curve in all conditions. The buffer 50mM Tris-HCl and 500 mM NaCl ($T_m = 48^\circ \text{C}$) stabilizes protein considerably compare to 50 MM Tris-HCl and 200 mM NaCl ($T_m = 32^\circ \text{C}$). The condition was repeated four times as indicated by the four curves in order to avoid pipetting error.

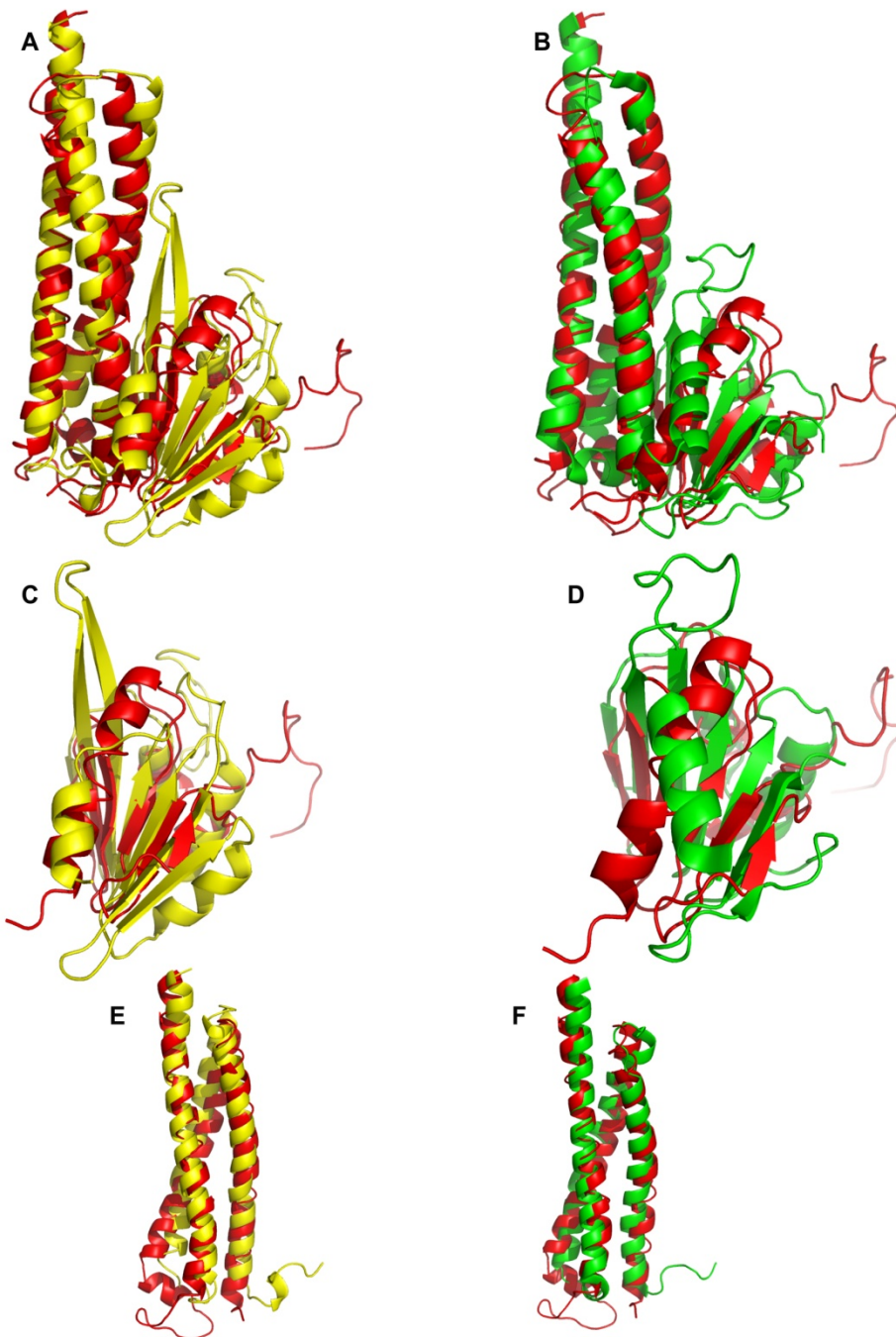
Supplementary Figure 1 Analytical size exclusion chromatography of Mrs2₄₈₋₃₀₈.



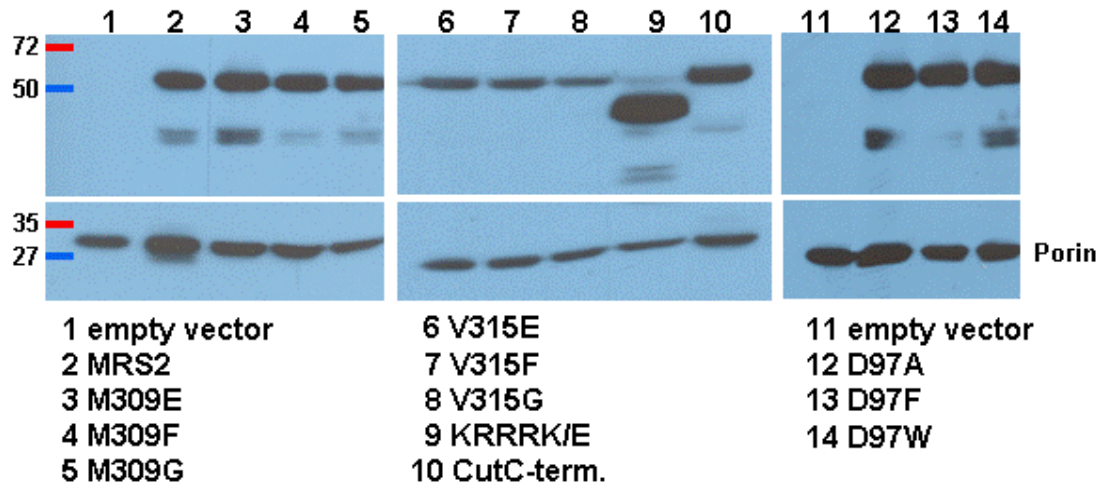
Supplementary Figure 2 Circular dichroism spectra of Mrs2₄₈₋₃₀₈.



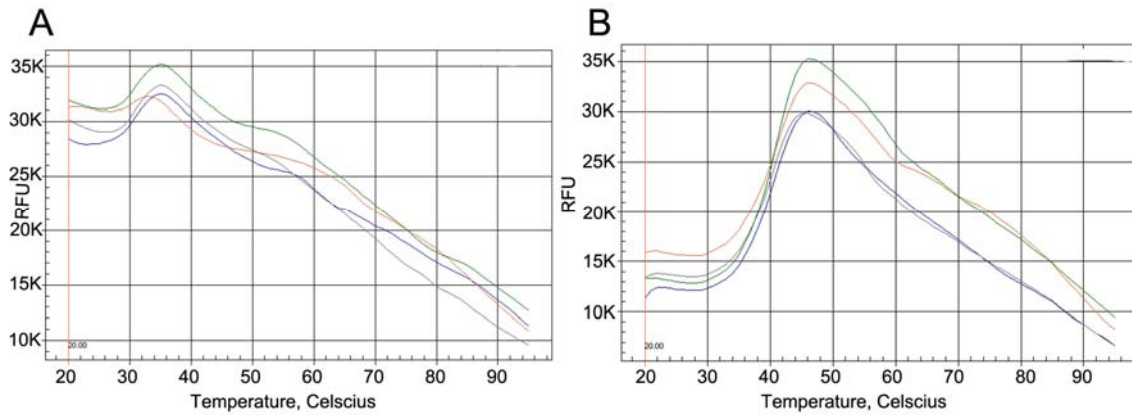
Supplementary Figure 3 Superposition of entire N-terminal moieties and of individual domains of CorA, ZntB on Mrs2₄₈₋₃₀₈ .



Supplementary Figure 4 Western Blot analysis of the expression levels of *MRS2* and the different *MRS2* mutant variants.



Supplementary Figure 5 Thermofluor-based stability optimization of Mrs2₄₈₋₃₀₈



Supplementary Table 1

Number of positively charged residues at the C-terminus of Mrs2 from different species

Name of species	Number of residues at C-terminus	Number of Positively charged residues
<i>Saccharomyces cerevisiae</i>	107	24
<i>Penicillium marneffeii</i>	116	21
<i>Penicillium chrysogenum</i>	122	22
<i>Ashbya gossypii</i>	78	16
<i>Kluyveromyces lactis</i>	79	15
<i>Magnaporthe oryzae</i>	198	29
<i>Yarrowia lipolytica</i>	42	14
<i>Debaryomyces hansenii</i>	69	15
<i>Vanderwaltozyma polyspora</i>	83	18
<i>Botryotinia fuckeliana</i>	65	18

MANUSCRIPT 3

Effect of mutations in the conserved GMN motif on ion transport and selectivity in the yeast magnesium transporter Mrs2p

Soňa Svidová, Gerhard Sponder, **Muhammad Bashir Khan**, Rudolf J. Schweyen, Oliviero Carugo, Kristina Djinović-Carugo

Submitted to *Biochim Biophys Acta*

Effect of mutations in the conserved GMN motif on ion transport and selectivity in the yeast magnesium transporter Mrs2p

Soňa Svidová¹, Gerhard Sponder¹, Muhammad Bashir Khan³, Rudolf J. Schweyen^{1†}, Oliviero Carugo², Kristina Djinović-Carugo^{3,4*}

¹Department of Microbiology, Immunobiology and Genetics, Max F. Perutz Laboratories, University of Vienna, Vienna, Austria

²Department of General Chemistry, University of Pavia, Pavia, Italy

³Department of Structural and Computational Biology, Max F. Perutz Laboratories, University of Vienna, Vienna, Austria

⁴Department of Biochemistry, Faculty of Chemistry and Chemical Technology, University of Ljubljana, Ljubljana, Slovenia

*Correspondence address: Campus Vienna Biocenter 5, A-1030 Vienna, Austria

Phone: +43-1-4277-52203/52201

Fax: +43-1-4277-9522

E-mail: kristina.djinovic@univie.ac.at

[†]Deceased on 15th of February 2009

Abstract

The highly conserved G-M-N motif of the CorA-Mrs2-Alr1 family of Mg²⁺ transporters has been proven to be essential for Mg²⁺ transport. We performed random mutagenesis of the G-M-N motif of *Saccharomyces cerevisiae* Mrs2p, and an unbiased genetic screen. We obtained a large number of mutants still capable of Mg²⁺ transport, albeit below the wild-type level, as assessed by measurements of Mg²⁺ influx into isolated mitochondria. Growth complementation assays in the presence of different concentrations of divalent cations (Ca²⁺, Co²⁺, Mn²⁺ and Zn²⁺), revealed some mutants with reduced growth in the presence of Mn²⁺ and Zn²⁺ ions. We hereby conclude that the G-M-N motif can be partially replaced by certain combinations of amino acids. We show that it plays a role in ion selectivity, together with the flanking negatively charged loop at the entrance of the channel, to which selectivity filter function has primarily been assigned.

Keywords: magnesium transport, Mrs2, G-M-N motif, *Saccharomyces cerevisiae*, mitochondria

1. Introduction

As the most abundant divalent cation within cells, magnesium is required for numerous cellular functions, including coordination to nucleotide triphosphates, membrane stability, regulation of gene transcription, DNA replication, enzyme catalysis, and protein synthesis [1; 2; 3; 4; 5]. Maintenance of Mg^{2+} concentrations within a certain range is therefore critical for cell viability. Cellular membranes are impermeable to divalent cations, which necessitates transmembrane channels or carriers that allow Mg^{2+} to pass through in a controlled manner.

Members of the large, heterogeneous CorA/Mrs2/Alr1 protein superfamily, found in prokaryotes, eukaryotic organisms, as well as in plants are high-affinity Mg^{2+} uptake systems enabling growth of bacterial and yeast cells even in very low external Mg^{2+} concentrations [6; 7; 8; 9; 10; 11]. Mutants lacking these transporters cannot survive without being provided with high external Mg^{2+} concentrations [7; 9; 12].

The *MRS2* gene encodes a 54 kDa integral protein of the inner mitochondrial membrane (Mrs2p). Yeast cells lacking *MRS2* are respiratory deficient and therefore exhibit a growth defect on non-fermentable substrates (“*petite* phenotype”) [13; 14; 15]. Besides Mrs2p, *S. cerevisiae* expresses a homologous protein known as Lpe10p/Mfm1p, essential for magnesium homeostasis and group II intron splicing in yeast [16]. Deletion of *LPE10/MFM1* also results in a “*petite* phenotype“ [17] and in a considerable reduction of the mitochondrial membrane potential ($\Delta\Psi$) [18].

Mrs2p is a distant relative of the bacterial Mg^{2+} transporter CorA, which three-dimensional crystal structure has already been solved [19; 20; 21]. Conservation of the primary sequences in the CorA/Mrs2/Alr1 protein superfamily is in the range of 15-20% [6; 8]. Despite of the low primary sequence homology there are several structurally conserved features, in particular the two α -helices (termed “willow helices”) in the large N-terminal part and two trans-membrane helices (TM1, TM2) near the C-terminus

connected by a short conformationally flexible loop (Figure 1) [17]. The sequence G-M-N, a motif at the end of TM1 and the presence of bulky hydrophobic amino acids in the predicted gate region at the intracellular/intramitochondrial end of the pore are the only universally conserved features, indicating an essential role for the function of these proteins [19; 20; 21].

Mrs2p-mediated Mg^{2+} transport has been extensively studied using the Mg^{2+} sensitive, fluorescent dye mag-fura-2, where it was shown that Mrs2p mediates rapid, highly regulated Mg^{2+} uptake into mitochondria [9]. Isolated mitochondria respond within seconds to a rise in the external magnesium concentration with a rapid increase of the mitochondrial free Mg^{2+} concentration ($150 \mu M s^{-1}$) [9]. The high conductance of ~ 150 pS obtained in patch-clamp recordings, characterizes Mrs2p as a channel [22] and preliminary data on the Mrs2p homologue, *Salmonella typhimurium* CorA, suggest a similarly high conductance [23]. The assumption of a common mechanism of Mg^{2+} transport for Mrs2p and CorA is supported by the fact that Mrs2p can be functionally replaced by CorA [17] and *vice versa* (this study). Furthermore, Mg^{2+} transport is in both cases inhibited by cobalt(III)-hexaammine, an analogue for the hydrated Mg^{2+} ion [22; 24; 25].

Mrs2p is able to mediate Ni^{2+} transport, albeit with a 3.5-fold lower conductance (~ 45 pS) compared to Mg^{2+} , whereas it is not permeable for Ca^{2+} , Mn^{2+} or Co^{2+} [22]. Additionally, suppression of Mg^{2+} currents in the presence of Co^{2+} was observed suggesting Co^{2+} to interact with the pore [22]. This is different to *S. typhimurium* CorA and yeast Alr1p for which transport of Ni^{2+} as well as of Co^{2+} has been reported [6; 24].

The G-M-N motif has been shown to be critical for the function of CorA and even conservative single point mutations completely abolish Mg^{2+} transport [26; 27]. This was also confirmed for Mrs2p where single mutations in the G-M-N motif were introduced [9]. This suggests that this sequence is indispensable for the function, possibly through suitably positioning the

periplasmic loop implicated in initial binding of the hydrated Mg^{2+} [19] and in assisting in the dehydration process [23].

The crystal structure of *Thermotoga maritima* CorA revealed that main-chain carbonyl groups of the G-M-N motif are exposed into the center of the pore entrance on the periplasmic side and form a polar strip suited for interaction with cations [20]. Lunin et al. proposed that the ring of five Asn314 side chains of the G-M-N motif in the CorA pentamer at the periplasmic entrance occlude the pore in the closed state [19].

In order to further investigate the importance and role of the G-M-N motif we performed random PCR mutagenesis on the G-M-N triplet to obtain mutants harbouring all possible amino acid combinations and identified those still capable of transporting Mg^{2+} . The active mutants were further characterized using *in vivo* and *in vitro* studies showing that the G-M-N motif can be in part functionally replaced by certain combinations of amino acids. Our results corroborate the notion that this motif plays an important role in ion selectivity.

2. Materials and Methods

2.1 Yeast and bacterial strains, growth media and genetic procedures

2.1.1 Bacterial cells

Escherichia coli DH10B F^- endA1 recA1 galE15 galK16 nupG rpsL Δ lacX74 Φ 80lacZ Δ M15 araD139 Δ (ara,leu)7697 mcrA Δ (mrr-hsdRMS-mcrBC) λ

Salmonella enterica serovar *Typhimurium* transmitter strain LB5010: metA22 metE551 ilv-452 leu-3121 trpC2 xyl-404 galE856 hsdL6 hsdSA29 hsdSB121 rpsL120 H1-b H2-e, n, x flaA66 nml (-) Fel-2(-).

Salmonella enterica serovar *Typhimurium* strain MM281 DEL485 (leuBCD)mgtB::MudJ;mgtA21::MudJ;corA45::mudJ;zjh1628::Tn10(cam).

Cam^R, Kan^R, Mg²⁺ dependent) was kindly provided by M.E. Maguire. It lacks all three major magnesium transport systems *CorA*, *MgtA* and *MgtB* and therefore requires medium containing Mg²⁺ concentrations in the millimolar range.

Salmonella enterica serovar Typhimurium strain MM 1927 DEL485 (leuBCD);mgtB::MudJ;mgtA21::MudJ;corA45::mudJ;zjh1628::Tn10(cam) Cam^R, Kan^R, pALTER-CorA (Amp^R).

Strains were grown in LB medium (1% tryptone, 0.5% yeast extract, 1% NaCl) with ampicillin (100 µg/ml). MM281 required addition of 10 mM MgCl₂. LB plates contained 2% Difco Agar Noble minimizing possible Mg contamination.

2.1.2 Yeast cells

The yeast *S. cerevisiae* DBY747 *mrs2*Δ deletion strain (DBY *mrs2*-1, short) has been described previously [13; 14; 15]. Yeast cells were grown in rich medium (1% yeast extract, 2% peptone) with 2% glucose as a carbon source (YPD) [11].

2.1.3 Plasmid constructs

The construct YEp351 MRS2-HA was described previously [17].

For cloning of *MRS2* into the vector pGEX-3X with IPTG-inducible promoter the primers M2GEXfw: 5'-CGCGGATCCCCAATCGGCGTCTCCTGG-3' and MRS2HiXrev: 5'-TGCTCTAGATCAATGGTGATGGTGATGG-3' were used. The resulting PCR fragment was cloned into the vector via BamHI and XbaI restriction sites.

2.1.4 Random PCR mutagenesis

In order to introduce various amino acid substitutions in *Mrs2p*, overlap extension PCR according to Pogulis et al. [28] was used. No additional mutations were found by sequencing.

Random mutagenesis of the GMN motif of *MRS2* was performed with the mutagenic forward primer 5'-GCATCTGTTCTGCCGGCGTTCTATNNNNNNNNNTTAAAGAATTCATCGA GGAGAGTG -3' and the reverse primer 5'-CACTCTCCTCGATGAAATTCTTTAANNNNNNNNNATAGAACGCCGGCAG AACAGATGC -3' according to standard protocols.

PCR products were digested with XhoI and EcoRI and cloned into an XhoI and EcoRI digested pGEX-MRS2 construct. For transformation into the DH10B *Escherichia coli* strain standard calcium chloride method was used. Correctly ligated constructs were identified by deletion of the BsmI restriction site of the *MRS2* gene, resulting in a silent mutation from an adenine to a guanine.

2.2 Identification of tolerated substitutions

A total of 45,600 constructs were pooled and transformed into the *S. typhimurium* transmitter strain LB5010. A total of 46,848 construct were pooled and transformed into the *S. typhimurium* strain MM281, plated on LB plates supplemented with 10 mM MgCl₂ and replicaplated on LB plates containing 0.05 mM IPTG to induce protein expression. 49 mutants able to grow on this medium were sequenced. No additional mutations were found by sequencing.

2.3 Serial dilutions

For serial dilutions on plates, cells were grown in liquid LB medium containing 10 mM MgCl₂ at 37°C over night, washed twice with LB medium, adjusted to an A₆₀₀ of 1 and diluted to an A₆₀₀ 0.1, 0.01 and 0.001. Serial dilutions were spotted onto LB medium plates containing different concentrations of MgCl₂, IPTG, MnCl₂ or ZnCl₂ and incubated for 24 h.

2.4 Isolation of mitochondria and measurement of changes in the intramitochondrial Mg²⁺ concentrations by spectrofluorimetry

Isolation of mitochondria by differential centrifugation and ratiometric determination of intramitochondrial Mg²⁺ concentrations ([Mg²⁺]_m) dependent

on various external concentrations ($[Mg^{2+}]_e$) was performed as previously reported [9].

3. Results and discussion

3.1 Screening of triple G-M-N mutants

According to the studies of Szegedy and Maguire [26] and of Kolisek et al. [9], single amino acid substitutions in the G-M-N motif of CorA or Mrs2p are sufficient to abolish Mg^{2+} transport. Since single conservative mutations in the G-M-N motif are poorly tolerated, we performed a triple site random mutagenesis screen in order to address the question whether any other amino acid combination can substitute for this unique and universally conserved motif.

Since large-scale isolation of mitochondria from yeast is extremely time consuming and thus not suitable for high throughput analyses, we decided to develop a bacterial system for screening for functional G-M-N mutants. Based on the fact, that Mrs2p can be functionally replaced by its bacterial homologue CorA [17], we assumed that Mrs2p expressed in the *S. typhimurium* strain MM281 depleted of all major Mg^{2+} transport systems (CorA, MgtA and MgtB), could complement the Mg^{2+} transport deficiency. *S. typhimurium* strain MM1927 lacking the magnesium uptake systems MgtA and MgtB and over-expressing only CorA was used as the positive control. As depicted in Figure 2, growth of MM281 cells was only supported at a high magnesium concentration of 10 mM. MM281 cells expressing Mrs2p virtually grew like MM1927 also without addition of external $MgCl_2$. This experiment clearly proved the ability of Mrs2p to complement the *corAΔmgtAΔmgtBΔ* induced Mg^{2+} deficiency of strain MM281 and enabled us to investigate our G-M-N mutants of Mrs2p in bacteria.

After transforming the mutant library into strain MM281, we replicaplated the transformants on LB plates without additional Mg^{2+} but

supplemented with 0.05 mM IPTG to induce protein expression. These conditions restrict growth exclusively to mutants still able to transport Mg^{2+} .

We obtained a considerable amount of mutants able to grow without additional Mg^{2+} supplementation. 62 mutants were sequenced, 7 of which contained the G-M-N motif itself (showing the functional dominance of this sequence), while 55 contained mutations of the G-M-N motif, 6 of which appeared twice, resulting in 9 different mutations. These 49 mutants were analyzed further using a growth complementation assay on plates supplemented with different IPTG concentrations to investigate, how their Mg^{2+} transport ability differs from wild-type Mrs2p. The assays were scored with four symbols “+” for cells able to grow at all four dilution steps, while “-” represents no growth at all on the plate (Tab. 1).

Bacterial cells transformed with wild-type *MRS2* were able to grow on plates with only 0.03 mM IPTG. In contrast, the analyzed mutants exhibited only poor growth at this IPTG concentration or did not grow at all. Upon stronger expression (IPTG concentrations of 0.035 – 0.05 mM) viability and growth of most of the mutants improved (Tab. 1). These results indicate that several G-M-N triple mutants still exhibited Mg^{2+} transport albeit at lower efficiency than wild-type Mrs2p.

3.2 Sequences of the functional mutants

The prominent feature of the amino acid sequences of the functional mutants is their divergence from the canonical G-M-N motif. A glycine at the first position is observed only twice (4%), a methionine appears twice (4%) at the second position, and in only one case there is an asparagine at the third position. The only mutant resembling the wild type protein is characterized by the presence of a G-T-N tripeptide instead of G-M-N.

Interestingly, about 80% of the functional mutants have a positively charged residue at the G-M-N motif. In 59% of the cases this occurs at the first position, in 18% of the cases at the second position, and only in 4% of the cases at the third position. However, the co-presence of two positively

charged amino acids is uncommon (only in about 10% of the cases). There is only one evident correlation between two positions: in the 59% of the cases in which the first position is occupied by a positively charged residue, a small and hydrophobic amino acid (Val, Ile or Leu) occupies the third position.

In contrast, few negatively charged residues are observed in the functional mutants, i.e. only six times at the first position and twice at the other two positions. No other clear trends were observed.

In a previous mutation analysis of the G-M-N motif of *S. typhimurium* CorA, none, even the most conservative single mutations (A-M-N, G-A-N, G-C-N, G-I-N, G-M-A, G-M-L, G-M-Q) were tolerated [26]. A mutational study of Mrs2p performed by Kolisek et al. [9] also confirmed the importance of the G-M-N motif: mutation to A-M-N reduced Mg^{2+} uptake to the level of the *mrs2Δ* mutant. These findings are in agreement with our results, as neither these mutants nor any other single point mutation - with the exception of the rather poorly growing G-T-N mutant - were found amongst the functional mutants, which are notably diverse from the native motif G-M-N. It might be hypothesised that while single mutations within the canonical G-M-N motif are evolutionary not tolerated by Nature, multiple adjacent mutations, though unlikely to occur in Nature, result in functional molecules.

3.3 The effect of mutations of the G-M-N sequence on cation selectivity of Mrs2p

We performed a growth complementation assay on plates containing 0.05 mM IPTG and different concentrations of divalent cations (Ca^{2+} , Co^{2+} , Mn^{2+} and Zn^{2+}), known substrates of the yeast plasma membrane Mg^{2+} uptake system Alr1p, a homologue of Mrs2p [29]. We selected 10 mutants for this assay (Tab. 2, 3), in which we examined if the presence of the aforementioned divalent cations in the growth medium influenced cell growth compared to wild-type Mrs2p.

Seven of the chosen mutants had a positively charged amino acid (K, R, H) at the first position and a small, hydrophobic residue at the third position (like 35% of the mutants of Table 1). The last three mutants did not fit in the pattern “positively charged – X – hydrophobic”, and were chosen as representatives of well (R-A-W), medium (R-R-T) and poorly (R-V-H) complementing mutant variants.

In case of Ca^{2+} and Co^{2+} we did not observe any difference (results not shown) in the growth complementation assay compared to plates not supplemented with cations, suggesting that no transport or blockage of the channel by these ions occurred. In a study employing patch clamp electrophysiology on giant lipid vesicles fused with inner-mitochondrial membranes, Mrs2p was permeable for Mg^{2+} and Ni^{2+} but not for Ca^{2+} , Mn^{2+} or Co^{2+} . However, suppression of Mg^{2+} currents in the presence of Co^{2+} was observed [22]. In our case no effect of Co^{2+} was observed, both on wild-type Mrs2p and on the investigated mutants. This might be due to different techniques used: patch-clamp recordings on single ion channels allow very precise measurements of the ion currents and tight control of ionic conditions on both sides of the channel which is not possible in a growth complementation assay on plates. Furthermore, ion concentrations used in the patch-clamp experiments were much higher (~ 1000x in this case) than concentrations used *in vivo*, and as a consequence, we cannot properly compare the results of the growth complementation assay and the patch-clamping experiments.

The tested concentrations of MnCl_2 reduced growth of all mutants, whereas growth of cells harboring wild-type *MRS2* remained unaffected. The negative effect of MnCl_2 increased with increasing concentrations of the cation (Table 2). Furthermore, the growth defect was differently pronounced in the mutants: the top three least affected are characterized by positively charged residues at the first and the second position (K-R-L; R-R-T), while the two most affected mutants carry Arg at the first, and Leu at the third position (R-Q-L; R-V-L) (Table 2).

The effect of ZnCl_2 was similar to MnCl_2 , however the growth defect of the mutants was slightly less pronounced (Table 3). The three least affected and the two most affected mutants were the same as those identified in the Mn^{2+} assay.

The R-V-H, R-A-W and R-R-T mutants do not significantly differ from the “positively charged - X - hydrophobic” set, suggesting that the absence of a hydrophobic amino acid at the third position does not critically affect ion selectivity, when combined with a small hydrophobic or positively charged residue on the second place.

Amongst the reasons for the manganese and zinc dependent negative effects on growth complementation assays, it is possible to hypothesize that both Mn^{2+} and Zn^{2+} either cross the channel and enter into the cells or block the entrance of the pore, stopping the flux of Mg^{2+} . Both explanations might be coherent with the experimental observation that increasing cation concentrations correlate with negative effects on cell growth. However, it is impossible to determine exactly the underlying mechanism of the negative effects, given the comparable ionic radii of Mg^{2+} , Mn^{2+} and Zn^{2+} (0.72 Å, 0.82 Å, 0.75 Å, respectively) and the consequent similarity between the hexa-aquaions [30]. It is on the other hand clear that Mn^{2+} and Zn^{2+} did not affect growth of cells hosting wild type Mrs2, suggesting that the G-M-N motif is involved in ion selectivity.

Apart from the size of the hydrated and non-hydrated ions, the water exchange rate of the hydrated ion appears to be an important parameter for the transport activity of the channel. Mg^{2+} has a very slow water exchange rate of 10^5 s^{-1} compared to Mn^{2+} and Zn^{2+} for which exchange rates are at least one to two orders of magnitude higher [31]. The incoming Mg^{2+} ion has to be at least partially dehydrated to enter the channel. The sequence G-M-N and the loop residues might generate a unique structural environment specially suited for the interaction and dehydration of Mg^{2+} . Consequently, alterations of the G-M-N motif could lead to a more or less productive

interaction with ions different from Mg^{2+} and thereby alter the selectivity of the channel.

3.4 Mg^{2+} influx into isolated mitochondria

In order to directly investigate Mg^{2+} influx into isolated mitochondria of selected mutants we used the Mg^{2+} -sensitive dye mag-fura-2 (Figure 3). The mutants were selected on the basis of good (R-M-V, R-F-V, R-C-V), medium (R-Q-L) or poor (R-V-H) growth complementation capacity in *S. typhimurium* strain MM281 (Table 1). After addition of $MgCl_2$ to a concentration of 1 mM Mg^{2+} a lack of the characteristic rapid Mg^{2+} influx [9] was observed in most mutants, together with significantly lower steady-state Mg^{2+} levels (Figure 3). The only exception was the R-Q-L mutant, which lacked rapid Mg^{2+} influx, but finally reached a mitochondrial Mg^{2+} concentration comparable to the wild-type level during the subsequent 100 seconds. After addition of $MgCl_2$ to the final concentration of 3 mM Mg^{2+} , we observed Mg^{2+} influx in all mutants, however, it did not reach the final steady-state level of wild-type Mrs2p. The differences between mutants were minimal, with the exception of the R-Q-L mutant, which reached almost wild-type Mg^{2+} levels. At the same time this mutant was found amongst the variants exhibiting the strongest growth reduction on plates supplemented with Mn^{2+} and Zn^{2+} . This mutation strongly affected ion selectivity but at the same time had only a minor effect on the conductivity of the channel for Mg^{2+} , implying that ion conduction and ion selectivity are two independent processes.

These results show that all investigated mutants maintained a certain ability to transport Mg^{2+} in *S. typhimurium* cells (Table 1) and mutants R-V-H, R-M-V, R-F-V, R-C-V and R-Q-L also in yeast mitochondria (Figure 3), albeit in both systems the transport activity was significantly decreased compared to the wild type protein.

4. Conclusions

The asparagine residues of the G-M-N motif have been proposed to block the entrance of the channel in the closed conformation [19; 23]. Furthermore, this motif has been implicated in suitably orienting the flexible, negatively charged loop at the mouth of the pore for interaction with the hydrated magnesium ion. The loop connecting TM1 and TM2 appears to form the initial interaction site for hydrated Mg^{2+} and likely participates in the dehydration process of the ion required prior to its entrance into the pore of the channel [23]. The high conductance of Mrs2p [22] and CorA [23] channels were proposed to be based on a mechanism which involves electrostatic interactions of the loop residues with the hydration shell of Mg^{2+} and not with the ion itself [23].

Our study on the G-M-N motif identified viable triple mutants hosting a positively charged residue primarily on the first but also on the third position. At a first glance, the presence of positively charged residues in functional mutants might seem counterintuitive as these mutations could in fact hinder the transport of Mg^{2+} ions by electrostatic repulsion. However, since it is structurally unfeasible for all three amino acid residues of the motif to be in direct contact with the ion [27], it is plausible to envisage that these residues form a structural motif critical for ion uptake, which can be partially accomplished by different amino acid combinations, eventually leading to a functionally equivalent structure.

In order to assess the impact of mutations in the G-M-N motif on the selectivity of Mrs2p, we performed growth complementation assays on plates supplemented with different cations (Ca^{2+} , Co^{2+} , Mn^{2+} and Zn^{2+}). Our results show that mutations in the G-M-N motif lead to reduced growth of the cells in presence of Mn^{2+} and Zn^{2+} while Ca^{2+} and Co^{2+} did not influence their viability. This can take place *via* two possible competitive mechanisms: (i) Mn^{2+} and Zn^{2+} are transported through the pore and the growth defect is caused by Mn^{2+}/Zn^{2+} overdose, or (ii) Mn^{2+} and Zn^{2+} ions are trapped and block the channel for Mg^{2+} transport causing in this way the growth defect by Mg^{2+} deficiency.

In summary we conclude that despite its high degree of conservation, the G-M-N motif can be functionally replaced by certain combinations of amino acid residues. Most frequently a positively charged residue in the first and a hydrophobic residue in the third position were found in functional mutants. Our studies suggest that the G-M-N motif plays a role in ion selectivity, being therefore part of the selectivity filter together with the flanking negatively charged loop, at the entrance of the Mrs2p channel. The concurrent involvement of the G-M-N motif in the gating process and in ion selectivity as well, might be the molecular basis for its universal conservation throughout the phyla.

5. Acknowledgements

We thank Michael Maguire (Case Western Reserve University) for providing the *Salmonella typhimurium* strains MM281. We thank Elisabeth Froschauer (Max F. Perutz Laboratories, Univ. Vienna, Austria) for fruitful discussions. Rainer Schindl, Julian Weghuber and Christoph Romanin (Univ. Linz, Austria) are kindly acknowledged for critical reading of the manuscript. MBK, GS, SS were recipients of a PhD fellowship from FWF (P20141) and from WWTF (LS05021). MBK was partially supported by the University of Vienna funds. The BIN-III initiative of the Austrian GEN-AU for financial support is acknowledged.

6. References

- [1] J.A. Cowan, Metallobiochemistry of magnesium. Coordination complexes with biological substrates: site specificity, kinetics and thermodynamics of binding, and implications for activity. *Inorg. Chem.* 30 (1991) 2740-2747.
- [2] J.A. Cowan, Metal Activation of Enzymes in Nucleic Acid Biochemistry. *Chem Rev* 98 (1998) 1067-1088.
- [3] J.A. Cowan, T. Ohyama, K. Howard, J.W. Rausch, S.M. Cowan, and S.F. Le Grice, Metal-ion stoichiometry of the HIV-1 RT ribonuclease H domain: evidence for two mutually exclusive sites leads to new mechanistic insights on metal-mediated hydrolysis in nucleic acid biochemistry. *J Biol Inorg Chem* 5 (2000) 67-74.
- [4] C.E. Dann, 3rd, C.A. Wakeman, C.L. Sieling, S.C. Baker, I. Irnov, and W.C. Winkler, Structure and mechanism of a metal-sensing regulatory RNA. *Cell* 130 (2007) 878-92.
- [5] G.J. Quigley, M.M. Teeter, and A. Rich, Structural analysis of spermine and magnesium ion binding to yeast phenylalanine transfer RNA. *Proc Natl Acad Sci U S A* 75 (1978) 64-8.
- [6] R.C. Gardner, Genes for magnesium transport. *Curr Opin Plant Biol* 6 (2003) 263-7.
- [7] A. Graschopf, J.A. Stadler, M.K. Hoellerer, S. Eder, M. Sieghardt, S.D. Kohlwein, and R.J. Schweyen, The yeast plasma membrane protein Alr1 controls Mg²⁺ homeostasis and is subject to Mg²⁺-dependent control of its synthesis and degradation. *J Biol Chem* 276 (2001) 16216-22.
- [8] V. Knoop, M. Groth-Malonek, M. Gebert, K. Eifler, and K. Weyand, Transport of magnesium and other divalent cations: evolution of the 2-TM-GxN proteins in the MIT superfamily. *Mol Genet Genomics* 274 (2005) 205-16.
- [9] M. Kolisek, G. Zsurka, J. Samaj, J. Weghuber, R.J. Schweyen, and M. Schweigel, Mrs2p is an essential component of the major electrophoretic Mg²⁺ influx system in mitochondria. *EMBO J* 22 (2003) 1235-44.
- [10] M. Wachek, M.C. Aichinger, J.A. Stadler, R.J. Schweyen, and A. Graschopf, Oligomerization of the Mg²⁺-transport proteins Alr1p and Alr2p in yeast plasma membrane. *FEBS J* 273 (2006) 4236-49.
- [11] J. Weghuber, F. Dieterich, E.M. Froschauer, S. Svidova, and R.J. Schweyen, Mutational analysis of functional domains in Mrs2p, the mitochondrial Mg²⁺ channel protein of *Saccharomyces cerevisiae*. *FEBS J* 273 (2006) 1198-209.
- [12] S.P. Hmiel, M.D. Snavely, J.B. Florer, M.E. Maguire, and C.G. Miller, Magnesium transport in *Salmonella typhimurium*: genetic characterization and cloning of three magnesium transport loci. *J Bacteriol* 171 (1989) 4742-51.
- [13] H. Koll, C. Schmidt, G. Wiesenberger, and C. Schmelzer, Three nuclear genes suppress a yeast mitochondrial splice defect when present in high copy number. *Curr Genet* 12 (1987) 503-9.
- [14] G. Wiesenberger, M. Waldherr, and R.J. Schweyen, The nuclear gene MRS2 is essential for the excision of group II introns from yeast mitochondrial transcripts in vivo. *J Biol Chem* 267 (1992) 6963-9.
- [15] J. Gregan, M. Kolisek, and R.J. Schweyen, Mitochondrial Mg(2+) homeostasis is critical for group II intron splicing in vivo. *Genes Dev* 15 (2001) 2229-37.
- [16] J. Gregan, D.M. Bui, R. Pillich, M. Fink, G. Zsurka, and R.J. Schweyen, The mitochondrial inner membrane protein Lpe10p, a homologue of Mrs2p, is essential for magnesium homeostasis and group II intron splicing in yeast. *Mol Gen Genet* 264 (2001) 773-81.
- [17] D.M. Bui, J. Gregan, E. Jarosch, A. Ragnini, and R.J. Schweyen, The bacterial magnesium transporter CorA can functionally substitute for its putative homologue Mrs2p in the yeast inner mitochondrial membrane. *J Biol Chem* 274 (1999) 20438-43.

- [18] G. Sponder, S. Svidova, R. Schindl, S. Wieser, R.J. Schweyen, C. Romanin, E.M. Froschauer, and J. Weghuber, Lpe10p modulates the activity of the Mrs2p-based yeast mitochondrial Mg²⁺ channel. *FEBS J* 277 3514-25.
- [19] V.V. Lunin, E. Dobrovetsky, G. Khutoreskaya, R. Zhang, A. Joachimiak, D.A. Doyle, A. Bochkarev, M.E. Maguire, A.M. Edwards, and C.M. Koth, Crystal structure of the CorA Mg²⁺ transporter. *Nature* 440 (2006) 833-7.
- [20] S. Eshaghi, D. Niegowski, A. Kohl, D. Martinez Molina, S.A. Lesley, and P. Nordlund, Crystal structure of a divalent metal ion transporter CorA at 2.9 angstrom resolution. *Science* 313 (2006) 354-7.
- [21] J. Payandeh, and E.F. Pai, A structural basis for Mg²⁺ homeostasis and the CorA translocation cycle. *EMBO J* 25 (2006) 3762-73.
- [22] R. Schindl, J. Weghuber, C. Romanin, and R.J. Schweyen, Mrs2p forms a high conductance Mg²⁺ selective channel in mitochondria. *Biophys J* 93 (2007) 3872-83.
- [23] A.S. Moomaw, and M.E. Maguire, Cation selectivity by the CorA Mg²⁺ channel requires a fully hydrated cation. *Biochemistry* 49 5998-6008.
- [24] R.L. Smith, and M.E. Maguire, Microbial magnesium transport: unusual transporters searching for identity. *Mol Microbiol* 28 (1998) 217-26.
- [25] L.M. Kucharski, W.J. Lubbe, and M.E. Maguire, Cation hexaamines are selective and potent inhibitors of the CorA magnesium transport system. *J Biol Chem* 275 (2000) 16767-73.
- [26] M.A. Szegedy, and M.E. Maguire, The CorA Mg(2+) transport protein of *Salmonella typhimurium*. Mutagenesis of conserved residues in the second membrane domain. *J Biol Chem* 274 (1999) 36973-9.
- [27] J. Payandeh, C. Li, M. Ramjeesingh, E. Poduch, C.E. Bear, and E.F. Pai, Probing structure-function relationships and gating mechanisms in the CorA Mg²⁺ transport system. *J Biol Chem* 283 (2008) 11721-33.
- [28] R.J. Pogulis, A.N. Vallejo, and L.R. Pease, In vitro recombination and mutagenesis by overlap extension PCR. *Methods Mol Biol* 57 (1996) 167-76.
- [29] C.W. MacDiarmid, and R.C. Gardner, Overexpression of the *Saccharomyces cerevisiae* magnesium transport system confers resistance to aluminum ion. *J Biol Chem* 273 (1998) 1727-32.
- [30] R.D. Shannon, Revised Effective Ionic Radii and Systematic Studies of Interatomic Distances in Halides and Chalcogenides. *Acta Crystallographica A* 32 (1976) 751-76.
- [31] M.E. H. Diebler, G. Ilgenfritz, G. Maab, R. Winkler, Kinetics and Mechanism of Reactions of Main Group Metal Ions with Biological Carriers. *Appl. Chem.* 20 (1969) 93-115.

Table 1

S. typhimurium strain MM281 was transformed with plasmids indicated, serially diluted and replicaplated on plates with increasing IPTG concentrations. The number of “+” symbols corresponds to the number of dilution steps exhibiting growth.

Sequence	0.03 mM IPTG	0.035 mM IPTG	0.04 mM IPTG	0.045 mM IPTG	0.05 mM IPTG
G-M-N	++++	++++	++++	++++	++++
R-F-V*	+	++++	++++	++++	++++
R-I-L	+	++++	++++	++++	++++
R-M-V	+	++++	++++	++++	++++
R-Q-I	+	++++	++++	++++	++++
R-Q-L*	+	++++	++++	++++	++++
R-V-L*	+	++++	++++	++++	++++
L-R-C	++	+++	+++	++++	++++
R-A-W	+	++++	+++	++++	++++
R-V-M	+	++++	+++	++++	++++
I-R-I	++	+++	++	++++	++++
K-A-I	-	++++	+++	++++	++++
K-R-L	-	++++	+++	++++	++++
R-F-I	+	++++	+++	++++	+++
R-V-I	+	++++	+++	++++	+++
R-N-L	-	+++	+++	++++	++++
R-P-L	+	+++	+++	++++	+++
C-F-L	++	++	++	+++	++++
R-G-F	+	+++	+++	+++	+++
R-S-V	+	+++	+++	++++	++
R-C-V	-	++	++	++++	++++
F-R-L*	+	++	++	+++	+++
D-F-G	+	++	+	+++	+++
K-A-M	-	++	++	+++	+++
R-F-Y	+	++	++	+++	++
R-R-T	-	++	++	+++	+++
V-R-A	+	++	++	++	+++
V-R-C	+	++	++	++	+++
D-F-P*	+	++	+	++	+++
E-F-P	+	++	++	++	++
K-H-V	-	++	++	+++	++
E-Q-V	+	++	+	++	++
G-D-M	+	++	+	++	++
K-Y-I	-	++	++	++	++
R-T-Y	-	++	++	++	++
E-F-A	+	+	+	++	++
G-T-N	+	+	+	++	++
K-M-L	-	++	+	++	++
P-D-L*	-	+	++	++	++
R-F-Q	-	++	+	++	++
R-V-H	-	+	+	+++	++
R-Y-S	-	++	++	++	+
R-F-S	-	+	+	++	++
T-S-E	+	+	+	+	++
E-S-K	-	+	+	++	+
F-R-E	-	+	+	++	+
K-I-T	-	+	+	++	+
P-N-V	-	+	+	+	+
P-R-L	-	+	+	+	+
P-T-L	-	-	-	+	+

* Mutants which appeared two times.

Table 2

S. typhimurium strain MM281 was transformed with plasmids indicated, serially diluted and replicaplated on plates with 0.05 mM IPTG and different MnCl₂ concentrations. The number of “+” symbols corresponds to the number of dilution steps exhibiting growth.

Sequence	0 mM MnCl ₂	0.01 mM MnCl ₂	0.1 mM MnCl ₂
G-M-N	++++	++++	++++
K-R-L	++++	+++	++
R-A-W	++++	+++	++
R-R-T	+++	+++	++
K-A-I	++++	++	+
R-M-V	++++	++	+
R-C-V	++++	+	+
R-F-V	++++	+	+
R-Q-L	++++	+	+
R-V-L	++++	+	+
R-V-H	++	++	+

Table 3

S. typhimurium strain MM281 was transformed with plasmids indicated, serially diluted and replicaplated on plates with 0.05 mM IPTG and different ZnCl₂ concentrations. The number of “+” symbols corresponds to the number of dilution steps exhibiting growth.

Sequence	0 ZnCl ₂	0.01 mM ZnCl ₂	0.1 mM ZnCl ₂
-	-	-	-
G-M-N	++++	++++	+++
K-R-L	++++	+++	++
R-R-T	+++	+++	++
R-A-W	++++	++	+
K-A-I	++++	++	+
R-C-V	++++	++	+
R-F-V	++++	++	+
R-M-V	++++	++	+
R-Q-L	++++	++	+
R-V-L	++++	++	+
R-V-H	++	++	++

Figure 1 Schematic representation of the Mrs2p pentamer.

Position of the G-M-N motif at the end of the TM1 helix is marked, together with TM1 and N- and C- termini of subunits. Flexible loop connecting TM1 and TM2 is depicted in red.

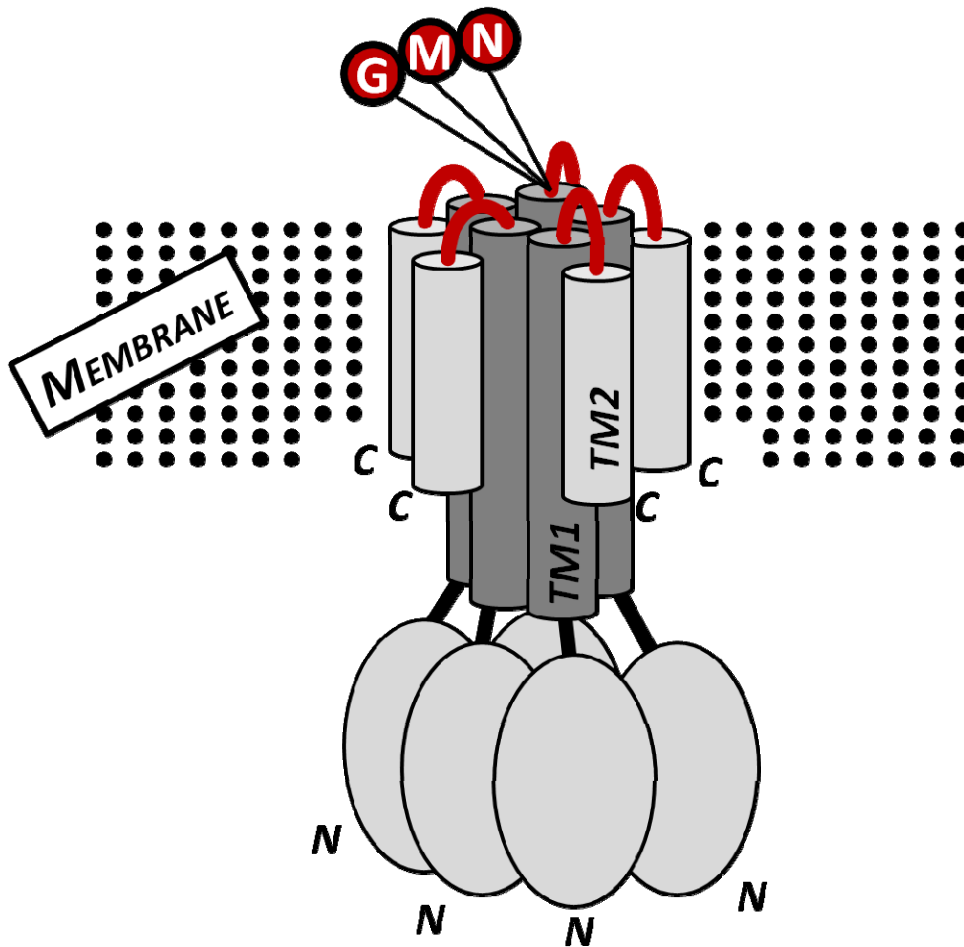


Figure 2 Growth complementation assay of the MM281 mutant strain by Mrs2p. Over night cultures of MM1927 and MM281 were transformed with plasmids indicated, serially diluted and spotted on LB medium plates with 10 mM magnesium chloride or 0.05 mM and 0.025 mM IPTG concentrations and incubated on 37°C for 24 hours.

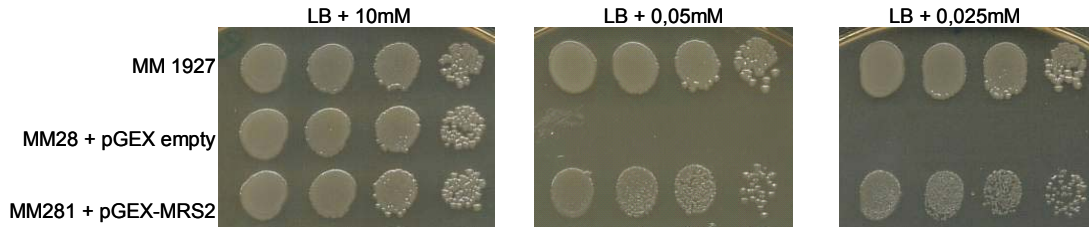
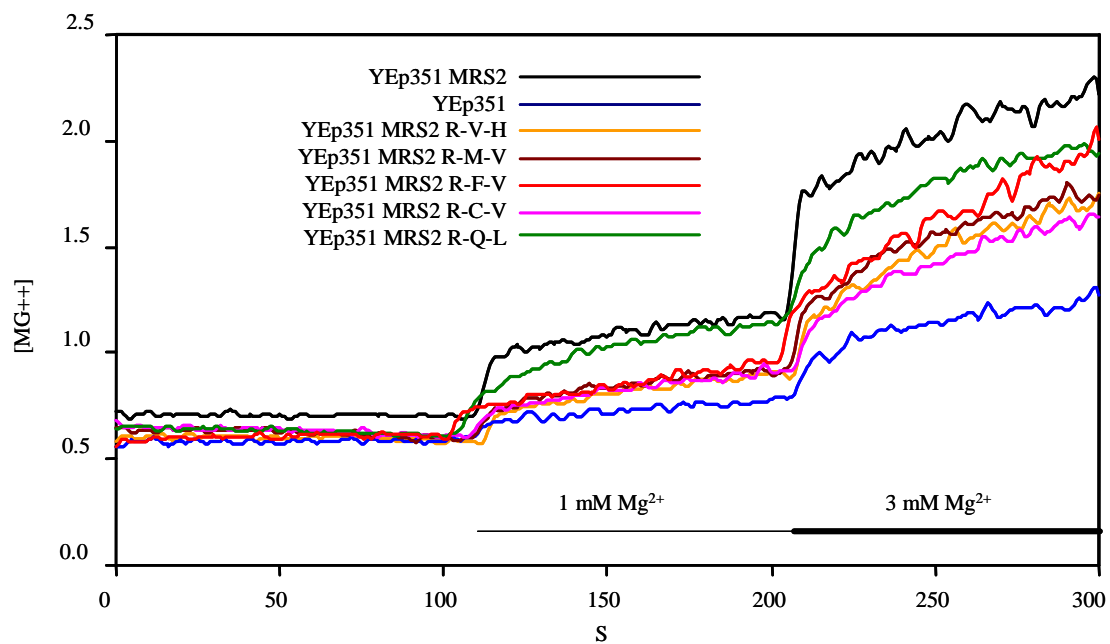


Figure 3 Representative recordings of $[Mg^{2+}]$ uptake.

S. cerevisiae strain DBY747 *mrs2* Δ was transformed with the indicated plasmids and mitochondria were isolated. The representative recordings show changes in fluorescence intensity of mag-fura-2 monitored over 300 seconds after step-wise addition of $MgCl_2$.



DISCUSSION

Structural studies on Mrs2

The yeast *Saccharomyces cerevisiae* Mrs2 is a well known member of the 2-TM-GxN eukaryotic magnesium transporter family, capable for substituting the prokaryotic CorA transporter. In my thesis, the yeast Mrs2 was taken as the archetype for this protein family to address the structural and functional characterization of the Mrs2 transporter, which is essential for the Mg²⁺ homeostasis in *Saccharomyces cerevisiae* (Kolisek et al, 2003; Papp-Wallace & Maguire, 2007; Quamme, 2010; Zsurka et al, 2001). The yeast Mrs2 protein belongs to the large superfamily of the 2-TM-GxN type transporters, forming a membrane potential-driven, ion-selective channel/transporter in the membrane to control Mg²⁺ homeostasis (Kolisek et al, 2003). This family of proteins is widely distributed in the eukaryotic as well as the prokaryotic world (Papp-Wallace & Maguire, 2007). It includes the bacterial CorA transporters, the fungal Alr1 and Alr2 like homologues, found from yeast to human. The typical features of this protein family are a large N-terminal moiety, 2 transmembrane helices (TM1 and TM2) with a highly conserved GMN motif (generally YGMNF) at the very end of the first transmembrane helix (TM1) and a comparatively short C-terminus. Generally, members of the CorA-Mrs2-Alr1 family of divalent metal ion transporters show low sequence homology and distinct structural features compare to other transporters (Lunin et al, 2006; Weghuber et al, 2006).

At present, the knowledge of the molecular/structural basis of Mg²⁺ homeostasis is still poorly understood, although many components of the Mg²⁺ transport network have been investigated. Extensive data are available for the existence of various Mg²⁺ transporters in different domain of life (Odblom & Handy, 1999; Quamme & Rabkin, 1990; Schweigel et al, 2006; Schweigel et al, 2000). Only the crystal structure of the prokaryotic magnesium transporter CorA from *Thermatoga maritima* (Tm-CorA) is solved in the closed conformation of 2-TM-GxN protein family (Eshaghi et al, 2006; Lunin et al, 2006). The crystal structure of the magnesium transporter MgtE from *Thermus thermophilus* is also accessible at 3.9 Å

but this transporter is not belonging to the Mrs2 superfamily (Hattori et al, 2007a). It is still not clear in molecular detail how these types of transporters differentiate magnesium from other metal ions, how magnesium is dehydrated and how magnesium propagates through the transporter conduction pathway (Lunin et al, 2006; Payandeh & Pai, 2006). In addition, little structural information is available about the common features in the CorA-Mrs2-Alr1 superfamily of transporters (Eshaghi et al, 2006; Lunin et al, 2006; Payandeh & Pai, 2006).

Overall structure of Mrs2₄₈₋₃₀₈ and its comparison with prokaryotic magnesium transporter Tm-CorA and Zinc transporter ZntB

In the beginning of this work, we designed a series of constructs in order to find an autonomously folded domain which is amenable to crystallization, based on bioinformatics, limited proteolysis and autocatalysis of the already expressed constructs. Most of the investigated constructs represented the soluble domain while some of them included the transmembrane helices as well as the full-length protein.

Most of the constructs were purified and characterized biochemically. Details on the purification and crystallization are reported in (Khan et al, 2010). The soluble constructs of Mrs2 included the entire N-terminal domain located in the mitochondrial matrix. Analytical size exclusion chromatography and dynamic light scattering (DLS) showed that the Mrs2 N-terminal constructs behaved as monomers in high ionic strength buffers and as homopentamers in low ionic strength buffers. In addition, the circular dichroism (CD) spectrum of the constructs showed that the protein is rich in α -helices. Together, these data suggest that most of our construct is autonomously folded into the native conformation in solution and that the protein solution is monomeric at a high ionic strength and pentameric at a low ionic strength (Khan et al., manuscript submitted).

One of the constructs of the soluble domain encompassing residues 48-308 (Mrs2₄₈₋₃₀₈, in the first publication denoted as Mrs2₄₈₋₂₇₆) was crystallized in a monomeric form (Khan et al., manuscript submitted). The Mrs2₄₈₋₃₀₈ monomer is broadly composed of two closely associated sub-domains, an N-terminal $\alpha/\beta/\alpha$

sandwich sub-domain (residues 48–164) and a C-terminal helical/coiled-coil sub-domain (residues 167–305).

The folds of prokaryotic and eukaryotic magnesium transporters are similar, to a certain extent. Each protomer can be divided into one N-terminal alpha/beta domain followed by an alpha domain. While the first one is a compact alpha-beta-alpha sandwich, the second one contains a triple coiled-coil that enters, at the end of the third, into the membrane with a transmembrane helix (TM-helix).

While the coiled-coil domain is almost identical in Tm-CorA and Mrs2₄₈₋₃₀₈, the N-terminal domain is rather different. The central beta sheet is formed by seven anti-parallel strands in Tm-CorA and by six strands in Mrs2₄₈₋₃₀₈. Despite differences in the length, the last four strands are topologically identical in the two proteins – a series of three beta hairpins. The first beta strands are topologically different. The alpha helix, that follows the strand N2, and the strand N3 is missing in Mrs2₄₈₋₃₀₈, making the eukaryotic N-terminal domain smaller than the prokaryotic one (Figure 1D, manuscript 2). It seems that in Mrs2 deletions of the first helix and the third strand of Tm-CorA have occurred during molecular evolution. Evolutionary relationships cannot be predicted just assuming the structural data. However, it is self-explanatory, that any structural based sequence alignment of these structures would be extremely deceptive, as the N-terminal domains of Tm-CorA and Mrs2₄₈₋₃₀₈ have different folds.

The Dali web-server (Holm & Sander, 1996) was employed to find out the structural neighbors of Mrs2₄₈₋₃₀₈. Tm-CorA and Vp-ZntB are the most structurally similar to Mrs2₄₈₋₃₀₈ at the level of the monomer. Moreover, the monomer and pentamer structures cannot be superimposed because, the relative orientation of the helical and the $\alpha/\beta/\alpha$ sub-domains are different.

The major differences of the three types of proteins occur at the N-terminus of the proteins. The $\alpha 1$ and C1 of Mrs2₄₈₋₃₀₈ did not superpose on any of the structural elements of Tm-CorA. The major structural difference between the two structures is the length and orientation of $\alpha 4$ of Mrs2₄₈₋₃₀₈ with respect to the β sheets. Other differences can be found in the loop regions between the C2 and C3. The stalk helix

$\alpha 7$ in case of Tm-CorA is bent near the membrane, while in case of Mrs2₄₈₋₃₀₈ the corresponding helix ($\alpha 7$) is much straighter. This might be due to the fact that the Tm-CorA structure is in a closed conformation, in a functional pentameric form. As a result it is more rigid and does not allow as much flexibility as Mrs2₄₈₋₃₀₈, which is in a monomeric form and most likely will represent the open conformation of the transporter.

Similarly, superposition of the Mrs2₄₈₋₃₀₈ and Vp-ZntB intracellular domain from *Vibrio parahaemolyticus* also shows that most of the variations occur at the $\alpha/\beta/\alpha$ domain, the first two β -strands, i.e. N1 and N2 of Mrs2₄₈₋₃₀₈ do not superpose on the Vp-ZntB transporter and more the $\alpha 4$ of Mrs2₄₈₋₃₀₈ does not superimpose on any of the structural elements of Vp-ZntB. As the available structure of Vp-ZntB only comprises the soluble domain and does not exhibit the kink in the stalk helix ($\alpha 7$ helix), this helix superposed quite well. This evidence supports the idea that the funnel domain of Vp-ZntB is in open conformation, as there is no bound divalent cation in the structure.

The different RMSDs values for the individuals domains seem to be either due to different orientations of the two N-terminal domains or to different types of folds of the three transporters (Khan et al., manuscript submitted).

Structural analysis clearly demonstrates that the prokaryotic proteins Tm-CorA and Vp-ZntB are structurally more similar to each other than to the eukaryotic protein Mrs2₄₈₋₃₀₈. Furthermore, Vp-ZntB contains a mixed seven-stranded beta sheet which is more similar to that of Tm-CorA and different from the six-stranded sheet of Mrs2₄₈₋₃₀₈. Moreover, it can be hypothesized that some structural variability between the three proteins may be related to the different level of funnel opening/closing of the transporter, which in-turn is reflected in the reorientation of the coiled-coil moiety, and which are influenced by the magnesium ion concentration.

Model of Mrs2₄₈₋₃₀₈ funnel

The funnel model was regenerated from the monomeric crystal structure of Mrs2₄₈₋₃₀₈ by superposing the helical domains of Tm-CorA and Vp-ZntB. The residues at the C-terminus of the funnel structure based on Tm-CorA came unfavourably close. This may be because of the structure of Tm-CorA, which has been reported in a closed conformation while the monomeric Mrs2₄₈₋₃₀₈ is more relaxed and may represent the open conformation of the transporter (Lunin et al, 2006). On the other hand, in the funnel model generated on Vp-ZntB, the residues at the C-terminus are at reasonably favoured distances from each other. It might be due to the structure of Vp-ZntB, which would represent the open conformation as there is no bound metal ion, the same is true for the monomeric Mrs2₄₈₋₃₀₈ which is also more relaxed and may be represent the open conformation of the transporter (Tan et al, 2009).

The structural analysis of the funnel model based on the Tm-CorA structure indicates that there are five hydrogen bonding interactions and one salt bridge between adjacent protomers. Similarly, the interactions between the two adjacent protomers in the funnel model generated on Vp-ZntB are via two hydrogen bonds and two salt bridges. On the other hand, eight hydrogen bonds and eight salt bridges can be identified in the crystal structure of the funnel domain of Vp-ZntB (PDB code 3CK6) (Tan et al, 2009), and sixteen hydrogen bonds and fifteen salt bridges in the crystal structure of Tm-CorA (PDB code 2BBJ) (Lunin et al, 2006). Although the interfaces of the proposed Mrs2 funnel were not optimized, the presence of fewer hydrogen bonds and salt bridges may explain the higher sensitivity of Mrs2 to elevated salt concentrations (Khan et al., manuscript submitted).

Analysis of the electrostatic surface potential of the structure of Mrs2₄₈₋₃₀₈, showed that the $\alpha 7$ helices, making the inner wall of the entire funnel in the functional pentameric form are rich with negative or hydroxyl-containing residues. Such an arrangement of charged residues is not only found in Mrs2₄₈₋₃₀₈, but also in other monovalent cation (KcsA) and divalent cation (CorA, ZntB) transporters/channels and possibly serve as an electrostatic sink to enhance the local ion concentration (Roux & MacKinnon, 1999).

Effect of metal ions on the pentameric Mrs2₄₈₋₃₀₈ susceptibility to protease

In Tm-CorA the elbow formed in the funnel domain by the helices ($\alpha 5$ - $\alpha 6$) move in connection with the metal site occupancy at the metal binding site (Payandeh & Pai, 2006). It has been shown that the metal stabilizes the Tm-CorA but is not required for the pentamerization of the protein (Eshaghi et al, 2005; Payandeh & Pai, 2006). Furthermore, it has been demonstrated that Tm-CorA becomes resistant to trypsin cleavage in the presence of metal ions, which represents the closed state of the transporter (Payandeh & Pai, 2006). In order to investigate the structural changes occurring in presence and absence of metal ions (magnesium and cobalt) we carried out a protease susceptibility assay of the pentameric Mrs2₄₈₋₃₀₈ funnel domain in low ionic strength buffers.

The results showed that in the presence of EDTA the protein was protected from protease digestion. On the other hand, only presence of high concentrations of cobalt rendered Mrs2₄₈₋₃₀₈ less susceptible to trypsin cleavage, while presence of magnesium did not, irrespective of the incubation time (Fig. 3 in manuscript 2). The reaction conditions were tested both at 4 and 37°C for 4 and 15 hours.

These observations were quite different, rather reverse to what has been observed for Tm-CorA protease susceptibility (Payandeh & Pai, 2006). Interestingly, addition of EDTA protected the Mrs2₄₈₋₃₀₈ funnel domain from protease cleavage. This differential protease susceptibility of the Mrs2₄₈₋₃₀₈ funnel domain compared to Tm-CorA suggests distinct conformational changes, which may be either due to different folds of the two types of proteins and/or due to different changes in open and closed conformations and subsequent protease digestion. Further molecular details are necessary to find out the changes, in particular, regions (which are involved in the conformational changes of the two states) of the funnel domain of Mrs2 in the two different types of conformations.

Structure based sequence alignment of Mrs2₄₈₋₃₀₈ and Tm-CorA

The structure based sequence alignment (manually corrected) of Mrs2₄₈₋₃₀₈ with Tm-CorA explores important residues involved not only in formation of the hydrophobic gate of the transporter (see below regulation of magnesium transport in Mrs2 and Tm-CorA) but also in driving of magnesium across the ion conduction pathway in the Mrs2 type of transporters. Glu295 aligned with Asp277 of Tm-CorA, which is highly conserved and is responsible for making an “aspartate ring” and regulates transport in Tm-CorA (Eshaghi et al, 2006; Lunin et al, 2006). In TolC (the outer membrane protein of many multidrug efflux pumps) transport system, an “aspartate ring” formed by the carboxylates of three aspartate residues was shown to determine selectivity, as well as to form a binding site for inhibitory cations (Eshaghi et al, 2006; Higgins et al, 2004). The high conservation of Glu295 in eukaryotic Mrs2 transporters together with the localization at the entrance of the pore and orientation towards the centre of the conduction pathway in the funnel model, suggest that this residue is important for transport or regulation. Experimental evidences are needed to explore the importance of this residue in the regulation of the transporter.

Functional Studies on Mrs2

Regulation of magnesium transport in Mrs2 and Tm-CorA

Until now it is not completely understood how Tm-CorA differentiates between magnesium and other metal ions; it still needs to be studied at the molecular level, but the conserved signature sequence GMN in 2-TM-GxN seems to play a central role in magnesium selection (Eshaghi et al, 2006; Lunin et al, 2006; Payandeh et al, 2008; Payandeh & Pai, 2006). Two important reasons arguing for a role of the GMN motif in magnesium selection are its location at the membrane-periplasm interface and the high conservation of the sequence throughout the phyla (Eshaghi et al, 2006; Lunin et al, 2006; Payandeh & Pai, 2006).

As no three-dimensional structure of the full-length Mrs2 transporter is available, we performed a structure based sequence alignment (manually corrected) of Mrs2₄₈₋₃₀₈ with the soluble domain of Tm-CorA, extended the sequence alignment

at the C-terminus and modeled the complete Mrs2 transporter. Our alignment and model of the pentamer of Mrs2 suggest that Met309, and Val315 are putatively involved in the formation of a hydrophobic gate. A sequence alignment of eukaryotic Mrs2 magnesium transporters showed that Met309 is highly conserved in the whole family, and we named this amino acid gate 1. Analysis of the pentameric Mrs2 model constructed on the known structure of Tm-CorA shows the narrowest constriction of the pore at this residue corresponding to Tm-CorA Met291. In contrast to Met309, a sequence alignment of various eukaryotic Mrs2 homologues indicates that Val315 is less conserved than Met309. We named this amino acid gate 2 (Khan et al., manuscript submitted).

The amino acids, with different characteristics were substituted at these two positions (Met309 and Val315) in Mrs2: bulky (phenylalanine), small (glycine) and negatively charged (glutamic acid). All substitutions of Met309 demonstrated a strong growth reduction on non-fermentable carbon sources in contrast to cells harbouring wild-type *MRS2*. Phe, being a bulky amino acid at position 309 narrowed the pore diameter and thereby reduced Mg^{2+} influx in mag-fura 2 measurements. Substitution of Met309 with Glu increased the magnesium uptake in mag-fura 2 measurement maybe by the enhancement of a negatively charged ring. This may increase the magnesium conductance, either directly due to stronger electrostatic interaction of the Mg^{2+} ion or contribute to the negative charged ring generated by the residues from the tip of the $\alpha 5$ and $\alpha 6$. The dramatic effect was observed in the Gly mutant, which display very robust Mg^{2+} flux and inchoate signs of deregulation of the closing process (Khan et al., manuscript submitted). However, closing of the ion conduction pathway was not completely deregulated as noticed for mutations at position 294 in Tm-CorA (Svidova et al, 2010).

Substitution of Val315 to Glu and Phe had no dramatic effect on growth of the *Saccharomyces cerevisiae* on non-fermentable carbon sources. In line with this result, also Mg^{2+} uptake was less affected by mutations at this position. Mg^{2+} uptake in the Glu mutant was comparable to wild-type *MRS2*. Moreover, the bulky residue Phe was surprisingly well endured at this position and apparently does not constrict the ion conduction pathway to an extent leading to a substantial reduction of magnesium uptake. Only Gly at this position reduced growth partially, which was,

however, less pronounced than in the Met309 mutant. Based on the results from mag-fura 2 measurements this effect is again caused by stronger magnesium uptake due to a widening of the channel at this position.

In addition TMpred analysis (Online server Prediction of Transmembrane Regions and Orientation http://www.ch.embnet.org/software/TMPRED_form.html), using the primary sequence both of Tm-CorA and Mrs2 from *Saccharomyces cerevisiae*, shows that the first transmembrane helix consists of Val293 to Met313 in case of Tm-CorA while in case of Mrs2 it includes residues Val315 to Leu336. Based on the TMpred server prediction the two methionine residues of the hydrophobic gate i.e. Met291 (Tm-CorA) and Met309 (Mrs2) of the two transporters are located outside of the membrane, either in the cytoplasm or the mitochondrial matrix accordingly, while the second set of gating residues Leu294 in Tm-CorA and Val315 in case of Mrs2 are located in the membrane spanning regions of the helices (Khan et al., manuscript submitted).

These observations suggest a higher degree of regulation of the Mrs2 type of transporter relative to Tm-CorA. Mutations at only one of the several positions putatively involved in gating did not completely abolish the function of the transporter to close the pore. The higher negative membrane potential inside the mitochondria causes a strong driving force for the Mg^{2+} ion (Iwatsuki et al, 2000; Rodriguez-Zavala & Moreno-Sanchez, 1998; Sponder et al, 2010). A tight control of the transport activity at more than one site of the ion conduction pathway (pore) may therefore, be essential to ensure a proper Mg^{2+} level in the mitochondrial matrix.

The role of the conserved GMN motif for Mg^{2+} transport and ion selectivity

The GMN motif located at the end of the first transmembrane helix is universally conserved in the CorA-Mrs2-Alr1 superfamily (Knoop et al, 2005). Single mutations within the GMN sequence in *T. maritima* and *S. typhimurium* almost always abolish the transport capability of CorA (Lunin et al, 2006; Szegedy & Maguire, 1999). However, in nature sequence divergence from GMN to GVN or to GIN occurs, but

these transporter transport metals other than magnesium (Knoop et al, 2005). Based on the analyses of the Tm-CorA closed crystal structure, different functions were proposed for this motif. In a homo-pentameric Tm-CorA, the Asn ring of GMN motif obstructs the ion conduction pathway (Lunin et al, 2006; Payandeh & Pai, 2006).

Moreover, the GMN motif was suggested to be critical for positioning of the periplasmic loop (Lunin et al, 2006; Moomaw & Maguire, 2008). This short loop is presumably responsible for the initial binding of magnesium and is supposed to assist in the dehydration/rehydration of ions as well as it acts in cation selectivity (Lunin et al, 2006; Moomaw & Maguire, 2008). The carbonyl groups of the GMN main chain appear to be oriented towards the centre of the conduction pathway (pore) and putatively interact with the hydrated ion and as a result play a role in the dehydration of the metal ion (Moomaw & Maguire, 2008; Payandeh & Pai, 2006). Kolisek et al. (2003) mutated the GMN motif to AMN in Mrs2, which resulted in a completely abolished magnesium transport capability (Kolisek et al, 2003).

In our study, we carried out random mutagenesis of the GMN motif to all possible amino acid combinations in order to find out its potential role in magnesium ion conductance and ion selectivity. We used the *S. typhimurium* strain MM281 which is deficient for all major bacterial magnesium transport systems (CorA, MgtA, MgtB) and screened for mutants, which still retained magnesium transport capability (Svidova S. et al. manuscript submitted).

Interestingly, we found a number of mutants, which were still capable of transporting magnesium with amino acid combinations completely different from GMN. Nevertheless, these mutant variants of *MRS2* required higher expression levels to overcome the growth defect of MM281 cells, exhibiting diminished magnesium transport ability compared to wild-type Mrs2 (Svidova S. et al. manuscript submitted).

These observations indicate that the GMN motif can be replaced by different combinations of amino acids, even though GMN is highly conserved. Furthermore, the high divergence of the functional sequences from the native GMN is surprising. In our analysis of the mutants, a positively charged residue at the first and a

hydrophobic amino acid at the third position were often observed. The second amino acid (methionine) seems to be adaptable to any kind of amino acid.

Almost, all the observed variants showed altered ion selectivity leading to a growth defect on solid media supplemented with Zn^{2+} or Mn^{2+} . Given the fact that no patch clamping data are available for these mutant Mrs2 variants, one can postulate that these effects may be caused by a block of the ion conduction pathway or by excessive transport of these ions, leading to toxic effects (Svidova S. et al. manuscript submitted).

The GMN motif thus seems to work in a concerted manner with the periplasmic loop in selecting and dehydrating the magnesium ion. The GMN motif is located at the membrane-periplasm/inter-membrane space at the very end of the first transmembrane helix (TM1) (Lunin et al, 2006). This location at the entrance of the transporter seems an ideal strategic site for the ion selectivity and the dehydration of the incoming ion (Eshaghi et al, 2006; Payandeh & Pai, 2006). Furthermore, it reveals that not the individual amino acids of this motif are important, but the structural properties generated collectively by this motif. This can be partially accomplished by amino acid combinations of completely different individual properties. It seems that GMN is the best combination of amino acids in nature to ascertain high selectivity and accompanying high transport capability of Mrs2 (Svidova S. et al. manuscript submitted).

The role of the Mrs2 C-terminus

It has been reported that the Lpe10p-Mrs2 chimeric protein consists of the N-terminal moiety of Lpe10p and the C-terminal part of Mrs2, including the long $\alpha 7$ helix responsible for making the funnel domain showed enhance transport capability (Sponder et al, 2010). The higher transport capacity of this chimeric protein, compared to the wild Mrs2-Lpe10p protein may be because this fusion protein contains the conduction pathway of Mrs2 (Sponder et al, 2010). However, the exceptionally long C-terminus of Mrs2 also seems to play an important role in the conduction of Mg^{2+} ions. Based on the crystal structure of Tm-CorA, its biophysical aspects have been discussed and are proposed that the Tm-CorA C-terminus has a

role in the regulation of magnesium transport (Payandeh & Pai, 2006; Quamme, 2010).

Tm-CorA has a highly conserved positively charged sequence at the very C-terminus of TM2, mostly four lysine residues (KKKK) (Lunin et al, 2006). The orientation of the TM2 helices in the structure positions the short, extremely basic C-terminus of the protein at the intracellular side of the membrane, parallel to the two hydrophobic gates of the pore (Lunin et al, 2006; Payandeh & Pai, 2006; Svidova et al, 2010). Considering, the homo-pentameric nature of Tm-CorA, this positions at least 20 lysines residues just below the membrane, near the neck of the cytoplasmic funnel domain, creating a ring of positive charge, known as the “basic sphincter” (Eshaghi et al, 2006; Lunin et al, 2006; Payandeh & Pai, 2006). For the conduction of magnesium ion it seems that the basic sphincter, together with the hydrophobic constriction (hydrophobic gates) formed by Met291 and Leu294 seem to be the primary barrier for Mg²⁺ transport in Tm-CorA (Payandeh et al, 2008; Payandeh & Pai, 2006). This sphincter was proposed to draw the negative charge away from the conduction pathway at this level, in the close conformation and this obstruct the passage of the positively charged Mg²⁺ cation through the pore (Lunin et al, 2006).

According to Tmpred (an online server) TM2 of Mrs2 ends with 1 - 2 non conserved lysine residues. Considering the homo-pentameric nature of Mrs2 this position at least 5 - 10 lysines at the membrane-matrix interface, which resulting in a ring of positively charged residues. The Mrs2 subfamily has C-termini highly variable in length containing almost no conserved primary sequence motives (Weghuber et al, 2006). The Mrs2 family on average has about 20 % of positively charged residues at their C-terminus (Khan et al., manuscript submitted). In addition, the C-terminus of Mrs2 also contains an arginine-rich motif (ARM) (Weghuber et al, 2006). The ARM is located about 40 amino acids away from the end of TM2 in the primary sequence. As no structure information of the C-terminus of Mrs2 is available it is difficult to model a structure of this part as well as to predict its function. Despite its distance from TM2, the ARM of Mrs2 may be located near the membrane in a three dimensional structure and would make a potential candidate for a basic sphincter in Mrs2. Even so, our observations do not conclude any important role of this motif in regulation of transporter. According to Weghuber et al, (2006) deletion of this motif

(400-414 amino acids) resulted in anaemic Mg^{2+} uptake when expressed in low copy vector, but upon high copy expression no defect in growth was observed (Weghuber et al, 2006).

It cannot be ruled out that deletion of a whole motif could result in drastic structural changes and a different orientation of the C-terminus in respect to the funnel domain as well as to the conduction pathway. This makes it difficult to conclude here the importance of this motif for Mg^{2+} transport. To get more insight into the function of the positively charged KRRRK (402-406) stretch, we substitute Glu at these positions, in order to incorporate the opposite charge. This mutant had no defect in growth on non-fermentable carbon sources and slightly increased Mg^{2+} influx in mag-fura 2 measurements were observed. The observed enhanced transport activity may be caused by the negatively charged residues contributing to the formation of a negatively charged ring, which would eventually result in a stronger electrostatic interaction with the Mg^{2+} . On the other hand, this mutation had no pronounced effect on regulation of the transporter (Khan et al., manuscript submitted).

Interestingly, deletion of nearly the whole C-terminus (deletion after Thr376) turned out in a growth defect on non-fermentable carbon sources, equal to *mrs2Δ* cells. This is in line with the observed strong decrease of Mg^{2+} transport capacity in mag-fura 2 measurements of isolated mitochondria (Khan et al., manuscript submitted).

Taken together, the small, non-conserved positively charged stretch (KRRRK, 402-406) at the C-terminus seems not to be critical for the function of Mrs2 transporter. On the other hand, deletion of the C-terminus (deletion of 94 residues at the C-terminus), diminish the transport activity. Likewise the ARM, the whole C-terminus of Mrs2 displays an excess of positively charged amino acid residues (24 positively charged out of 107 of total). The C-terminus deletion did not caused instability of the protein; rather protein levels were slightly raised. These observations demonstrate that the KRRRK-stretch is not important for the function of Mrs2 transporter, but the overall surplus of positively charged residues at the C-terminus of Mrs2 might fulfill a similar function like that of the “basic sphincter” in Tm-

CorA. This is also in agreement with the measurement of Mg^{2+} influx of the two chimeric Mrs2/Lpe10p proteins, where the fusion protein Mrs2-Lpe10p with out the Mrs2 C-terminus demonstrated weaker Mg^{2+} uptake in isolated mitochondria magnifera 2 measurements (Sponder et al, 2010).

Moreover, it has been proposed for Tm-CorA that the C-terminus is directly involved in opening and closing of the transporter by pulling out the negatively charged residues from the ion conduction pathway. Accordingly, deletion of the whole C-terminus may result in decreasing opening and closing capabilities of the transporter.

Magnesium sensing sites in Mrs2 and Tm-CorA

Two divalent cation binding sites have been identified by Eshaghi et al. at the protomer-protomer interface within the funnel domain of Tm-CorA (Eshaghi et al, 2006; Lunin et al, 2006; Payandeh et al, 2008) and have been characterized as a “divalent cation sensor (DCS)”. The two sites coordinate the metal ion differently: the first was found to bind the cation directly by two carboxylates of Asp89 and Asp253, while the second, composed of Glu88, Asp175, Asp253 and His257, coordinating the hydrated metal cation indirectly (Eshaghi et al, 2006). According to a model for regulation of Tm-CorA, a torque is produced at the bottom of the stalk helix ($\alpha 7$) by releasing bound magnesium from the magnesium binding sites and move up toward the hydrophobic gate of the ion conduction pathway (Payandeh et al, 2008; Payandeh & Pai, 2006).

Based on the structural comparison of Tm-CorA and our model of the Mrs2₂₄₈₋₃₀₈ funnel, we identified the residues that would form a potential DCS in Mrs2, Asp97 from one subunit and Glu270 from adjacent subunit, corresponding to the DCS1 of Tm-CorA. A sequence alignment of eukaryotic magnesium transporters reveals that the Asp97 and Glu270 residues, possibly coordinating the metal ion, are highly conserved in the whole subfamily. In the Mrs2₂₄₈₋₃₀₈ crystal structure Glu270 is located at the N-terminus of $\alpha 7$ corresponding to the position of Asp253 in Tm-CorA.

Many efforts have been made to co-crystallize a monomer of Mrs2 with magnesium as well as to soak in the metals but no electron density has been observed for the metal ion. The addition of magnesium in the crystallization environment did not change the structure of the native protein and corroborate the notion that DCS is composed of ligands coming from adjacent subunits in the pentamer. Consequently, a single subunit cannot bind divalent ions with high affinity.

In order to test the involvement of these amino acids in regulation of the channel, we performed site-directed mutagenesis of Asp97 to Ala, Phe and Trp. Amazingly, these mutants do not displayed any growth defect on non-fermentable carbon sources. Accordingly, no significant differences between wild-type Mrs2 and the mutant proteins in Mg^{2+} uptake measurements in isolated mitochondria could be observed, suggesting that a magnesium sensing site(s) composed of multiple ligand residues cannot be abrogated by a single residue mutation in Mrs2.

REFERENCES

Altura BM (1994) Introduction: importance of Mg in physiology and medicine and the need for ion selective electrodes. *Scand J Clin Lab Invest Suppl* **217**: 5-9

Anderson GG, Yahr TL, Lovewell RR, O'Toole GA (2010) The *Pseudomonas aeruginosa* magnesium transporter MgtE inhibits transcription of the type III secretion system. *Infect Immun* **78**: 1239-1249

Ausubel FM, Brent, R., Kingston, R. E., Moore, D. D., Seidman, J. G., Smith, J. A., and Struhl, K. (1994) *Current Protocols in Molecular Biology*, New York: Greene Publishing Associates and Wiley-Interscience.

Banachowicz E (2006) Light scattering studies of proteins under compression. *Biochim Biophys Acta* **1764**: 405-413

Blanc-Potard AB, Groisman EA (1997) The *Salmonella* selC locus contains a pathogenicity island mediating intramacrophage survival. *EMBO J* **16**: 5376-5385

Blattner FR, Plunkett G, 3rd, Bloch CA, Perna NT, Burland V, Riley M, Collado-Vides J, Glasner JD, Rode CK, Mayhew GF, Gregor J, Davis NW, Kirkpatrick HA, Goeden MA, Rose DJ, Mau B, Shao Y (1997) The complete genome sequence of *Escherichia coli* K-12. *Science* **277**: 1453-1462

Borgstahl GE (2007) How to use dynamic light scattering to improve the likelihood of growing macromolecular crystals. *Methods Mol Biol* **363**: 109-129

Bruce Alberts AJ, Julian Lewis, Martin Raff, Keith Roberts, and Peter Walter (2002) *Molecular Biology of the Cell*, Vol. 4, 4th edn. New York.

Bui DM, Gregan J, Jarosch E, Ragnini A, Schweyen RJ (1999) The bacterial magnesium transporter CorA can functionally substitute for its putative homologue Mrs2p in the yeast inner mitochondrial membrane. *J Biol Chem* **274**: 20438-20443

Callera GE, He Y, Yogi A, Montezano AC, Paravicini T, Yao G, Touyz RM (2009) Regulation of the novel Mg²⁺ transporter transient receptor potential melastatin 7 (TRPM7) cation channel by bradykinin in vascular smooth muscle cells. *J Hypertens* **27**: 155-166

Carvalho AL, Trincao J, Romao MJ (2009) X-ray crystallography in drug discovery. *Methods Mol Biol* **572**: 31-56

Cecere D, Bruno A, Minutolo P, D'Alessio A (2003) DLS measurements on nanoparticles produced in laminar premixed flames. *Synthetic Metals* **139**: 653-656

Chayen N, Dieckmann M, Dierks K, Fromme P (2004) Size and Shape Determination of Proteins in Solution by a Noninvasive Depolarized Dynamic Light Scattering Instrument. *Annals of the New York Academy of Sciences* **1027**: 20-27

Chubanov V, Waldegger S, Mederos y Schnitzler M, Vitzthum H, Sassen MC, Seyberth HW, Konrad M, Gudermann T (2004) Disruption of TRPM6/TRPM7 complex formation by a mutation in the TRPM6 gene causes hypomagnesemia with secondary hypocalcemia. *Proc Natl Acad Sci U S A* **101**: 2894-2899

Cregg JM, Cereghino JL, Shi J, Higgins DR (2000) Recombinant protein expression in *Pichia pastoris*. *Mol Biotechnol* **16**: 23-52

Cromie MJ, Shi Y, Latifi T, Groisman EA (2006) An RNA sensor for intracellular Mg(2+). *Cell* **125**: 71-84

D'Arcy A (1994) Crystallizing proteins - a rational approach? *Acta Crystallogr D Biol Crystallogr* **50**: 469-471

Daley DO, Rapp M, Granseth E, Melen K, Drew D, von Heijne G (2005) Global topology analysis of the *Escherichia coli* inner membrane proteome. *Science* **308**: 1321-1323

Diebler H, M. Eigen, G. Ilgenfritz, G. Maass, and R., Winkler. (1969) Kinetics and mechanism of reactions of main group metal ions with biological carriers. *Pure Appl Chem* **20**: 93-115

Elin RJ (1987) Assessment of magnesium status. *Clin Chem* **33**: 1965-1970

Elin RJ (1994) Magnesium: the fifth but forgotten electrolyte. *Am J Clin Pathol* **102**: 616-622

Ericsson UB, Hallberg BM, Detitta GT, Dekker N, Nordlund P (2006) Thermofluor-based high-throughput stability optimization of proteins for structural studies. *Anal Biochem* **357**: 289-298

Eshaghi S, Hedren M, Nasser MI, Hammarberg T, Thornell A, Nordlund P (2005) An efficient strategy for high-throughput expression screening of recombinant integral membrane proteins. *Protein Sci* **14**: 676-683

Eshaghi S, Niegowski D, Kohl A, Martinez Molina D, Lesley SA, Nordlund P (2006) Crystal structure of a divalent metal ion transporter CorA at 2.9 angstrom resolution. *Science* **313**: 354-357

Fan Y, Joachimiak A (2010) Enhanced crystal packing due to solvent reorganization through reductive methylation of lysine residues in oxidoreductase from *Streptococcus pneumoniae*. *Journal of Structural and Functional Genomics* **11**: 101-111

Fontana A, de Laureto PP, Spolaore B, Frare E, Picotti P, Zamboni M (2004) Probing protein structure by limited proteolysis. *Acta Biochim Pol* **51**: 299-321

Gao X, Bain K, Bonanno JB, Buchanan M, Henderson D, Lorimer D, Marsh C, Reynes JA, Sauder JM, Schwinn K, Thai C, Burley SK (2005) High-throughput limited proteolysis/mass spectrometry for protein domain elucidation. *J Struct Funct Genomics* **6**: 129-134

Garcia-Calderon CB, Casadesus J, Ramos-Morales F (2007) Rcs and PhoPQ regulatory overlap in the control of *Salmonella enterica* virulence. *J Bacteriol* **189**: 6635-6644

Garcia Vescovi E, Soncini FC, Groisman EA (1996) Mg^{2+} as an extracellular signal: environmental regulation of *Salmonella* virulence. *Cell* **84**: 165-174

Gardner RC (2003) Genes for magnesium transport. *Curr Opin Plant Biol* **6**: 263-267

Gebert M, Meschenmoser K, Svidova S, Weghuber J, Schweyen R, Eifler K, Lenz H, Weyand K, Knoop V (2009) A root-expressed magnesium transporter of the MRS2/MGT gene family in *Arabidopsis thaliana* allows for growth in low- Mg^{2+} environments. *Plant Cell* **21**: 4018-4030

Goytain A, Quamme GA (2005a) Functional characterization of ACDP2 (ancient conserved domain protein), a divalent metal transporter. *Physiol Genomics* **22**: 382-389

Goytain A, Quamme GA (2005b) Functional characterization of human SLC41A1, a Mg^{2+} transporter with similarity to prokaryotic MgtE Mg^{2+} transporters. *Physiol Genomics* **21**: 337-342

Goytain A, Quamme GA (2005c) Identification and characterization of a novel mammalian Mg^{2+} transporter with channel-like properties. *BMC Genomics* **6**: 48

Graschopf A, Stadler JA, Hoellerer MK, Eder S, Sieghardt M, Kohlwein SD, Schweyen RJ (2001) The yeast plasma membrane protein Alr1 controls Mg^{2+} homeostasis and is subject to Mg^{2+} -dependent control of its synthesis and degradation. *J Biol Chem* **276**: 16216-16222

Gregan J, Bui DM, Pillich R, Fink M, Zsurka G, Schweyen RJ (2001a) The mitochondrial inner membrane protein Lpe10p, a homologue of Mrs2p, is essential for magnesium homeostasis and group II intron splicing in yeast. *Mol Gen Genet* **264**: 773-781

Gregan J, Kolisek M, Schweyen RJ (2001b) Mitochondrial $Mg(2+)$ homeostasis is critical for group II intron splicing in vivo. *Genes Dev* **15**: 2229-2237

Groisman EA (1998) The ins and outs of virulence gene expression: Mg^{2+} as a regulatory signal. *Bioessays* **20**: 96-101

Groisman EA (2001) The pleiotropic two-component regulatory system PhoP-PhoQ. *J Bacteriol* **183**: 1835-1842

- Grubbs RD, Maguire ME (1987) Magnesium as a regulatory cation: criteria and evaluation. *Magnesium* **6**: 113-127
- Gunzel D, Amasheh S, Pfaffenbach S, Richter JF, Kausalya PJ, Hunziker W, Fromm M (2009) Claudin-16 affects transcellular Cl⁻ secretion in MDCK cells. *J Physiol* **587**: 3777-3793
- Gunzel D, Kucharski LM, Kehres DG, Romero MF, Maguire ME (2006) The MgtC virulence factor of *Salmonella enterica* serovar Typhimurium activates Na⁽⁺⁾,K⁽⁺⁾-ATPase. *J Bacteriol* **188**: 5586-5594
- Hanahan D (1983) Studies on transformation of *Escherichia coli* with plasmids. *J Mol Biol* **166**: 557-580
- Hattori M, Iwase N, Furuya N, Tanaka Y, Tsukazaki T, Ishitani R, Maguire ME, Ito K, Maturana A, Nureki O (2009) Mg²⁺-dependent gating of bacterial MgtE channel underlies Mg²⁺ homeostasis. *EMBO J* **28**: 3602-3612
- Hattori M, Tanaka Y, Fukai S, Ishitani R, Nureki O (2007a) Crystal structure of the MgtE Mg²⁺ transporter. *Nature* **448**: 1072-1075
- Hattori M, Tanaka Y, Fukai S, Ishitani R, Nureki O (2007b) Crystallization and preliminary X-ray diffraction analysis of the full-length Mg²⁺ transporter MgtE. *Acta Crystallogr Sect F Struct Biol Cryst Commun* **63**: 682-684
- Higgins MK, Eswaran J, Edwards P, Schertler GF, Hughes C, Koronakis V (2004) Structure of the ligand-blocked periplasmic entrance of the bacterial multidrug efflux protein TolC. *J Mol Biol* **342**: 697-702
- Hmiel SP, Snavelly MD, Florer JB, Maguire ME, Miller CG (1989) Magnesium transport in *Salmonella typhimurium*: genetic characterization and cloning of three magnesium transport loci. *J Bacteriol* **171**: 4742-4751
- Hmiel SP, Snavelly MD, Miller CG, Maguire ME (1986) Magnesium transport in *Salmonella typhimurium*: characterization of magnesium influx and cloning of a transport gene. *J Bacteriol* **168**: 1444-1450
- Holm L, Sander C (1996) Mapping the protein universe. *Science* **273**: 595-603
- Hubner CA, Jentsch TJ (2008) Channelopathies of transepithelial transport and vesicular function. *Adv Genet* **63**: 113-152
- Ignoul S, Eggermont J (2005) CBS domains: structure, function, and pathology in human proteins. *Am J Physiol Cell Physiol* **289**: C1369-1378
- Ikari A, Okude C, Sawada H, Yamazaki Y, Sugatani J, Miwa M (2008) TRPM6 expression and cell proliferation are up-regulated by phosphorylation of ERK1/2 in renal epithelial cells. *Biochem Biophys Res Commun* **369**: 1129-1133

Invitrogen. A Manual of Methods for Expression of Recombinant Proteins in *Pichia pastoris*. *Pichia Expression Kit*, Carlsbad.

Invitrogen. (2002) pPIC3.5K/pAO815. In Invitrogen (ed.). Invitrogen Corporation., Vol. D, pp. 25-0156

Iseri LT, French JH (1984) Magnesium: nature's physiologic calcium blocker. *Am Heart J* **108**: 188-193

Iwatsuki H, Lu YM, Yamaguchi K, Ichikawa N, Hashimoto T (2000) Binding of an intrinsic ATPase inhibitor to the F(1)FoATPase in phosphorylating conditions of yeast mitochondria. *J Biochem* **128**: 553-559

Jamieson A M, Mc DME (1979) Structural Characterization of Polymers in Solution by Quasielastic Laser Light Scattering. In *Probing Polymer Structures* Vol. 174, 10, pp 163-205. AMERICAN CHEMICAL SOCIETY

Kato A, Groisman EA (2008) The PhoQ/PhoP regulatory network of *Salmonella enterica*. *Adv Exp Med Biol* **631**: 7-21

Kehres DG, Lawyer CH, Maguire ME (1998) The CorA magnesium transporter gene family. *Microb Comp Genomics* **3**: 151-169

Kehres DG, Maguire ME (2002) Structure, properties and regulation of magnesium transport proteins. *Biometals* **15**: 261-270

Khan MB, Sjoblom B, Schweyen RJ, Djinovic-Carugo K (2010) Crystallization and preliminary X-ray diffraction analysis of the N-terminal domain of Mrs2, a magnesium ion transporter from yeast inner mitochondrial membrane. *Acta Crystallographica Section F* **66**: 658-661

Kier LD, Weppelman RM, Ames BN (1979) Regulation of nonspecific acid phosphatase in *Salmonella*: *phoN* and *phoP* genes. *J Bacteriol* **138**: 155-161

Kim Y, Quartey P, Li H, Volkart L, Hatzos C, Chang C, Nocek B, Cuff M, Osipiuk J, Tan K, Fan Y, Bigelow L, Maltseva N, Wu R, Borovilos M, Duggan E, Zhou M, Binkowski TA, Zhang RG, Joachimiak A (2008) Large-scale evaluation of protein reductive methylation for improving protein crystallization. *Nat Methods* **5**: 853-854

Knoop V, Groth-Malonek M, Gebert M, Eifler K, Weyand K (2005) Transport of magnesium and other divalent cations: evolution of the 2-TM-GxN proteins in the MIT superfamily. *Mol Genet Genomics* **274**: 205-216

Kolisek M, Launay P, Beck A, Sponder G, Serafini N, Brenkus M, Froschauer EM, Martens H, Fleig A, Schweigel M (2008) SLC41A1 is a novel mammalian Mg²⁺ carrier. *J Biol Chem* **283**: 16235-16247

Kolisek M, Zsurka G, Samaj J, Weghuber J, Schweyen RJ, Schweigel M (2003) Mrs2p is an essential component of the major electrophoretic Mg²⁺ influx system in mitochondria. *EMBO J* **22**: 1235-1244

- Kucharski LM, Lubbe WJ, Maguire ME (2000) Cation hexaammines are selective and potent inhibitors of the CorA magnesium transport system. *J Biol Chem* **275**: 16767-16773
- Kyte J, Doolittle RF (1982) A simple method for displaying the hydropathic character of a protein. *J Mol Biol* **157**: 105-132
- Laemmli UK (1970) Cleavage of structural proteins during the assembly of the head of bacteriophage T4. *Nature* **227**: 680-685
- Lalonde S, Wipf D, Frommer WB (2004) Transport mechanisms for organic forms of carbon and nitrogen between source and sink. *Annu Rev Plant Biol* **55**: 341-372
- Lee J-m, Gardner R (2006a) Residues of the yeast ALR1 protein that are critical for Magnesium uptake. *Current Genetics* **49**: 7-20
- Lee JM, Gardner RC (2006b) Residues of the yeast ALR1 protein that are critical for magnesium uptake. *Curr Genet* **49**: 7-20
- Li L, Tutone AF, Drummond RS, Gardner RC, Luan S (2001) A novel family of magnesium transport genes in Arabidopsis. *Plant Cell* **13**: 2761-2775
- Lunin VV, Dobrovetsky E, Khutoreskaya G, Zhang R, Joachimiak A, Doyle DA, Bochkarev A, Maguire ME, Edwards AM, Koth CM (2006) Crystal structure of the CorA Mg²⁺ transporter. *Nature* **440**: 833-837
- Lusk JE, Kennedy EP (1969) Magnesium transport in Escherichia coli. *J Biol Chem* **244**: 1653-1655
- MacDiarmid CW, Gardner RC (1998) Overexpression of the Saccharomyces cerevisiae magnesium transport system confers resistance to aluminum ion. *J Biol Chem* **273**: 1727-1732
- Maguire ME (1992) MgtA and MgtB: Prokaryotic P-type ATPases that mediate Mg influx. *Journal of Bioenergetics and Biomembranes* **24**: 319-328
- Maguire ME (2006) Magnesium transporters: properties, regulation and structure. *Front Biosci* **11**: 3149-3163
- Maguire ME, Cowan JA (2002) Magnesium chemistry and biochemistry. *Biometals* **15**: 203-210
- Maguire ME, Snavely MD, Leizman JB, Gura S, Bagga D, Tao T, Smith DL (1992) Mg²⁺ transporting P-type ATPases of Salmonella typhimurium. Wrong way, wrong place enzymes. *Ann N Y Acad Sci* **671**: 244-255; discussion 255-246
- Mobasher A, Mobasher R, Francis MJ, Trujillo E, Alvarez de la Rosa D, Martin-Vasallo P (1998) Ion transport in chondrocytes: membrane transporters involved in

intracellular ion homeostasis and the regulation of cell volume, free $[Ca^{2+}]$ and pH. *Histol Histopathol* **13**: 893-910

Moncrief MB, Maguire ME (1998) Magnesium and the role of MgtC in growth of *Salmonella typhimurium*. *Infect Immun* **66**: 3802-3809

Monsieurs P, De Keersmaecker S, Navarre WW, Bader MW, De Smet F, McClelland M, Fang FC, De Moor B, Vanderleyden J, Marchal K (2005) Comparison of the PhoPQ Regulon in *Escherichia coli* and *Salmonella typhimurium*. *Journal of Molecular Evolution* **60**: 462-474

Monteilh-Zoller MK, Hermosura MC, Nadler MJ, Scharenberg AM, Penner R, Fleig A (2003) TRPM7 provides an ion channel mechanism for cellular entry of trace metal ions. *J Gen Physiol* **121**: 49-60

Moomaw AS, Maguire ME (2008) The unique nature of Mg^{2+} channels. *Physiology (Bethesda)* **23**: 275-285

Nadler MJ, Hermosura MC, Inabe K, Perraud AL, Zhu Q, Stokes AJ, Kurosaki T, Kinet JP, Penner R, Scharenberg AM, Fleig A (2001) LTRPC7 is a Mg.ATP-regulated divalent cation channel required for cell viability. *Nature* **411**: 590-595

Nelson DL, Kennedy EP (1971) Magnesium transport in *Escherichia coli*. Inhibition by cobaltous ion. *J Biol Chem* **246**: 3042-3049

Neurath H (1980) Limited proteolysis, protein folding and physiological regulation. In *Protein Folding*. Elsevier/North Holland Biomedical Press, Amsterdam-New York: 501-504

Niegowski D, Eshaghi S (2007) The CorA family: Structure and function revisited. *Cellular and Molecular Life Sciences* **64**: 2564-2574

Niesen FH, Berglund H, Vedadi M (2007) The use of differential scanning fluorimetry to detect ligand interactions that promote protein stability. *Nat Protoc* **2**: 2212-2221

Odblom MP, Handy RD (1999) A novel DIDS-sensitive, anion-dependent $Mg(2+)$ efflux pathway in rat ventricular myocytes. *Biochem Biophys Res Commun* **264**: 334-337

Papp-Wallace KM, Maguire ME (2007) Bacterial homologs of eukaryotic membrane proteins: the 2-TM-GxN family of $Mg(2+)$ transporters. *Mol Membr Biol* **24**: 351-356

Papp KM, Maguire ME (2004) The CorA Mg^{2+} transporter does not transport Fe^{2+} . *J Bacteriol* **186**: 7653-7658

Park MH, Wong BB, Lusk JE (1976) Mutants in three genes affecting transport of magnesium in *Escherichia coli*: genetics and physiology. *J Bacteriol* **126**: 1096-1103

- Payandeh J, Li C, Ramjeesingh M, Poduch E, Bear CE, Pai EF (2008) Probing structure-function relationships and gating mechanisms in the CorA Mg²⁺ transport system. *J Biol Chem* **283**: 11721-11733
- Payandeh J, Pai EF (2006) A structural basis for Mg²⁺ homeostasis and the CorA translocation cycle. *EMBO J* **25**: 3762-3773
- Pisat NP, Pandey A, Macdiarmid CW (2009) MNR2 regulates intracellular magnesium storage in *Saccharomyces cerevisiae*. *Genetics* **183**: 873-884
- Quamme GA (2010) Molecular identification of ancient and modern mammalian magnesium transporters. *Am J Physiol Cell Physiol* **298**: C407-429
- Quamme GA, Rabkin SW (1990) Cytosolic free magnesium in cardiac myocytes: identification of a Mg²⁺ influx pathway. *Biochem Biophys Res Commun* **167**: 1406-1412
- Retamal P, Castillo-Ruiz M, Mora GC (2009) Characterization of MgtC, a virulence factor of *Salmonella enterica* Serovar Typhi. *PLoS ONE* **4**: e5551
- Rodriguez-Zavala JS, Moreno-Sanchez R (1998) Modulation of oxidative phosphorylation by Mg²⁺ in rat heart mitochondria. *J Biol Chem* **273**: 7850-7855
- Romani A (2007) Regulation of magnesium homeostasis and transport in mammalian cells. *Arch Biochem Biophys* **458**: 90-102
- Romani A, Scarpa A (1992) Regulation of cell magnesium. *Arch Biochem Biophys* **298**: 1-12
- Roux B, MacKinnon R (1999) The cavity and pore helices in the KcsA K⁺ channel: electrostatic stabilization of monovalent cations. *Science* **285**: 100-102
- Rude RK (1998) Magnesium Deficiency: A Cause of Heterogenous Disease in Humans. *Journal of Bone and Mineral Research* **13**: 749-758
- Ryazanova LV, Rondon LJ, Zierler S, Hu Z, Galli J, Yamaguchi TP, Mazur A, Fleig A, Ryazanov AG (2010) TRPM7 is essential for Mg²⁺ homeostasis in mammals. *Nat Commun* **1**: 109
- Rypniewski WR, Holden HM, Rayment I (1993) Structural consequences of reductive methylation of lysine residues in hen egg white lysozyme: an X-ray analysis at 1.8-Å resolution. *Biochemistry* **32**: 9851-9858
- Saier MH, Jr. (2000) A functional-phylogenetic classification system for transmembrane solute transporters. *Microbiol Mol Biol Rev* **64**: 354-411
- Schlingmann KP, Weber S, Peters M, Niemann Nejsum L, Vitzthum H, Klingel K, Kratz M, Haddad E, Ristoff E, Dinour D, Syrrou M, Nielsen S, Sassen M, Waldegger S, Seyberth HW, Konrad M (2002) Hypomagnesemia with secondary hypocalcemia

is caused by mutations in TRPM6, a new member of the TRPM gene family. *Nat Genet* **31**: 166-170

Schmitz C, Perraud AL, Johnson CO, Inabe K, Smith MK, Penner R, Kurosaki T, Fleig A, Scharenberg AM (2003) Regulation of vertebrate cellular Mg²⁺ homeostasis by TRPM7. *Cell* **114**: 191-200

Schock I, Gregan J, Steinhäuser S, Schweyen R, Brennicke A, Knoop V (2000) A member of a novel Arabidopsis thaliana gene family of candidate Mg²⁺ ion transporters complements a yeast mitochondrial group II intron-splicing mutant. *Plant J* **24**: 489-501

Schweigel M, Park HS, Etschmann B, Martens H (2006) Characterization of the Na⁺-dependent Mg²⁺ transport in sheep ruminal epithelial cells. *Am J Physiol Gastrointest Liver Physiol* **290**: G56-65

Schweigel M, Vormann J, Martens H (2000) Mechanisms of Mg(2+) transport in cultured ruminal epithelial cells. *Am J Physiol Gastrointest Liver Physiol* **278**: G400-408

Shaul O (2002) Magnesium transport and function in plants: the tip of the iceberg. *Biometals* **15**: 309-323

Shaul O, Hilgemann DW, de-Almeida-Engler J, Van Montagu M, Inz D, Galili G (1999) Cloning and characterization of a novel Mg(2+)/H(+) exchanger. *EMBO J* **18**: 3973-3980

Silver S (1969) Active transport of magnesium in escherichia coli. *Proc Natl Acad Sci U S A* **62**: 764-771

Silver S, Clark D (1971) Magnesium transport in Escherichia coli. *J Biol Chem* **246**: 569-576

Simon DB, Lu Y, Choate KA, Velazquez H, Al-Sabban E, Praga M, Casari G, Bettinelli A, Colussi G, Rodriguez-Soriano J, McCredie D, Milford D, Sanjad S, Lifton RP (1999) Paracellin-1, a renal tight junction protein required for paracellular Mg²⁺ resorption. *Science* **285**: 103-106

Smith DL, Tao T, Maguire ME (1993a) Membrane topology of a P-type ATPase. The MgtB magnesium transport protein of Salmonella typhimurium. *J Biol Chem* **268**: 22469-22479

Smith RL, Banks JL, Snavelly MD, Maguire ME (1993b) Sequence and topology of the CorA magnesium transport systems of Salmonella typhimurium and Escherichia coli. Identification of a new class of transport protein. *J Biol Chem* **268**: 14071-14080

Smith RL, Kaczmarek MT, Kucharski LM, Maguire ME (1998a) Magnesium transport in Salmonella typhimurium: regulation of mgtA and mgtCB during invasion of epithelial and macrophage cells. *Microbiology* **144 (Pt 7)**: 1835-1843

- Smith RL, Maguire ME (1995) Distribution of the CorA Mg²⁺ transport system in gram-negative bacteria. *J Bacteriol* **177**: 1638-1640
- Smith RL, Maguire ME (1998) Microbial magnesium transport: unusual transporters searching for identity. *Mol Microbiol* **28**: 217-226
- Smith RL, Szegedy MA, Kucharski LM, Walker C, Wiet RM, Redpath A, Kaczmarek MT, Maguire ME (1998b) The CorA Mg²⁺ transport protein of Salmonella typhimurium. Mutagenesis of conserved residues in the third membrane domain identifies a Mg²⁺ pore. *J Biol Chem* **273**: 28663-28669
- Snavely MD, Florer JB, Miller CG, Maguire ME (1989) Magnesium transport in Salmonella typhimurium: 28Mg²⁺ transport by the CorA, MgtA, and MgtB systems. *J Bacteriol* **171**: 4761-4766
- Snavely MD, Miller CG, Maguire ME (1991) The mgtB Mg²⁺ transport locus of Salmonella typhimurium encodes a P-type ATPase. *J Biol Chem* **266**: 815-823
- Soncini FC, Garcia Vescovi E, Solomon F, Groisman EA (1996) Molecular basis of the magnesium deprivation response in Salmonella typhimurium: identification of PhoP-regulated genes. *J Bacteriol* **178**: 5092-5099
- Sponder G, Svidova S, Schindl R, Wieser S, Schweyen RJ, Romanin C, Froschauer EM, Weghuber J (2010) Lpe10p modulates the activity of the Mrs2p-based yeast mitochondrial Mg²⁺ channel. *FEBS J* **277**: 3514-3525
- Stephenson K, Hoch JA (2002) Histidine kinase-mediated signal transduction systems of pathogenic microorganisms as targets for therapeutic intervention. *Curr Drug Targets Infect Disord* **2**: 235-246
- Svidova S, Sponder G, Schweyen RJ, Djinojic-Carugo K (2010) Functional analysis of the conserved hydrophobic gate region of the magnesium transporter CorA. *Biochim Biophys Acta*
- Szegedy MA, Maguire ME (1999) The CorA Mg(2+) transport protein of Salmonella typhimurium. Mutagenesis of conserved residues in the second membrane domain. *J Biol Chem* **274**: 36973-36979
- Tan K, Sather A, Robertson JL, Moy S, Roux B, Joachimiak A (2009) Structure and electrostatic property of cytoplasmic domain of ZntB transporter. *Protein Sci* **18**: 2043-2052
- Tao T, Snavely MD, Farr SG, Maguire ME (1995) Magnesium transport in Salmonella typhimurium: mgtA encodes a P-type ATPase and is regulated by Mg²⁺ in a manner similar to that of the mgtB P-type ATPase. *J Bacteriol* **177**: 2654-2662
- Teramoto T, Lambie EJ, Iwasaki K (2005) Differential regulation of TRPM channels governs electrolyte homeostasis in the C. elegans intestine. *Cell Metab* **1**: 343-354

- Townsend DE, Esenwine AJ, George J, 3rd, Bross D, Maguire ME, Smith RL (1995) Cloning of the *mgtE* Mg^{2+} transporter from *Providencia stuartii* and the distribution of *mgtE* in gram-negative and gram-positive bacteria. *J Bacteriol* **177**: 5350-5354
- Vescovi EG, Ayala YM, Di Cera E, Groisman EA (1997) Characterization of the bacterial sensor protein PhoQ. Evidence for distinct binding sites for Mg^{2+} and Ca^{2+} . *J Biol Chem* **272**: 1440-1443
- Wabakken T, Rian E, Kveine M, Aasheim HC (2003) The human solute carrier SLC41A1 belongs to a novel eukaryotic subfamily with homology to prokaryotic *MgtE* Mg^{2+} transporters. *Biochem Biophys Res Commun* **306**: 718-724
- Walter TS, Meier C, Assenberg R, Au KF, Ren J, Verma A, Nettleship JE, Owens RJ, Stuart DI, Grimes JM (2006) Lysine methylation as a routine rescue strategy for protein crystallization. *Structure* **14**: 1617-1622
- Warren MA, Kucharski LM, Veenstra A, Shi L, Grulich PF, Maguire ME (2004) The *CorA* Mg^{2+} transporter is a homotetramer. *J Bacteriol* **186**: 4605-4612
- Weghuber J, Dieterich F, Froschauer EM, Svidova S, Schweyen RJ (2006) Mutational analysis of functional domains in *Mrs2p*, the mitochondrial Mg^{2+} channel protein of *Saccharomyces cerevisiae*. *FEBS J* **273**: 1198-1209
- Wiesenberger G, Waldherr M, Schweyen RJ (1992) The nuclear gene *MRS2* is essential for the excision of group II introns from yeast mitochondrial transcripts in vivo. *J Biol Chem* **267**: 6963-6969
- Wipf D, Ludewig U, Tegeder M, Rentsch D, Koch W, Frommer WB (2002) Conservation of amino acid transporters in fungi, plants and animals. *Trends Biochem Sci* **27**: 139-147
- Worlock AJ, Smith RL (2002) *ZntB* is a novel Zn^{2+} transporter in *Salmonella enterica* serovar Typhimurium. *J Bacteriol* **184**: 4369-4373
- Xia Y, Lundback AK, Sahaf N, Nordlund G, Brzezinski P, Eshaghi S (2011) Co^{2+} Selectivity of *Thermotoga maritima* *CorA* and Its Inability to Regulate Mg^{2+} Homeostasis Present a New Class of *CorA* Proteins. *J Biol Chem* **286**: 16525-16532
- Yan Q (2003) *Membrane Transporters Methods and Protocols*, Vol. 227: Humana Press.
- Zhou H, Clapham DE (2009) Mammalian *MagT1* and *TUSC3* are required for cellular magnesium uptake and vertebrate embryonic development. *Proc Natl Acad Sci U S A* **106**: 15750-15755
- Zsurka G, Gregan J, Schweyen RJ (2001) The human mitochondrial *Mrs2* protein functionally substitutes for its yeast homologue, a candidate magnesium transporter. *Genomics* **72**: 158-168

ACKNOWLEDGEMENTS

All praises and thanks to the grace of God (**ALLAH ALMIGHTY**) Who is the supreme source of all knowledge to a human being. HE gave human being with rational power and understanding supremacy and renders him spiritual insights enabling him to discover his “Self” knows his Creator through His wonders and conquers Nature. Submit in obeisance, I before my Lord, WHO bestows me to fortitude and impetus to achieve this task and enlighten a drop of already existing ocean of knowledge. WHO made me reach at present pedestal of knowledge with the ability of doing thrilling, sensational, adventurous, novel and path bearing.

It appears impossible to pay thanks to my kind supervisor **Kristina Djinović-Carugo** her keen interest, genial behavior and guidance throughout this task, helped me to complete the desired task in time. I also feel very grateful to Prof. Rudolf J. Schweyen (late) from the Department of Microbiology, Immunobiology and Genetics for a useful discussion during the initial phase of my study.

Extremely thanks to **Björn Sjöblom** for his kind scientific teaching, starting from cloning to structure analysis.

Thanks to **Oliviero Carugo**, especially in the beginning of the study and at the ending.

Special thanks to **Peggy Stolt-Bergner** for being very kind and helpful when ever I need her assistance, I always find her lab open, free accessible at any time.

This acknowledgement will be prenominal, and I am confident will be failing in my duty if I do not pay exceptional thanks to **Claudia Schreiner** for innovating into

Vienna style of life, maintenance of clean and organized laboratory and providing cookies, whenever I need energy and chatting in deutscher Sprache (Danke Claudia).

Extremely thanks to **Gerhard Sponder**, **Soňa Svidová** and Markus Aleschko as well for their help in functional studies of different mutants and fruitful discussion.

Extremely thanks to Patrizia Abrusci for her kind help, especially in cloning of *Pichia*

Thanks to Florian a diploma student for helping in speeding up the work in the middle stages.

Thanks to all my PhD, Post docs, diploma students and the technical gang Eirini, George, Julius, Mads, small Bettina, Maria, Kerstin, Christian, Ajda, Kira, Brazilian Anita, Austrian Anita, Jana, Christoph, Euripedes, Jaegeun, Adekunle, Nikos, Irina and Ulrich.

Thanks to Prof Robert Konrat and all colleagues from his group, for being provided a nice and friendly working atmosphere.

Many thanks to Dr. Abdul Ghafoor KHAN, Keni VIDILASERIS and Faisal KHAN Bangash for their company whenever I need them.

Thank to Werner König for helping in solving computer problems, Ursula Talhammer and Karin Pfeiffer for helping in all office works.

Muhammad Bashir Khan

CURRICULUM VITAE

Muhammad Bashir Khan, M.Sc

Personal Data

Born: 3rd August 1977, F.R. Lakki Marwat, Pakistan

Citizenship: Pakistani

Current position: PhD student

Institute: Department for Structural and Computational Biology, Max F. Perutz Laboratories, University of Vienna, Vienna, Austria Campus Vienna Biocenter 5 A-1030 Vienna, Austria

E-mail: Muhammad.Bashir.Khan@univie.ac.at
mbashirjan@hotmail.com

Education and Scientific Experience

Since 09/2006 **Department for Structural and Computational Biology, Max F. Perutz Laboratories, University of Vienna, Vienna, Austria**
PhD student
Advisor: Prof. Dr. Kristina Djinović-Carugo
Thesis : **“Structural and functional studies on yeast mitochondrial magnesium transporter Mrs2”**
Funding: WWTF, Wiener Wissenschafts-, Forschungs- und Technologiefonds, (Vienna Science and Technology Fund)

05/2006-09/2006 **Internship** in the laboratory of Prof. Dr. Hubert Kalbacher University of Tübingen
“purification and identification of carboxy peptidase from human sweat”

2002-2005 **Research Fellow** University of Karachi, Karachi Pakistan
“purification and Identification of biologically active molecules from plants and snake venom”

2001-2002 **Lecturer** of Chemistry at Islamabad Model College for Boys, F-10/3 Islamabad, Pakistan.

- 02/2001-07/2001 **Master Thesis** Department of Chemistry Gomal University D.I.Khan
“Identification of mineral contents in *Triticum aestivum*”
- 1998-2001 **Master of Science**, in Chemistry and Biochemistry, Gomal University D.I.Khan
- 1995-1997 **Bachelor of Science**, University of the Punjab

Publication

- 2011 **Muhammad Bashir Khan**, Gerhard Sponder, Björn Sjöblom, Soňa Svidová, Oliviero Carugo, Rudolf J. Schweyen, Kristina Djinović-Carugo “Structural and Functional Characterization of the N-terminal Moiety of Mrs2 – the Mg²⁺ Transporter from Yeast Inner Mitochondrial Membrane” (Submitted)
- 2011 Soňa Svidová, Gerhard Sponder, **Muhammad Bashir Khan**, Rudolf J. Schweyen, Oliviero Carugo, Kristina Djinović-Carugo “Effect of mutations in the conserved GMN motif on ion transport and selectivity in the yeast magnesium transporter Mrs2p” (Submitted)
- 2010 **Muhammad Bashir Khan**, Björn Sjöblom, Rudolf J. Schweyen, Kristina Djinović-Carugo. Crystallization and preliminary X-ray diffraction analysis of the N-terminal domain of Mrs2, a magnesium ion transporter from yeast inner mitochondrial membrane. *Acta Cryst.* (2010). F66, 658–661
- 2006 Saeed, S., Rasool, S.A., Ahmed, S., Khanum, T., **Khan M.B.**, Abbasi, A., and Ali, S.A. (2006) New insight in staphylococcin research: bacteriocin or / and bacteriocin-like inhibitory substance(s) produced by *S. aureus* AB188. *World J. Microbiol. Biotechnol.*, 22: 713-722.
- 2004 Pirzada, Z.A., Ali, S.A., **Khan, M.B.** and Rasool, S.A. Production and Physico-chemical Characterization of Bacteriocins-like Inhibitory Substances from Marine Bacterium ZM81. *Pak. J. Biol. Sci.*, (2004)7: 2026-2030.

Oral Presentations

- 2011 Vienna Bruker Workshop 19-21 January 2011, Univ. Vienna.

Title, “**S-SAD Phasing with highly redundant in-house data of Mrs2 Protein**”.

- 2010 MFPL annual presentation 18th November, Univ. Vienna.
 Title, “**Structural and functional studies on yeast mitochondrial Mg⁺² transporter Mrs2**”.
- 2009 MFPL PhD and Post Doc Recess, 19-21 October, Krumbach Austria.
 Title, “**An N-terminal domain of Eukaryotic Crystal structure of Mg⁺² Channel/Transporter from yeast inner mitochondrial membrane and its comparison with prokaryotic Mg⁺² transporter CorA**”.
- 2009 Workshop on advanced strategies for the expression of proteins and protein complexes in Yeast, 19-21 November, Barcelona, Spain.
 Title, “**Crystal Structure of N-terminal Domain of Mrs2 - Mg⁺² Channel/Transporter from Yeast Inner Mitochondrial Membrane at 1.4 Å**”.
- 2008 11th Heart of Europe Bio-Crystallography meeting, Greifswald, Germany 25-27. September.
 Title, “**Structural studies on the Mrs2p: a eukaryotic Mg⁺² channel protein**”

Poster Presentation

- 2003 Symposium on Protein Structure and Function Relationship, Jan 20 - 24, 2003, Karachi, Pakistan.
 Title, “Purification and Characterization of 25 kDa Alkaline Serine Protease from The Seeds of *Citrullus colocynthis*”.
- 2005 International Conference on Protein Structure and Function Relationship, Jan 07-10, 2005, Karachi, Pakistan.
 Title, “Isolation, Purification and Biochemical Characterization of a 25 kDa Novel Alkaline Serine Protease from Seeds of *Citrullus colocynthis*”.

Fellowships

- 2000 Academic Merit Scholarship of Gomal University D.I.Khan.
- 2005 CNPq-TWAS 2005 Post Graduate Fellowship.
- 03-12-2008 Research Fellowship 2008 of the University of Vienna
